UNIVERSITÀ DEGLI STUDI DI SALERNO

UNIVERSITÀ DEGLI STUDI DI SALERNO

Dipartimento di Farmacia

PhD Program

in **Drug Discovery and Development**

Cycle XXXVIII–Academic Year 2024/2025

PhD Thesis in

Multi-omics analysis on prokaryotic model to explore the targets of bioactive natural molecules

Candidate

Raffaella Nocera

Tutor

Prof. *Nunziatina De Tommasi*

Co-Tutor

Prof. *Fabrizio Dal Piaz*

PhD Program Coordinator: Prof. Dr. *Alessandra Tosco*

Secondo la relatività, il tempo non scorre uguale per tutti: ciò che per me è passato, per l'universo potrebbe essere ancora presente. Forse, in quel presente, tu esisti ancora e mi osservi da una curva che non possiamo ancora calcolare.

"La distinzione tra passato, presente e futuro è solo un'illusione, anche se ostinata."

Albert Einstein

Al mio immenso, unico ed eterno papà.

Index

Abstract

The threat of bacterial resistance to antibiotics is a major concern, thus making the discovery of new molecules with antimicrobial activity a central goal of biomedical research. This PhD project aims to identify plant derived molecules with antimicrobial activity and elucidate their mechanisms of action. During the first year, the study of the labdane diterpenoid manool, a specialized metabolite of *Salvia* genus, Lamiaceae, was carried out. Firstly, the antimicrobial activity of manool was tested on different bacterial strains, both GRAM+ and GRAM-, and the most promising activity was observed towards *Streptococcus mutans*. Drug Affinity Responsive Target Stability (DARTS) assay coupled with mass spectrometry was used as a reliable approach to identify the putative molecular target(s) of manool in *S. mutans*. DARTS was preliminary performed on protein extract (pe-DARTS) of *S. mutans* in presence or not of manool, and subsequently it was carried out on live bacteria. However, applying DARTS to bacterial systems presents intrinsic challenges due to the rapid replication and short generation times of prokaryotic cells. These fast dynamics can quickly trigger regulatory responses, such as transcriptional and translational changes, which can make it difficult to interpret DARTS results. Based on this evidence, experimental conditions were optimized to enable the effective application of DARTS in bacterial cells, to preserve

the integrity of the protein/ligand interaction snapshot that DARTS aims to obtain. These approaches allowed the identification of manool interacting proteins belonging to the ATP-binding cassette (ABC) superfamily. These proteins form a large family involved in the active transport of several molecules, using ATP to move substrates across cell membranes. During the second year of this PhD program, the putative targets of manool in *Streptococcus mutans* were validated. To confirm ABC transporters as potential targets of manool, amino acid and sugar uptake assays were performed using LC-MS and NMR analyses. Several studies have shown that ABC transporters are involved in the trafficking of various substrates across membranes, suggesting they may play a key role in bacterial susceptibility to antibiotics. Therefore, inhibition of ABC transporters by manool could enhance the efficacy of other antibacterial drugs. To test this hypothesis, LC-MS analysis of the supernatants of *S. mutans* incubated with and without manool in combination with kanamycin was performed, along with experiments measuring the Fractional Inhibitory Concentration Index (FICI) for manool and kanamycin. In order to elucidate the possible stress response and the principal pathway involved in manool treatment, *S. mutans* was subjected to differential proteomics studies. The results showed regulation of ABC transporters and several proteins involved in stress responses. Based on these results, the downstream effects of manool in *S. mutans* were investigated during the third year. Firstly, *S. mutans* was cultured in co-culture with

human gingival fibroblasts (HGF-1). Incubating manool and *S. mutans* in co-culture with eukaryotic cells allowed studying the role of the diterpene in the adhesion and invasion of *S. mutans* in HGF-1. Subsequently, an evolution experiment was conducted to study *S. mutans'* response to a prolonged exposure to increasing concentrations of manool. After eight weeks, proteomics and genomics analyses were performed to investigate the possible mutations induced in bacteria by manool treatment. The experimental design used for investigation of manool's target on *S.mutans* was applied to ammoresinol, a sesquiterpenoid coumarin from *Ferula ammoniacum* (Apiaceae), that exhibited an interesting antimicrobial activity. As a starting point, the antibacterial activity of specialized metabolites from *F. ammoniacum* against bacteria was investigated. Ammoresinol was selected after antimicrobial screening as it showed promising activity against *Listeria monocytogenes*. Proteins involved in peptidoglycan synthesis and bacterial virulence were identified as putative ammoresinol targets by DARTS experiments on protein extracts (pe-DARTS) and bacterial cells (bc-DARTS). The two DARTS experiments led to the identification of prfA as a major putative target of ammoresinol in *L. monocytogenes*. Based on these results, a targeted proteomics assay was performed to confirm the interaction between ammoresinol and prfA.

Chapter 1

Introduction

1.1 Antimicrobial resistance: the silent treat to global health

Antibiotics represent one of the most pivotal classes of pharmaceuticals and stand among the most transformative medical innovations of the twentieth century. Their introduction has profoundly benefited human society, saving millions of lives by effectively combating bacterial infections (Muteeb et al., 2023). However, the global rise in infections caused by multidrug-resistant (MDR) bacteria has become increasingly alarming, with the threat of untreatable diseases, since the early 2000s (Bobate et al., 2023). Antibiotics have enabled the advancement of numerous medical fields, such as facilitating successful surgical procedures, immunosuppressive therapies, and management of infectious complications. The emergence of antimicrobial resistance (AMR) poses a formidable challenge to healthcare systems worldwide (Nazir et al., 2025). As all living organisms adapt to survive selective pressures, AMR is an inevitable evolutionary outcome. Bacteria will continue to develop resistance mechanisms if antibacterial agents are present in their environment. Microorganisms such as bacteria are living entities capable of adapting to environmental changes over time. Their fundamental biological imperative is to replicate, survive and spread as efficiently as possible. Consequently, bacteria evolve mechanisms that enhance their survival, particularly when exposed to threats such as antibiotics (Zhang & Cheng, 2022). When antimicrobial agents inhibit bacterial growth, genetic mutations may arise that confer

resistance, allowing the organism to persist despite treatment (Coculescu 2009). This evolutionary response is a natural consequence of selective pressure and is central to the development of antimicrobial resistance (AMR). Multidrug-resistant pathogens are responsible for a wide range of infections and are associated with significantly higher rates of morbidity and mortality. The escalation of antibiotic resistance and the frequent recurrence of common infections pose a serious threat to public health and have profound societal implications. Recent studies estimate that by 2050, deaths caused by antimicrobial resistance could surpass 10 million annually, potentially exceeding mortality rates from other infectious diseases and certain cancers (Oliveira, et al., 2024). This escalating crisis not only threatens public health but also undermines economic stability. According to the World Health Organization's 2019 report, AMR is responsible for approximately 700,000 deaths annually, with projections estimating up to 20 million fatalities by 2050 (Naghavi et al., 2024) and a global economic burden exceeding $2.9 trillion (Figure 1).

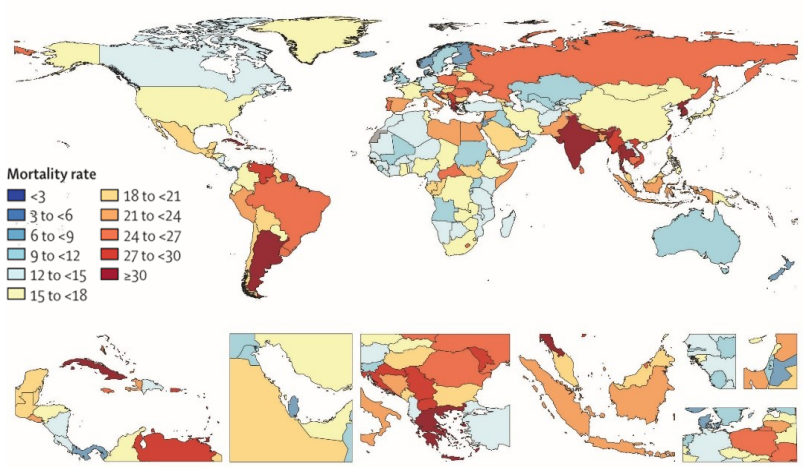

Figure 1. *Death rate attributable to Antimicrobial Resistance (AMR), all ages, 2050. (Naghavi et al., 2024)*

The aetiology of antibiotic resistance is multifactorial and extends beyond microbial adaptation. Key contributing factors include the overuse and misuse of antibiotics, inaccurate diagnoses, inappropriate prescribing practices, loss of patient sensitivity, self-medication, substandard healthcare environments, poor hygiene and extensive use of antibiotics in agriculture (Mendoza et al., 2025). Recent advances in molecular biology and genomics have deepened our understanding of the genetic basis of resistance. The concept of the resistome, introduced by Wright (2007), encompasses the full repertoire of resistance genes present in pathogenic and non-pathogenic bacteria alike. This includes both intrinsic resistance elements and those acquired through horizontal gene transfer. The resistome serves as a reservoir from which clinically relevant resistance traits may emerge, especially

under selective pressure from antibiotic use. Antibiotic resistance can be broadly categorized into two main types: natural (intrinsic) and acquired resistance. Natural resistance may be either *innate*, where resistance traits are constitutively expressed by the organism, or *inducible*, where resistance genes are present but only activated upon exposure to antibiotics. In contrast, acquired resistance arises through the uptake of foreign genetic material via transformation, conjugation, or transposition, or through spontaneous mutations in the bacterial chromosome (Galgano et al., 2025) (Figure 2). Mechanisms underlying antimicrobial resistance (AMR) can be divided into four principal strategies:

- Limitation of drug uptake;
- Modification of drug targets;
- Drug inactivation;
- Active drug efflux.

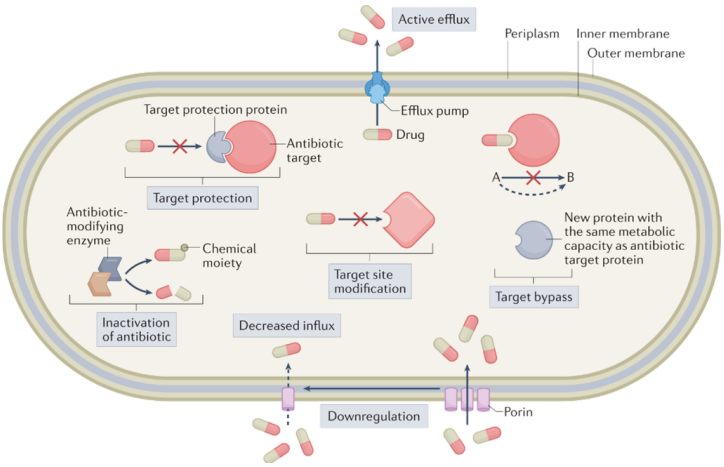

Figure 2. *Mechanisms underlying antimicrobial resistance (AMR) (Darby, E.M., et al., 2023).*

Due to structural differences, Gram-negative bacteria are capable of employing all four mechanisms, whereas Gram-positive bacteria are less likely to utilize drug uptake limitation and efflux, owing to the absence of an outer membrane and lipopolysaccharide (LPS) layer. Gram-negative bacteria possess an outer membrane enriched with LPS, which acts as a permeability barrier, reducing the penetration of many antibiotics. For example, glycopeptide antibiotics like vancomycin are ineffective against Gram-negative bacteria due to their inability to cross this barrier. Hydrophilic antibiotics such as β-lactams, tetracyclines, and certain fluoroquinolones are particularly affected by changes in membrane permeability. In Enterococci, reduced porin expression or substitution with non-selective channels impairs the entry of polar molecules, conferring intrinsic tolerance to aminoglycosides (Reygaert 2018). Mutations that downregulate porin channels have been

linked to resistance against carbapenems in *Enterobacterales*, *Acinetobacter spp.*, and *Pseudomonas spp.*, even in the absence of carbapenemase enzymes. Additionally, biofilm formation contributes to resistance by creating a protective matrix composed of polysaccharides, proteins, and DNA, which impedes antibiotic penetration. Efflux pumps actively expel antibiotics from bacterial cells, contributing significantly to intrinsic resistance in Gram-negative species (Pfeifer, Cullik & Witte, 2010). These pumps are classified into five major families based on their structure and energy source:

- ATP-Binding Cassette (ABC)
- Small Multidrug Resistance (SMR)
- Multidrug and Toxic Compound Extrusion (MATE)
- Resistance-Nodulation-Division (RND)
- Major Facilitator Superfamily (MFS)

While most families consist of single-component pumps operating across the cytoplasmic membrane, RND pumps are multi-component systems that span the entire cell envelope. A classic example is tetracycline resistance, mediated by Tet pumps (MFS family), which use proton exchange to extrude the drug. MDR efflux systems like MexAB-OprM in *P. aeruginosa* and AcrAB-TolC in *Enterobacterales* also contribute to resistance. Resistance to macrolides is often mediated by mef genes, which encode efflux pumps targeting erythromycin and related drugs. The MacAB-TolC tripartite pump (ABC family) is another well-characterized system for macrolide extrusion.

Bacteria can also neutralize antibiotics either by chemical modification or enzymatic degradation (Gaurav et al., 2023).

- Chemical Modification: enzymes may attach chemical groups (e.g., phosphoryl, acetyl, adenyl) to antibiotic molecules, preventing them from binding to their targets. Acetylation is common in resistance to aminoglycosides, chloramphenicol, streptogramins, and fluoroquinolones. Aminoglycoside-modifying enzymes (AMEs) alter hydroxyl or amino groups, rendering the drug inactive.
- Enzymatic Destruction: β-lactam antibiotics (e.g., penicillins, cephalosporins) share a four-membered β-lactam ring essential for activity. β-lactamases hydrolyze this ring, preventing the drug from binding to penicillin-binding proteins (PBPs), thus conferring resistance. Resistance can also result from structural or quantitative changes in the antibiotic's target site.
- Alterations in PBPs reduce the binding affinity of β-lactam antibiotics. For instance, the mecA gene in *Staphylococcus aureus* encodes a modified PBP that resists β-lactam binding.
- The erm gene family methylates 16S rRNA, modifying the ribosomal binding site and blocking macrolides, streptogramins, and lincosamides.
- Resistance to fluoroquinolones, which target DNA gyrase and topoisomerase IV, arises from mutations that alter these enzymes, diminishing drug binding. The global rise in microbial infectious diseases is increasingly driven by the growing

resistance of microorganisms to currently available antimicrobial agents (Nishino et al., 2021).

Given the complexity of the resistance processes there is a still unsolved demand for innovative antimicrobials that can successfully combat resistant clinical pathogens.

“There is a fascinating competition between microbes and humans: they are lucky to have a short generation time, but I hope we are smarted and stay one step ahead”

Jaap Wagenaar, University of Utrecht.

1.2 Nature’s silent warriors: plants molecules against superbags

There is no doubt that antibiotics have been revolutionary drugs, standing as a cornerstone in the fight against infectious diseases for decades and saving millions of lives. However, their effectiveness is increasingly compromised by the alarming rise of multidrug-resistant pathogens and the rapid spread of new infections. This growing crisis has prompted global health organizations and pharmaceutical industries to reconsider their strategies. Medicinal plants represent a rich reservoir of bioactive compounds with significant therapeutic potential (El-Saadony et al., 2025). Their natural origin, cultural relevance

and broad pharmacological spectrum make them promising candidates for the development of innovative drugs (Chaachouay & Zidane, 2024). Rich in natural antimicrobial compounds with diverse mechanisms of action, (Pérez-Flores et al., 2025) many of these plants have been used in traditional medicine for centuries and have demonstrated efficacy comparable to certain commercial antibiotics. Their huge biodiversity offers a vast array of bioactive compounds with diverse pharmacological properties, making them invaluable in the search for new drugs and treatments (Figure 3). Among the most studied bioactive constituents are alkaloids, flavonoids, terpenoids, phenolics and essential oils (Parham et al., 2020).

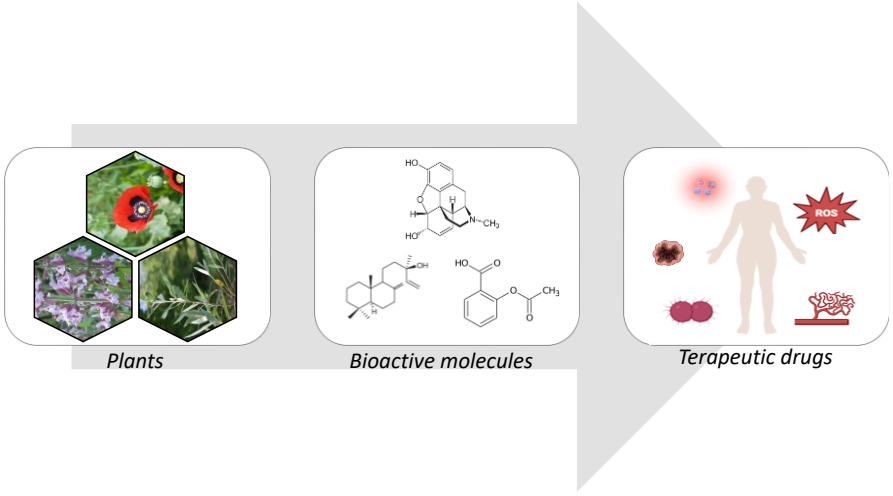

Figure 3. *Plants as a source for new bioactive compounds.*

These compounds exhibit a wide range of biological activities, including antibacterial, antioxidant, anti-inflammatory, anticancer, and immunomodulatory effects. Recent advancements in extraction technologies, analytical methods,

and phytochemical screening have greatly improved the identification and characterization of bioactive compounds. These scientific innovations have deepened understanding of the chemical and biological profiles of medicinal plants, paving the way for new therapeutic discoveries. The growing interest in traditional ethnomedicine is paving the way for the discovery of novel therapeutic agents. A plethora of specialised metabolites have served as precursors to pharmaceuticals currently employed in the treatment of diverse pathologies. Among them, some of the best-known plant-derived specialized metabolites are the *Vinca* alkaloid*s*, such as vincristine and vinblastine, widely used in the chemotherapy of haematological and lymphatic malignancies. These compounds, among the first microtubule-targeting agents approved for clinical use, act by disrupting mitotic spindle dynamics, leading to cell cycle arrest and cancer cell death (Banyal et al., 2023). Another example is morphine and its derivatives, widely used for the management of various types of pain. Morphine, a potent μ-opioid receptor agonist, remains one of the most effective analgesics available. However, its clinical use is limited by serious side effects such as respiratory depression, euphoria, and addiction. This has prompted ongoing efforts in medicinal chemistry to develop semi-synthetic derivatives of morphine and codeine that are safer, orally active, and less prone to abuse (Zarin et al., 2023). Only a small proportion of the known plant species on Earth (estimated at 250,000–500,000) has been studied for the

presence of antibiotic compounds, and only 1–10% of plants are used by humans (Borris 1996). Plants' antimicrobial properties are attributed to active compounds and secondary metabolites such as quinones, phenols, alkaloids, flavonoids, terpenoids, tannins, lignans and glucosinolates. These compounds represent one of the main sources of chemical diversity. Essential oils derived from aromatic medicinal plants (e.g. fennel, peppermint, thyme and lavender) contain mixtures of volatile substances such as monoterpenes, sesquiterpenes and/or phenylpropanoids and have been reported to be active against Gram-positive and Gram-negative bacteria, yeasts, fungi and viruses (Savoia 2012). The use of plant species guarantees the availability of compounds with antimicrobial activity. The reason for studying these compounds is to understand their therapeutic targets, mechanisms of action, and structure-activity relationships (Fischbach & Walsh, 2009). The primary aim is to develop new chemotherapeutic agents and antibiotic therapies that are effective, safe and have fewer side effects. Additionally, these new compounds are intended to serve as alternatives or complementary treatments to existing antimicrobials. This will help to overcome the growing challenge of antibiotic resistance. The objective of this research is to have the arsenal of available drugs expanded so that infectious diseases can be better managed and patient outcomes improved worldwide.

1.3 Targeting bacterial resistance: proteomics and DARTS-based approaches

Determining the specific biological molecule a drug interacts with is a fundamental step in the drug discovery process and is known as target identification. Identifying the protein targets of natural products is a valuable drug discovery strategy. By understanding the exact target, researchers can make improvements to drug design, enhance its efficacy and reduce unwanted side effects. However, the fact that most therapeutic compounds interact with multiple proteins complicates this process. In recent years, researchers have increasingly turned to chemical proteomics approaches to address this challenge (Jiang et al., 2024). These methods enable the unbiased and comprehensive profiling of protein targets for bioactive small molecules, offering deeper insights into their mechanisms of action (Zou et al., 2024). Proteomic analysis provides essential information about the function and regulation of protein complexes, which are complex structures that play a crucial role in various biological processes. It encompasses the entire set of proteins encoded by a genome and this can depend on factors such as the type of cell or tissue, age, disease state and environmental influences. Unlike the genome, which is static, proteomes are highly dynamic in both time and space; each profile captures a specific biological snapshot (Kopec, Bozyczko-Coyne & Williams, 2005). This versatility makes proteomics a powerful tool for comparing protein expression under different conditions, such as between drug-treated and

untreated cells, or between healthy and diseased tissues. Proteins are key functional molecules that drive and regulate most biochemical processes in living organisms. Their activity and structure can be altered through post-translational modifications (PTMs), which cannot be directly inferred from gene or transcript sequences. Indeed, proteomics is a crucial complement to genomics and transcriptomics. Over the past two decades, MS-based proteomics has emerged as the leading approach for high-throughput, detailed protein analysis (Birhanu et al., 2023). This technology has significantly advanced microbiological research in various fields, including the comprehensive mapping of bacterial proteomes, the characterisation of PTMs, the elucidation of pathogen-host interactions, the investigation of antimicrobial resistance and the identification of potential biomarkers. Furthermore, proteomic approaches coupled with mass spectrometry are widely used for the study of the mode of action of bioactive small molecules. Several promising proteomic methods have been introduced for directly isolating and identifying the protein targets of interest that are bound by active compounds or for visualizing enzymes whose activity is somehow affected by such compounds (Liao et al., 2017). Protein target identification research is an important part of the drug discovery process, requiring a significant investment of time and resources, crucial for understanding their mechanism of action. Prominent results in the discovery of drug targets have been achieved using a series of target screening techniques based on affinity

chromatography, isotopic tracers and fluorescence detection (Cho et al., 2019). Various experimental techniques have been developed over the years to identify drug targets, particularly at the biochemical level. These approaches are used most widely in two forms: affinity-based and label-free. Selecting the most appropriate approach depends on the specific requirements of the research project (Tabana et al., 2023). The main techniques used in target identification are summarised below:

Affinity-based pull-down methods: the process involves modifying a small molecule with a tag or linker to capture its binding partners from cell lysates. The small molecule is attached to a solid support (e.g. agarose beads) via a linker (e.g. PEG) and is then incubated with a cell lysate. Proteins that bind to the matrix are eluted and identified using mass spectrometry (Ha et al., 2021).

Biotin-tagged approach: a biotin tag is appended to the small molecule. This tagged molecule is then incubated with a cell lysate before being isolated using streptavidin beads. Proteins are identified using two methods: SDS-PAGE and mass spectrometry. This approach is easy to perform, low cost, widely used. Unfortunately, the strong biotin-streptavidin interaction requires harsh conditions (e.g. heat or SDS) to release the proteins. This may alter protein structure or affect cell permeability. It can also impact biological results (e.g. the immune response in living cells) (Cotton, Wells & Seiple, 2021).

Photoaffinity labelling (PAL): this uses a light-activated chemical probe that covalently binds to the target protein when exposed to light. These probes consist of a photoreactive group, a linker, and sometimes an affinity tag. Common photoreactive groups include: phenylazides (form nitrenes), phenyldiazirines (form carbenes); Benzophenones (form diradicals) (Murale et al., 2016).

These approaches primarily aim to increase traceability by modifying small molecules structures, thereby altering properties such as polarity, conformation and solubility, which can easily lead to false positive protein binding results (Rix & Superti-Furga, 2009). Another limitation is that structural modifications always occur at specific sites, such as hydroxyl and carboxyl groups. However, when large and structurally complicated types of natural small molecules are used, it can be difficult to achieve the selective modification of a chosen site. Therefore, target discovery, especially for natural products, remains uncertain and subject to change. In recent years, a series of label-free SM probes have been developed that can efficiently screen target proteins of small molecules without the need for chemical modification of their structures. These approaches leave the molecules in their natural state, without undergoing any chemical modifications to their structures, thus retaining their native conformation and functional properties.

This method is often preferred by researchers as it does not require modification or labelling of the primary molecule. However, although this approach avoids any potential problems with compound labelling, it does have a few limitations (Hedl et al., 2019). One of the most exploit label-free SM probe technology among chemical proteomics approaches is Drug Affinity Responsive Target Stability (DARTS), first proposed by Lomenick et al. in 2009 (Lomenick et al., 2009) (Figure 4).

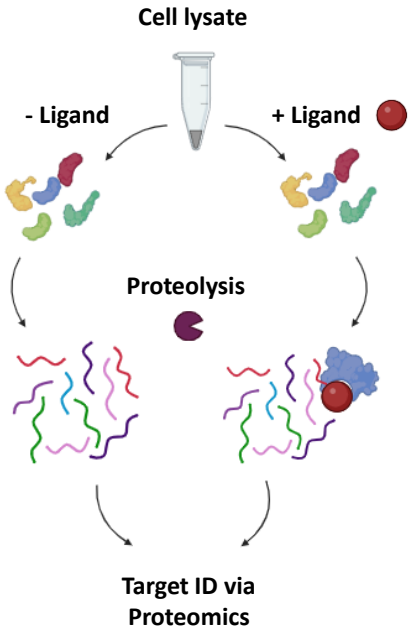

Figure 4. *Drug Affinity Responsive Target Stability Assay (DARTS)*

This strategy enables target proteins to be tracked and identified after their stability changes upon binding to SM. The connection between SMs and target proteins is typically formed through ionic bonds, hydrogen bonds, van der Waals forces

and other intermolecular forces, which maintain a stable complex structure. Therefore, when a protein binds to a small molecule, its stability is significantly enhanced compared to its unbound form (Lomenick et al., 2009). Such change in stability results in a modification of some properties of the protein, like susceptibility to enzymatic-catalysed proteolysis. Based on this, a classical DARTS experiment is carried out by subjecting to a limited proteolysis protein mixtures obtained from cell treated or not with a SM of interest. Those proteins whose digestion rate is affected by the treatment are considered putative interactors of the SM. DARTS is particularly favoured in the field of anti-cancer and anti-tumour drug research. Additionally, the DARTS strategy has been fully applied to elucidate the pharmacological mechanisms of anti-neurodegenerative, anti-angiogenesis, anti-inflammatory, anti-fungal and anti-toxin effects (Ren et al., 2021). Applying DARTS to bacterial systems presents intrinsic challenges due to the rapid replication and short generation times of prokaryotic cells. These fast dynamics can quickly trigger regulatory responses, such as transcriptional and translational changes, which can make it difficult to interpret DARTS results. Since DARTS is based on capturing a static snapshot of protein–ligand interactions before secondary cellular effects begin, the temporal resolution required in bacterial contexts is much lower. As a result, the probability of perturbation-induced artefacts rises, possibly undermining the specificity and reliability of target engagement evaluations. Based on this evidence, it is

clear that experimental conditions must be optimized to enable the effective application of DARTS in bacterial cells. It is essential to adapt the protocol to consider the rapid replication and dynamic cellular responses of bacteria in order to preserve the integrity of the protein–ligand interaction snapshot that DARTS aims to obtain.

Chapter 2

Disarming *Streptococcus mutans* by manool

Partially based on the manuscript

Nocera, R., Rosa, E., Parisi, V., Tuccinardi, T., Di Stefano, M., Donadio, G., Dal Piaz, F., De Tommasi, N. Disarming *Streptococcus mutans* in real time: live-cell DARTS uncovers ABC transporter targeting by manool. Submitted on *Communication Biology*, under review.

2.1 Introduction

2.1.1 Salvia genus

Salvia is a highly diverse and polymorphic genus belonging to Lamiaceae family, which include approximately 900 species, distributed across nearly every region of the world (Ghorbani & Esmaeilizadeh, 2017). Among them, *Salvia officinalis* is an herbaceous plant native to the Middle East and Mediterranean basin, though it has since become naturalized worldwide. It is commonly used as a culinary herb to flavour and season food (Figure 5). The plant's botanical name reflects its long-standing medicinal significance. The term "Salvia" originates from the Latin word *salvere*, meaning "to heal," while "officinalis" denotes its use in medicine (Moreira et al., 2013). Indeed, *S. officinalis* has a rich history in traditional medicine, where it has been employed to treat a wide array of ailments, including convulsions, ulcers, gout, rheumatism, inflammation, dizziness, tremors, paralysis, diarrhea, and hyperglycemia (Anagnostou et al., 2025). In recent years, this species has been the focus of extensive scientific research aimed at validating its traditional uses and uncovering new therapeutic properties. These studies have revealed a broad spectrum of pharmacological activities, such as antitumor, anti-inflammatory, antinociceptive, antioxidant, antimicrobial, antimutagenic, anti-dementia, hypoglycemic and hypolipidemic effects.

Figure 5. *Salvia officinalis L. (Lamiaceae), perennial aromatic subshrub, native to the Mediterranean region, widely cultivated for culinary and medicinal use.*

2.1.2 Terpenes and manool

Terpenoids and phenols have been identified as the primary products of secondary metabolism in *Salvia* genus (Avato et al., 2005). Terpenes are built from C5 isoprene units, whose number determines their classification: monoterpenes (C10), sesquiterpenes (C15), diterpenes (C20), triterpenes (C30), and carotenoids (C40) (Xavier et al., 2023). They exhibit diverse functional groups, including alcohols, aldehydes, phenols, ketones, ethers, and hydrocarbons, as exemplified by compounds such as linalool, citral, thymol, carvone, eucalyptol, and limonene. Terpenoids, which are abundant in nature, are produced in response to microbial attack and have huge potential against various microorganisms through diverse mechanisms, such as membrane disruption, anti-quorum

sensing, inhibition of protein synthesis and ATP (Sharma et al., 2020). Manool is a diterpene and is one of the most abundant components of sage essential oils and extracts (Ben Farhat et al., 2009) (Figure 6). This diterpene was purified from the leaf tissues of *S. officinalis* and *S. tingitana* by our research group (Iobbi et al., 2021). It has also been isolated from other sources in the Lamiaceae family, such as the essential oils of *Origanum scabrum* (Demetzos et al., 2001), *Origanum dayi* (Dudai et al., 2003) and *Thymus fallax* (Morteza-Semnani et al., 2004), as well as from other plant families, including Asteraceae, Malvaceae, Solanaceae and Apiaceae (Iobbi et al., 2021). The compound's only known commercial natural source is the pink pine (*Halocarpus biformis, Podocarpaceae*), a tree that grows in New Zealand and has the highest known content (up to 6-8% dry weight) (Brooker, Cambie and Cooper, 1989; Iobbi et al., 2021). Manool is a hydroxylated labdane-type diterpene, characterized by a bicyclic system derived from four isoprene units (Tran, Wong & Chai, 2017). Its basic structure consists of two main fragments: a fused decalin core (C1–C10) and a branched six-carbon side chain attached at C9. The remaining four carbons (C17–C20) are linked to C8, C4, and C10 of the decalin system, respectively. In manool, this core structure is further functionalized by two double bonds at positions 8 and 14 and by a hydroxyl group at C13. Interest in the study of labdane diterpenes has grown in recent decades due to their wide range of biological activities, such as antibacterial, antifungal, antimutagenic, cytotoxic, cytostatic and anti-

inflammatory effects, as well as modulation of immune cell functions (Tran, Wong & Chai, 2017). These compounds have emerged as new candidates for modern drug discovery. Manool has demonstrated antibacterial activity against Gram-positive bacteria, including MRSA (Iobbi et al., 2021), as well as against oral cavity bacteria, such as *S. mutans, S. mitis, S. sanguinis* and *L. casei* (Moreira et al., 2013). Several authors have highlighted diterpenes as an important class of plant small molecules with potential for the discovery of new antibacterial agents (Moreira et al., 2013). However, the mechanisms underlying their antibacterial activity remain poorly understood.

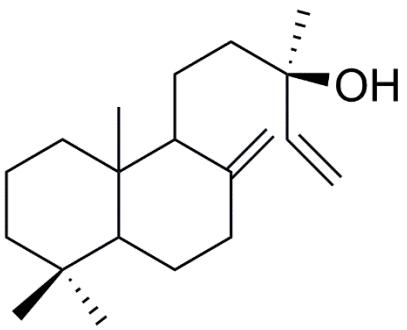

Figure 6. *Chemical structure of manool.*

2.1.3 Streptococcus mutans as a paradigm shift

In 1924, J. Clarke isolated an organism from carious lesions and named it *Streptococcus mutans*, believing that the oval-shaped cells he observed were mutant forms of streptococci (Figure 7). However, it wasn't until the late 1950s that *S. mutans*

began to attract significant attention within the scientific community. By the mid-1960s, both clinical and animal-based studies had identified *S. mutans* as a key etiological agent in dental caries. The natural habitat of *S. mutans* is the human oral cavity, specifically within dental plaque a multispecies biofilm that forms on the hard surfaces of teeth. Its cariogenic potential is widely attributed to three core characteristics:

1. The ability to synthesize large amounts of extracellular glucan polymers from sucrose, which facilitate stable colonization of tooth surfaces and contribute to the formation of the extracellular polymeric matrix.
2. The capacity to transport and metabolize a broad range of carbohydrates into organic acids (acidogenicity).
3. The resilience to environmental stress, particularly its ability to survive and thrive in low pH conditions (Lemos et al., 2019).

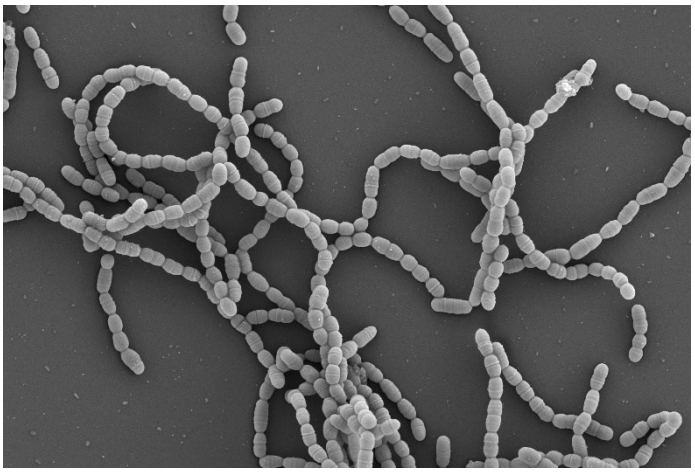

***Figure 7**. Scanning Electron Microscope (SEM) image of Streptococcus mutans. (Science Photo Library).*

Strains of *S. mutans* can be classified into four sero-logical groups (c, e, f, and k), based on the composition of cell-surface rhamnose-glucose polysaccharide, with ~75% of strains isolated from dental plaque belonging to serotype c, ~20% to serotype e and the remaining 5%classified as serotypes f or k (Nakano & Ooshima, 2009). As mentioned above, decades of epidemiological, biochemical and animal studies have identified bacteria as the primary cause of human dental caries. Although 200–300 bacterial species have been found in dental plaque, only *S. mutans* has been consistently linked to dental caries formation. Occasionally, it is linked to non-oral infections, most commonly bacterial endocarditis. Some *S. mutans* strains have also been connected to other extraoral diseases, including cerebral microhaemorrhages, IgA nephropathy and atherosclerosis (Ajdić et al., 2002; Lemos et al., 2019). As a lactic acid bacterium, *S. mutans* relies purely on glycolysis to produce energy. One of its defining characteristics is its ability

to metabolize a wide range of carbohydrates. The genome of the UA159 reference strain contains 14 phosphoenolpyruvate-dependent sugar phosphotransferase systems (PTS), each specialized for different mono- and disaccharides, along with two ATP-binding cassette (ABC) transporters, which are primarily responsible for importing oligosaccharides (Ajdić et al., 2002). The ability of *S. mutans* to rapidly adapt to significant environmental changes within dental plaque is a key factor in its role as a primary causative agent of dental caries. Fermentable carbohydrates consumed by the host serve as substrates for *S. mutans* and other lactic acid bacteria, leading to the production of acidic byproducts that accumulate within the biofilm (Lemos et al., 2008). Almost 15% of the total (ORFs) in the *S. mutans* genome encode transport proteins (Ajdić et al., 2002). Most of the identified transporters are ATP-dependent, a characteristic also observed in other organisms lacking an electron transport chain. There are three types of ATPase that transport solutes: type P, type F, and type ABC. ABC-type ATPases are the most abundant, with more than 60 transporters encoded in the genome, representing almost 10% of the total number of ORFs in *S. mutans* (Ajdić et al., 2002). Approximately one-third of all ABC transporters are categorized as importers, while the remainder are exporters, indicating that this microorganism can actively eliminate excess and harmful molecules. ABC transporters are composed of four main domains: two integral membrane domains and two ATPase subunits, the latter of which contain a distinctive ABC motif

(Webb, Homer & Hosie 2008). In prokaryotes, these domains are typically encoded as separate proteins that must assemble into a functional transporter. This active complex usually consists of homo- or heterodimers formed by ATPase and membrane domain subunits. These transporters are highly specific and capable of importing a wide variety \of substrates, including amino acids, carbohydrates, oligopeptides, osmo-protectants (such as proline, glycine betaine, and choline), inorganic ions (like Fe^{3+}, Co^{2+}, Mn^{2+}, Zn^{2+}, phosphate, nitrate, sulphate, and molybdenum), bacteriocins, and even DNA (Ajdić et al., 2002). Additionally, ABC transporters play a crucial role in exporting diverse compounds-antibiotics, metals, peptides, and lipids, making them key components of cellular efflux systems that contribute to drug resistance. *S. mutans* possesses several ABC transporters dedicated to amino acids uptake, specific or not specific for a single amino acid. This underscores the amino acid's vital role as a primary nitrogen source and a precursor for proteins biosynthesis. Sugar uptake is also central to *S. mutans* metabolism, with at least five ABC transport systems devoted to carbohydrate transport, including the MSM (multiple sugar metabolism binding) system (Russell et al., 2025). Moreover, the genome of *S. mutans* strain UA159 encodes 14 Two-Component Signal Transduction Systems (TCSTSs), that play a crucial role in bacterial adaptation, survival and virulence (Smith & Spatafora, 2012). Among these, ComDE, LevRS, VicRK, and the orphan regulator CovR have been extensively studied for their roles in regulating virulence

traits. LevRS is involved in carbohydrate metabolism, while ComDE regulates bacteriocin (mutacin) production and competence. VicRK is unique in being essential for *S. mutans* survival and influences responses to acid and oxidative stress, as well as competence (Senadheera et al., 2009). Evidence suggests crosstalk between VicRK and LiaFSR, another TCSTS, which contributes to surface adhesion, mutacin synthesis and resistance to environmental stressors such as cell envelope damage and heat shock (Shankar et al., 2015). The activation of quorum sensing for genetic competence requires at least six gene products encoded by the comCDE, comAB, and comX operons. The comC gene produces a precursor of the competence-stimulating peptide (CSP), which is processed and exported into the extracellular environment via a peptide-specific ABC transporter encoded by comAB. The comDE operon encodes a two-component system composed of a histidine kinase sensor protein (ComD) and its corresponding response regulator (ComE), which specifically detect and respond to CSP. When CSP reaches a critical concentration, it triggers autophosphorylation of ComD in neigh boring cells. The phosphate group is then transferred to ComE, which activates its target genes, including comX. The comX gene encodes a competence-specific sigma factor that recognizes a conserved sequence (known as the com-box) in the promoter regions of late competence genes, initiating the signalling cascade required for genetic competence. In *S. mutans*, this quorum sensing system represents a unique

regulatory mechanism, as it governs both bacteriocin production and the development of genetic competence (Yonezawa & Kuramitsu 2005). In light of these knowledges about *S. mutans* biology, pathogenicity and virulence, Jose ´A.Lemos et al. proposed it as a new Gram-positive paradigm (Figure 8).

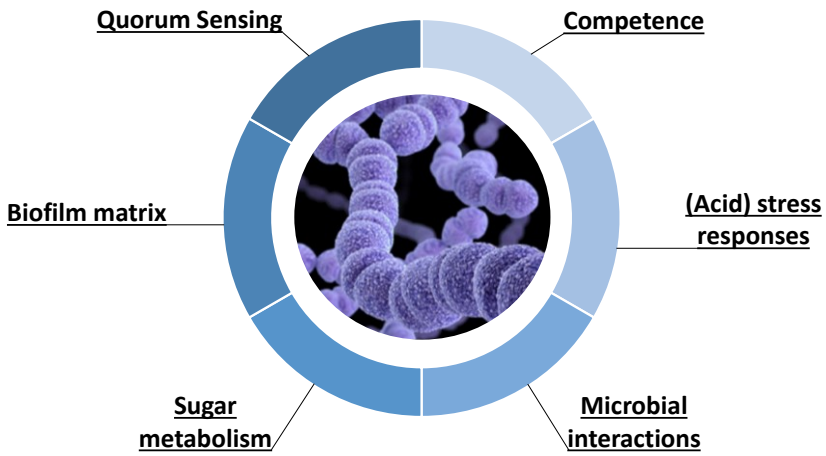

Figure 8. *The biology of Streptococcus mutans*

Although *Escherichia coli* and *Bacillus subtilis* have made important contributions to both basic and applied microbiological research, it is widely recognized that no single organism can fully represent the diversity of bacterial species. Many bacteria are difficult, or nearly impossible, to cultivate in laboratory conditions, some resist genetic and molecular manipulation and others pose significant safety risks. For these

reasons, model organisms will continue to play a vital role in advancing foundational research. In contrast to *E. coli* and *B. subtilis*, the dental pathogen *S. mutans* does not have a free-living lifestyle. Moreover, *S. mutans* is able to grow in multiple conditions and to resist several stresses, including some antibiotic agents, makes it an ideal model to characterize a new antibiotic compound. Finally, *S. mutans* is a genetically adaptable and relatively safe organism (Lemos et al., 2019).

2.2 Materials and Methods

2.2.1 Reagents and materials

Growth Media: Brain Heart Infusion Broth (Oxoid) and M9 Minimal Salts Base (Na2HPO4 7 H2O, KH2PO4, NaCl, NH4Cl) 5X were used. Solvents: Ultra-pure water (ROMIL-UpsTM Ultra purity), ultra-pure acetonitrile (ROMIL-UpsTM Ultra purity), ultrapure water (18 MΩ), and DMSO (Sigma-Aldrich) were utilized for the preparation of solutions and reagents. Buffers: The following buffers were used: Dulbecco's Modified Eagle's Medium (DMEM, Sigma-Aldrich), MOPS, Tris-HCl (1.5 M pH 8.8 and 1.0 M pH 6.8), Laemmli Buffer, TGS (Tris/Glycine/SDS buffer 5X, Bio-Rad), and AMBIC. Reagents: MTT (4,5-Dimethylthiazol-2-yl)-2,5-Diphenyltetrazolium Bromide (Invitrogen) was used for cell viability assays.

Other reagents included subtilisin, acrylamide 30% (AppliChem), sodium dodecyl sulfate (SDS), ammonium persulfate (APS), tetra-methylenediamine (TEMED),

dithiothreitol (DTT, AppliChem), iodoacetamide (IAA, AppliChem), and trypsin (proteomic grade, 0.0013 µg/µL). Standards: Kanamycin sulfate (ChemCruz), and chlorhexidine (MCE®) were used as standards in the experiments. The manool was previously purified by HPLC from *Salvia. officinalis* and was thus already available as a pure molecule (purity > 98%, see Appendix Figure A14). It was solubilized in DMSO at a concentration of 5 mg/ml and stored at -20°C prior to use.

2.2.2 Bacterial Culture

Streptococcus mutans Clarke NCTC (National Collection of Type Cultures) 10499 was grown in liquid Brain Heart Infusion (BHI) medium at 37°C under aerobic conditions for 18-24 hours. Solid culture was performed on BHI medium with 1.5% agar on a 60 cm² Petri dish (100 x 20 mm) at 37°C for 48 hours.

2.2.4 Minimum Inhibitory Concentration (MIC)

The minimum inhibitory concentration (MIC), defined as the lowest concentration of the molecule capable of inhibiting bacterial growth, was assessed using the serial dilution method, in accordance with the CLSI protocol (2009). Manool concentrations ranging from 40 µM to 2.5 µM were tested on *S. mutans*. Starting from a stock concentration of 5 mg/mL, the molecule was diluted with BHI (Brain Heart Infusion) to a maximum concentration of 40 µM. Serial dilutions were performed in a 96-well plate to achieve the desired antimicrobial concentrations (40 µM, 20 µM, 10 µM, 5 µM, 2.5

μM) with a volume of 100 μL per well. All tests were performed in triplicate. At this point, 100 μL of bacteria, previously diluted according to the initial OD values obtained from spectrophotometric measurements, was added to each well. *S. mutans* was inoculated into the plate at a density of 1 x 10^6 CFU/ml. The plate was then incubated at 37°C. After 24 hours, the bacterial growth inhibition values were evaluated using a spectrophotometer at a wavelength of 600 nm. The positive control was performed with the antibiotic chlorhexidine.

2.2.5 Bacterial Growth Curve

The growth curves of *S. mutans* were performed in flasks with and without manool. Four sterile 250 ml flasks, each containing 100 ml of BHI medium, were used. In each flask, an inoculum of the liquid bacterial culture was prepared, diluting it to an initial density of 0.05 OD/ml. Manool was added to three of the four flasks at concentrations of 2.5 μM, 5 μM, and 10 μM. The flasks were incubated at 37°C with shaking. Every 30 minutes 1 mL samples were taken from each of the four flasks, transferred to cuvettes, and bacterial growth was quantified using a spectrophotometer at a wavelength of 600 nm. The absorbance variation in each flask was monitored for 660 minutes. The microbial growth curve was obtained by plotting time on the x-axis and OD600 on the y-axis, allowing the identification of the different stages of microbial growth. The growth of *S. mutans* in the presence of manool was also evaluated starting from the exponential phase of the bacteria: under the same conditions,

an inoculum of the liquid bacterial culture was prepared in each of the four flasks, diluting it to a density of 0.2 OD/ml. Growth was monitored until an OD600 of 0.5 was reached, at which point manool was added at concentrations of 2.5 µM, 5 µM, and 10 µM. The flasks were incubated at 37°C with shaking. Bacterial growth was quantified using a spectrophotometer at a wavelength of 600 nm and monitored every 30 minutes for 210 minutes.

2.2.6. Drug Affinity Responsive Target Stability (DARTS)

The Drug Affinity Responsive Target Stability (DARTS) assay allows the identification of protein-ligand interactions, based on the principle that the binding of a small molecule to a target protein protects the protein, increasing its resistance to protease-catalysed hydrolysis (Dal Piaz et al., 2016). The DARTS assay was performed both on protein extract (pe-DARTS, Drug Affinity Responsive Target Stability Assay on protein extract) and on bacterial cells (bc-DARTS, Drug Affinity Responsive Target Stability Assay on bacterial cells).

2.2.6.1. Drug Affinity Responsive Target Stability Assay on protein extract (pe-DARTS)

The DARTS assay was initially performed by incubating manool with a protein extract (pe-DARTS) from *S. mutans*, followed by limited proteolysis, SDS-PAGE analysis of digestion products, and proteomic identification of the separated proteins. *S. mutans* cells from inoculum were centrifuged at 3000 rpm for

10 minutes; the pellets were then resuspended in 25 mM MOPS buffer to a density of 50 OD. Next, 50 OD of cells were lysed by sonication at an amplitude of 10 for 30 minutes, with 10 seconds ON and 10 seconds OFF. The lysates were centrifuged at 15,000 rpm for 20 minutes, and the supernatant was transferred into sterile Eppendorf tubes. The protein content of the supernatant was quantified using the Bradford method. For the DARTS assay, 50 µg of proteins were aliquoted for both control and treated samples. The treated sample for the pe-DARTS assay was incubated with manool (20 µM) for 30 minutes at 4°C. The lysates were then digested with subtilisin (enzyme:protein ratio of 1:3500) at 37°C for 30 minutes. The resulting protein mixtures were separated by one-dimensional polyacrylamide gel electrophoresis (SDS-PAGE). A gel with 12% polyacrylamide concentration was prepared as follows: “Resolving gel 12%” (for a final volume of 10 ml): 3.3 ml distilled H_2O, 4.0 ml 30% acrylamide, 2.5 ml Tris-HCl 1.5 M pH 8.8, 0.1 ml 10% SDS, 0.1 ml 10% ammonium persulfate (APS) (initiator), 0.004 ml TEMED (catalyst); “Stacking gel” (for a final volume of 3 ml): 2.1 ml distilled H_2O, 0.5 ml 30% acrylamide, 0.38 ml Tris-HCl 1.0 M pH 6.8, 0.03 ml 10% SDS, 0.03 ml 10% ammonium persulfate (APS), 0.03 ml TEMED. For sample resuspension and electrophoresis, the following solutions were used: “SDS gel-loading buffer” (Laemmli Buffer): Tris 0.125 M pH 6.8 (for protein denaturation), 4% SDS (w/v), 0.4% bromophenol blue (w/v) (dye), 40% glycerol (v/v) (to increase sample density for loading into wells), 10% β-

mercaptoethanol (v/v) (to break disulfide bonds between cysteines); “Running buffer” (for a final volume of 1 L): 800 ml deionized H_2O, 200 ml 5x TGS (Tris/Glycine/SDS buffer). Electrophoresis was performed at 100 V for 20 minutes and continued at 180 V for 40 minutes. After electrophoresis, the proteins were fixed in gel using the fixing solution (50% H_2O, 40% MeOH, 10% CH_3COOH), and 10 bands were excised from each lane and subjected to trypsin digestion. The tryptic digestion selectively cleaves peptide bonds on the carboxyl side of arginine and lysine residues, generating highly characteristic fragments for each protein. Each band was transferred into respective Eppendorf tubes and subjected to a washing step with acetonitrile (ACN) three times to dehydrate the gel fragments. After removing the ACN solution, 0.01 M DTT in 0.1 M ammonium bicarbonate (AMBIC) was added. The reduction reaction was carried out for 60 minutes at 56°C. Then, the supernatant was removed and another three washes with ACN were performed. After removing the ACN, a 0.055 M iodoacetamide (IAA) in AMBIC 0.1 M solution was added. The alkylation reaction was carried out for 30 minutes at room temperature in the dark. After removing the supernatant, the bands were washed again with ACN and dried in a Speed-Vac for 15 minutes. Subsequently, the actual digestion was performed: 30 µL of a trypsin solution (Proteomic grade, 0.0013 µg/µl) in 25 mM AMBIC was added to each band to cover them, and each was incubated at 4°C for 45 minutes to allow the enzyme to penetrate the gel bands. Finally, 20 µl of 25 mM

AMBIC was added to completely cover the gel fragments. The reaction was continued overnight at 37°C to optimize enzyme activity. After incubation, peptide extraction was performed. First, ACN was added and the eppendorfs were incubated for 15 minutes at 37°C. After the reaction, the supernatant was recovered and placed in clean Eppendorf tubes. The extraction solution containing the peptides of interest was dried in a Speed-Vac. The dried peptides were resuspended in 1% formic acid (FA) and analysed by mass spectrometry. The gel bands were then analysed by LC-MS/MS using the Orbitrap Q-Exactive mass spectrometer (Thermo Fisher Scientific), equipped with a nano-ESI source, coupled to an UHPLC nanoUltimate 3000 system (Thermo Fisher). Peptide separation was performed on a capillary RSLC C18 column (75 µm x 15 cm, 1.7 µm) (Thermo Fisher) using a 0.1% formic acid (A) aqueous solution and CH_3CN containing 0.1% formic acid (B) as the mobile phase, with a linear gradient from 5% to 50% in 60 minutes at a flow rate of 300 nl·min^{-1}. Mass spectra were acquired in the m/z range 375-1500. Protein identification was performed using the Proteome Discoverer (PD) software (Thermo Fisher Scientific).

2.2.6.2 Drug Affinity Responsive Target Stability Assay on Bacterial Cells (bc-DARTS)

The bc-DARTS assay involved the incubation of manool with *S. mutans* bacterial cells, followed by proteolysis, SDS-PAGE analysis and LC-MS. The *S. mutans* overnight inoculum was

centrifuged at 3000 rpm for 15 minutes and the cells were resuspended in BHI medium to a density of 0.05 OD/ml. The cells were incubated at 37°C and cultured to the established optical densities (0.5 OD/ml and 1 OD/ml). Then cells were centrifuged at 3000 rpm for 15 minutes. After discarding the supernatant, the pellet was resuspended in M9 minimal medium 1X supplemented with 0.4% glucose for both control and treated samples, at a density of 0,5 OD/ml and 1 OD/mL. The treated samples were incubated with manool at 5 µM and 10 µM for 90 minutes. The samples were then centrifuged at 3000 rpm for 10 minutes. After discarding the supernatant, the pellets were resuspended in 25 mM MOPS buffer. The cells were then lysed by sonication at an amplitude of 10 for 30 minutes, with 10 seconds ON and 10 seconds OFF. The lysates were centrifuged at 15,000 rpm for 20 minutes, and the supernatant was transferred into sterile Eppendorf tubes. The protein content of the supernatant was quantified using the Bradford method. For the DARTS assay, 50 µg of proteins were aliquoted for control and treated samples. The lysates were then digested with subtilisin (enzyme:protein ratio of 1:3500) at 37°C for 30 minutes. The resulting protein mixtures were separated by SDS-PAGE. The gel bands were digested following the previously described protocol and subsequently analysed by LC-MS under the same conditions.

2.2.7 Ethidium bromide accumulation assay

An ethidium bromide (EtBr) accumulation assay for *S. mutans* was adapted following the procedure of Rodrigues et al (Rodrigues et al., 2011). One colony of *S. mutans* was inoculated in 10 mL of BHI medium and grown overnight with shaking at 37 °C. Cells were washed twice in PBS buffer to remove the rich BHI medium and resuspended in PB S buffer at 0.6 OD_{600}/mL. Cells were incubated in PBS. Manool was tested at different concentrations (2.5 to 10 µM) with EtBr at a final concentration of 2 µg/mL. Negative controls were performed using DMSO each. Samples were prepared in separate wells of a 96-well plate. Ethidium bromide was added to each well to a final concentration of 2 µg/mL, allowing an accumulation into cells without causing significant inhibition of growth. The 96-well plate was placed in a Tecan Infinite 200 Pro spectrofluorometer, and fluorescence data were recorded every 60 s for 60 min at 37 °C using an excitation wavelength of 525 nm and an emission wavelength of 605 nm. Fluorescence intensity was monitored over time, measuring EtBr accumulation.

2.2.8 Determination of Activity in Combination with other antibiotics

The combination of antibiotics with plant specialized metabolites that possess antimicrobial activity can be beneficial for the cooperative action of the two compounds. The

combination of manool with the antibiotic kanamycin against *S. mutans* was evaluated. First, using the serial dilution method, the minimum inhibitory concentration (MIC) was determined to extrapolate the MIC100 of kanamycin, which completely inhibits the growth of the tested strain. Antibiotic concentrations ranging from 227 µM to 14.2 µM were tested. Subsequently, any synergy between manool and kanamycin was evaluated by using sub-MIC concentrations of kanamycin, in the presence of a single concentration of manool (10 µM), corresponding to its MIC_{50}. The assay was performed in 96-well plates: serial dilutions were performed to obtain the desired concentrations of the antibiotic (kanamycin: 227 µM, 113.5 µM, 56.75 µM, 28.37 µM; 14.2 µM) with a volume of 100 µL per well, in duplicate. Then, 100 µL of bacteria at a density of 1 x 10^6 CFU/ml were inoculated into each well. Finally, manool was added at a final concentration of 10 µM. The plate was incubated at 37°C. After 24 hours, the values of bacterial growth inhibition were evaluated using a spectrophotometer at a wavelength of 600 nm. The action between two molecules with antimicrobial activity is synergistic if the effect developed by the combination of the two exceeds the sum of their individual effects.

The results were interpreted by calculating the fractional inhibitory concentration (FIC) index for kanamycin and quantifying the nature of the pharmacological interaction in vitro (synergy, additivity, indifference, or antagonism). The FIC index

indicates the microbiological activity determined by an antibiotic combination (Botelho 2000).

$$FIC_{Kanamycin} = \frac{MIC_{Kanamycin\ in\ presence\ of\ manool}}{MIC_{Kanamycin}}$$

The FICI (Fractional Inhibitory Concentration Index) or ∑FIC is calculated as:

$$FICI = \mathrm{FIC}_{\mathrm{kanamycin}} + FIC_{manool}$$

The interpretation of the FICI is as follows:

FICI ≤ 0.5: Synergy (the combined effect is stronger than the sum of the individual effects of the agents); 0.5 < FICI ≤ 1: Additivity (the combined effect is equal to the sum of the individual effects of the agents); 1 < FICI ≤ 4: Indifference (the combined effect is equal to the effect of one of the individual agents); FICI > 4: Antagonism (the combined effect is weaker than the sum of the individual effects of the agents or weaker than the effect of both individual agents).

2.2.9 LC-MS analysis for kanamycin quantification

To preserve the analytical capacity of the column, the sample was also diluted 1:1000 for this analysis. The samples analysed

were as follows: the supernatant of the medium with kanamycin at 28.37 µM; the supernatant of the medium with kanamycin at 56.75 µM; the supernatant of the medium with kanamycin at 28.37 µM and manool at 2.5, 5 and 10 µM; the supernatant of the medium with kanamycin at 56.75 µM and manool at 2.5, 5 and 10 µM. The quantitative determination was performed using an ABSCIEX API 6500 QTRAP® mass spectrometer coupled to a Nexera X2 UPLC Shimadzu system, operating in positive ion mode. A Luna® Omega 100 × 1.6 mm, 3 µm (100 Å) column (Phenomenex®, Castel Maggiore, Bologna, Italy) with H_2O containing 0.1% v/v formic acid as solvent A and CH_3CN containing 0.1% v/v formic acid as solvent B (Lane 2015). The method started with a linear gradient of 2% of B for 5 minutes, followed by a fast gradient of 5% of B for 5 minutes and a final wash at 100% B. The flow rate was 0.30 mL/min, and the column oven was 40°C.

2.2.10 LC-MS analysis for amino acids quantification

To quantify the amino acids in the *S. mutans* supernatants, the medium was diluted 1:1000 in H_2O and the samples were analysed by HR-ESI-LC-MS/MS, the dilution was done to avoid overwhelming the analytical capacity of the chromatography column (Lane 2015). The samples analysed were as follows: the supernatant of the medium without manool treatment; the supernatant of the medium with manool treatment at 2.5 µM; the supernatant of the medium with manool treatment at 5 µM; the supernatant of the medium with manool treatment at 10 µM.

The quantitative determination was performed using an ABSCIEX API 6500 QTRAP® mass spectrometer coupled to a Nexera X2 UPLC Shimadzu system, operating in positive ion mode. A Luna® Omega 100 × 1.6 mm, 3 µm (100 Å) column (Phenomenex®, Castel Maggiore, Bologna, Italy) with H_2O containing 0.1% v/v formic acid as solvent A and CH_3CN containing 0.1% v/v formic acid as solvent B (Lane 2015). The method started with a linear gradient of 2% of B for 5 minutes, followed by a fast gradient of 20% of B for 5 minutes and a final wash at 100% B. The flow rate was 0.30 mL/min, and the column oven was 40°C. Compounds L-Arginine, L-Valina, L-Tryptophan, L-Phenylalanine, L-Glutamic acid, L-Glutamine, L-Metionine and L-Proline were used as standard. The calibration curve for each amino acid was acquired at a concentration range from 10 ng/mL to 10 µg/mL.

2.2.11 NMR sample preparation

NMR sample preparation was performed as previously reported by Palama et al., 2016 with slight modifications. Supernatants for NMR analysis were collected as described into paragraph *2.2.5* and centrifuge at 10000 g for 5 minutes at 4°C to remove the particulate matter. 540 µL of obtained clear supernatants were added to 60 µL of a mono-potassium phosphate solution (90 mM KH_2PO_4 in D_2O, pH 6.5) and transferred to 5 mm NMR tubes. Trimethylsilyl propionic-2,2,3,3-d_4 acid, sodium salt (TSP-d4 0.01% in D_2O) was used as an internal reference for alignment of NMR spectra.

2.2.11.1 NMR spectroscopy and processing

The NMR experiments were performed as previously reported by Iobbi et al. (2023), with slight modifications to optimise the acquisition parameters. Spectra were acquired on a Bruker Avance 600 spectrometer equipped with a 5 mm ATMA cryo-probe operating at 298 K and a SampleJet changer. TopSpin V3.2 software (Bruker Biospin,Wissembourg, France) was used for NMR data acquisition and processing, and its IconNMR module controlled the automation of acquisition (locking, tuning, matching, and shimming). ^{1}H NMR spectra were recorded using a 1D-NOESY (noesygppr1d) pulse sequence with water signal suppression (Grimaldi et al., 2020). The acquisition parameters were: 19K data points, 2782.7 Hz (11 ppm) spectral width, 4 dummy and 128 scans, a recycle delay of 5 s, and a fixed value for receiver gain for all samples. To achieve a high confidence level of metabolites annotations, 2D NMR experiments (HSQC, HMBC, COSY) and 1D TOCSY were also recordered. Phase corrections and baseline editing were performed manually for all spectra using TOPSPIN version 3.2.

2.2.11.2 NMR data analysis

^{1}H NMR spectra were processed using NMRProcFlow 1.4.28 (INRA UMR 1332 BFP, Bordeaux Metabolomics Facility, Villenave d'Ornon, France (Jacob, D., et al., 2017). The ppm calibration was made using the internal standard at 0 ppm and

the peaks alignment was applied on all ^{1}H NMR spectra. Variable size bucketing was used to integrate the signals of key metabolites. The data matrix was exported, and the areas obtained were used to determine the level of selected metabolites in bacteria supernatants. The metabolites annotation was achieved using Chenomx NMR-Suite v12 (Chenomx Inc.), online databases (HMDB, SpectraBase) and in-house library. 2D NMR spectra were analysed using TOPSPIN version 3.2.

2.2.12 Homology Modelling

All the primary sequences were obtained from the SWISS-PROT protein sequence database. Sequence similarity searches were carried out using Blast. The crystal structure of the multiple sugar-binding protein (6PUW) was taken from the Protein Data Bank. The sequence alignment of the chosen protein was performed by Modeller 10.5[2] with a gap creation penalty of 900 and a gap extension penalty of 50. Five structures were generated by means of the Automodel protocol, as implemented in Modeller, and the best receptor model was chosen on the basis of the Discrete Optimized Protein Energy (DOPE) assessment method and minimized. The backbone conformation of the resulting receptor structures was evaluated by inspection of the Ramachandran plot. The protein was minimized using Amber22 software (Case et al., 2023) and ff14SB force field at 300 K. The protein was placed in a rectangular parallelepiped water box; the TIP3P explicit solvent

model for water was used and the complex was solvated with a 15 Å water cap. Chlorine ions were added as counterions to neutralize the system. Two steps of minimization were then carried out. In the first stage, we kept the protein fixed with a position restraint of 500 kcal/mol·Å^2 and we solely minimized the positions of the water molecules. In the second stage, we minimized the entire system through 5000 steps of steepest descent followed by conjugate gradient (CG) until a convergence of 0.05 kcal/Å mol.

2.2.12.1 MD Simulations

The minimized protein was used as input structures for the MD simulations, which were run using Particle Mesh Ewald (PME) electrostatics, a cutoff of 10 Å for the non-bonded interactions and all the parameters reported above. SHAKE algorithm was used to constrain all bonds involving hydrogen atoms and a time step of 2.0 fs was thus used for the simulation. Initially, a MD heating stage of 50 ns, in which the temperature of the system was raised from 0 to 300 K, was performed using constant-volume periodic boundary conditions. In all these steps all α carbons of the protein were subjected to a harmonic potential of 10 kcal/mol•Å^2. Finally, a production step of 350 ns was performed maintaining the same temperature and pressure conditions but removing any harmonic restraint, thus leaving the system totally free. In total, the protein was thus subjected to 400 ns of MD simulation.

2.2.12.2 Docking studies.

The compound cpd01 was docked into the final 200 conformations of the multiple sugar-binding transport ATP-binding protein using Autodock-GPU (Santos-Martins et al., 2021) with the ADP molecule from 3PUW defining the centre of the binding site. For each docking calculation, the following parameters were used: 100 LGA runs with 10000000 score evaluations, 10000000 generations and 500 as population size per run. An RMSD clustering tolerance of 2.0 Å was used. The 400 docking solutions were clustered by using an in-house python script and by considering only clusters with a population of at least 40 docking results. The resulting clusters were then subjected to MD simulations. For each protein-ligand complex, all parameters reported above were used. General Amber force field (GAFF) parameters were used for the ligand, whose partial charges were assigned using the Antechamber suite of Amber22, based on the AM1-BCC method. As reported above, two steps of minimization were then carried out. In the first stage, we kept the protein fixed with a position restraint of 500 kcal/mol·Å^2 and we solely minimized the positions of the water molecules. In the second stage, we minimized the entire system through 5000 steps of steepest descent followed by conjugate gradient (CG) until a convergence of 0.05 kcal/mol•Å. For the MD simulations, a MD heating stage of 50 ns, in which the temperature of the system was raised from 0 to 300 K, was performed using constant-volume periodic boundary conditions with all α carbons of the protein subjected

to a harmonic potential of 10 kcal/mol•Å^2. Then, a production step of 350 ns was performed maintaining the same temperature and pressure conditions. In total, each complex analyzed was thus subjected to 400 ns of MD simulation. The final structure of the protein-ligand complex corresponded to the average of the last 350 ns of MD simulation minimized by the CG method until a convergence of 0.05 kcal/mol•Å^2. The average structures were obtained using the Cpptraj program implemented in Amber22, which was also used for RMSD and H-bond analyses.

2.2.12.3 Binding Energy Evaluation

The evaluation of the binding energy associated with the four protein-ligand complexes analysed through MD simulations was carried out using AMBER22. The trajectories relative to the last 350 ns of each simulation were extracted and used for the calculation for a total of 350 snapshots (at time intervals of 1 ns). Van der Waals, electrostatic and internal interactions were calculated with the SANDER module of AMBER22, whereas polar energies were calculated using the Poisson-Boltzman methods with the MM-PBSA module of AMBER22. Dielectric constants of 1 and 80 were used to represent the gas and water phases, respectively. The entropic term was considered as approximately constant in the comparison of the ligand-protein energetic interactions.

2.2.13 Proteomic analysis

Proteomics analysis involved the incubation of manool with *S. mutans* bacterial cells during different growth phases, followed SDS-PAGE analysis and LC-MS. The *S. mutans* overnight inoculum was centrifuged at 3000 rpm for 15 minutes and the cells were resuspended in BHI medium to a density of 0.05 OD/mL. The cells were incubated at 37°C and cultured to the established optical densities (0.250, 0.5 and 1 OD/mL). Once reaching the established OD value, manool was added at sub-MIC concentrations (5 and 10 µM) and bacteria were incubated with the diterpene for 30 minutes. Following the treatment, cells were collected and centrifuged at 3000 rpm for 15 minutes; the pellets were then resuspended in 25 mM MOPS buffer to a density of 50 OD/mL. Next, 50 OD of cells were lysed by sonication at an amplitude of 10 for 30 minutes, with 10 seconds ON and 10 seconds OFF. The lysates were centrifuged at 15,000 rpm for 20 minutes and the supernatant was transferred into sterile Eppendorf tubes. The protein content of the supernatant was quantified using the Bradford method. The resulting protein mixtures were separated by one-dimensional polyacrylamide gel electrophoresis (SDS-PAGE). After electrophoresis, the proteins were fixed in gel using the fixing solution (50% H_2O, 40% MeOH, 10% CH_3COOH) and 10 bands were excised from each lane and subjected to trypsin digestion. The dried peptides were resuspended in 1% formic acid (FA) and analysed by LC-MS/MS using the Orbitrap Q-Exactive mass spectrometer (Thermo Fisher Scientific),

equipped with a nano-ESI source, coupled to an UHPLC nanoUltimate 3000 system (Thermo Fisher). Peptide separation was performed on a capillary RSLC C18 column (75 µm x 15 cm, 1.7 µm) (Thermo Fisher) using a 0.1% formic acid (A) aqueous solution and CH_3CN containing 0.1% formic acid (B) as the mobile phase, with a linear gradient from 5% to 50% in 60 minutes at a flow rate of 300 nl·min^{-1}. Mass spectra were acquired in the m/z range 375-1500. Protein identification was performed using the Proteome Discoverer (PD) software (Thermo Fisher Scientific).

2.2.14 Quantitative real time PCR of vicK gene

The *S. mutans* overnight inoculum was centrifuged at 3000 rpm for 15 minutes and the cells were resuspended in BHI medium to a density of 0.05 OD/mL. The cells were incubated at 37°C and cultured to the established optical densities (0.250 and 0.5 OD/mL). Once reaching the established OD value, manool was added at sub-MIC concentrations (2.5, 5 and 10 µM) and bacteria were incubated with the diterpene for 30 minutes. Following the treatment, cells were collected to obtain a final concentration of 3 OD for each condition. Total RNA was extracted as follow: 5% Phenol/ 95% Ethanol pre-chilled solution (5 part bacteria: 1 part Phenol/Ethanol) was added and then centrifuged at 3000 rpm for 15 minutes. Pellets were resuspended in 1 mL of pre-chilled TRIzol (Thermo Fisher Scientific, Germany), according to the manufacturer's protocol, and incubated for 5 minutes at room temperature. After that,

bacteria were lysed at 6000 × g for 15 seconds for 3 times using Precellys® 24 Touch Homogenizer. Following, 0.2 mL of pre-chilled chloroform was added and incubated for 5 minutes at 4°C. Subsequentially, samples were centrifugated for 15 minutes at 12000 × g at 4°C. Once obtained separated phases, the aqueous phase, containing RNA, was transferred to a new tube. Then, 0.5 mL of pre-chilled isopropanol was added to the aqueous phase and incubated on ice for 10 minutes. Samples were centrifugated for 10 minutes at 12000 × g at 4°C. The pellet was then washed with 75% Ethanol. Finally, RNA was resuspended in diethylpyrocarbonate-treated H_2O. RNA concentration was estimated spectrophotometrically by measuring the absorbance at 260 (1 OD260nm = 40 µg/mL). For complementary DNA (cDNA) synthesis, the RevertAid First-strand cDNA Synthesis kit was used (Thermo Fisher Scientific, Germany) and then the cDNA was quantified spectrophotometrically. 50 ng of cDNA per reaction were used for quantitative RT-PCR using CFX 96 real-time PCR (Bio-Rad Laboratories, Munich, Germany) along with SsoAdvanced Universal IT SYBRGreen Smx (Bio-Rad Laboratories, Munich, Germany). The amplification parameters comprised as initial activation step (95-98°C for 3-10 min), followed by 39-40 cycles of denaturation (95-98°C for 15 s), annealing (56°C for 15-30 s) and extension (65-72°C for 15-30 s). The following primers were used for target genes, and 16s ribosomal RNA was used as the reference gene for data normalization.

- VicK_fw. CGGCGTGATGAATATGATGAA
- VicK_rv: GAGGTTAATGGTGTCCGCAGT
- 16S rRNA_fw: AGCGTTGTCCGGATTTATTG
- 16S rRNA_rv: CTACGCATTTCACCGCTACACA

The relative gene expression was compared using the $2^{-\Delta\Delta Ct}$ method as described elsewhere (Schmittgen & Livak, 2008). A value of significance was established when $p < 0.05$ and variances are displayed as standard errors. All statistical analyses were performed using GraphPad Prism 9.

2.2.15 Human Gingival Fibroblasts (HGF-1) cell line

Experiments were conducted on Human Gingival Fibroblasts (HGF-1) (ATCC). HGF-1 were grown in DMEM 1X and F-12 DMEM 1X in a ratio of 3:1 (3 parts for DMEM 1X and 1 part of F-12 DMEM), supplemented with 10 % of Fetal Bovine Serum (FBS) and maintained in a humidified atmosphere of 5% CO2 at 37°C with a medium change every two days.

2.2.15.1 Analysis of metabolic activity of HGF-1 by Alamar blue assay

The CellTiter-Blue® Cell Viability Assay provides a homogeneous, fluorometric method for estimating the number of viable cells present in multiwell plates (Rich Moravec & Riss 2003). It uses the indicator dye resazurin to measure the metabolic capacity of cells, an indicator of cell viability. Viable cells retain the ability to reduce resazurin into resorufin, which

is highly fluorescent. Nonviable cells rapidly lose metabolic capacity, do not reduce the indicator dye, thus do not generate a fluorescent signal. HGF-1 cell line was plated in a black 96-well plate at the density of 5×10^3 cells/well. After 24 hours, cells were treated with several concentrations of manool (2.5 μM to 160 μM) and incubated at 37°C for 3 hours. After incubation, 10% of Alamar Blue reagent (v/v) was added to each well. The plate was then insert in Tecan for 24 hours, measuring absorbance in 60 min cycle at λ=595 nm and fluorescence with λ=560 nm excitation and λ=590 nm emission wavelengths. Results showed in paragraph 2.4 Appendix.

2.2.16 Adhesion and invasion assay

For adhesion and invasion experiments, HGF-1 were plated in 24-well plates at the confluence of 8×10^5 cells/well. Once cells were confluent, manool was added at the concentrations of 2.5,5 and 10 μM. Subsequentially, cells were infected with *S. mutans* using a Multiplicity of Infection (MOI) of 30.

2.2.16.1 Invasion Experiments

For the invasion experiment, cells were incubated for 3 hours. After incubation, cells were washed with HBSS 1X for 3 times. In order to kill all extracellular bacteria, cells were treated with Gentamycin (200 μg/mL) for 90 minutes. Subsequentially, cells were washed with HBSS 1X for 2 times. Then cells were lysate with a Lysis Buffer (Trypsin solution from porcine pancreas (w/o EDTA) 1X (0,5 g/L), Triton X 0.1% w/v, DTT in DPBS 0.1% w/v,

DNAse 0.1 mg/mL. The DNAse was added to the Lysis Buffer fresh before use every time). Once added lysis buffer for each well, cells were lysate for 30 minutes in shacking at room temperature. Subsequentially cells were scraped and 100 µL of intracellular bacteria and diluted 1:10, were plated on BHI agar plates and incubated at 37°C for 48 hours. Finally, colonies were counted. The experiments were performed in biological triplicate.

2.2.16.2 Adhesion Experiments

For the adhesion experiment, after infection, cells were centrifuged at 3000g for 5 minutes to promote the adhesion of bacteria to host cells. Then cells were incubated for 15 minutes at 37°C. After incubation cells were washed with HBSS 1X for 5 times. Subsequentially cells were lysate following the same protocol applied for the invasion experiment (see 2.2.16.1). Finally, adherent cells were plated on BHI agar plates and incubated at 37°C for 48 hours. The experiments were performed in biological triplicate.

2.2.17 Evolution experiment

To investigate long-term adaptive responses, bacterial populations were continuously exposed to manool for a period of eight weeks. Cultures were maintained with regular passaging to ensure viability and to allow for the accumulation of adaptive mutations. At the end of the experimental period, samples from the evolved strain were collected for proteomic

and genomic analysis. Starting from week 0, after an overnight pre-inoculum, the optical density (OD) of *S. mutans* was adjusted to a final density of 0.05 OD/mL, after which it was incubated with manool for 24 hours. After this time, the *S. mutans* cultures (control and treatment) were transferred to a fresh medium with and without manool every day. Then, the manool concentration was increased every week. More specifically, manool was added at the following concentrations: 2.5 μM in the first week; 3.4 μM in the second week; 5 μM in the third week; 6.8 μM in the fourth week; 10 μM in the fifth week; 13.5 μM in the sixth week; 20 μM in the seventh week; and 30 μM in the eighth week. Before increasing the manool concentration each week, the bacteria were plated to verify bacterial proliferation and five colonies were chosen and cryopreserved for further experiments. Finally, the MIC of evolved strain was determinate and grow studies of evolved strain were performed following the previous procedures (see 2.2.4 and 2.2.5). The experiments were performed in biological triplicate.

2.2.17.1 Proteomic studies of S. mutans evolved strain

Proteomics analyses of *S. mutans* evolved strain compared to *S. mutans* wild-type were performed, followed SDS-PAGE analysis and LC-MS. Proteomic analysis were performed in *S. mutans* after eight weeks of manool treatment. After overnight inoculum, *S. mutans* evolved strain and *S. mutans* wild type were centrifuged at 3000 rpm for 15 minutes and the pellets

were then resuspended in 25 mM MOPS buffer to a density of 50 OD/mL. Next, 50 OD of cells were lysed by sonication at an amplitude of 10 for 30 minutes, with 10 seconds ON and 10 seconds OFF. The lysates were centrifuged at 15,000 rpm for 20 minutes and the supernatant was transferred into sterile Eppendorf tubes. The protein content of the supernatant was quantified using the Bradford method. The resulting protein mixtures were separated by one-dimensional polyacrylamide gel electrophoresis (SDS-PAGE). After electrophoresis, the proteins were fixed in gel using the fixing solution (50% H_2O, 40% MeOH, 10% CH_3COOH) and 10 bands were excised from each lane and subjected to trypsin digestion. The dried peptides were resuspended in 1% formic acid (FA) and analysed by LC-MS/MS using the Orbitrap Q-Exactive mass spectrometer (Thermo Fisher Scientific), equipped with a nano-ESI source, coupled to an UHPLC nanoUltimate 3000 system (Thermo Fisher). Peptide separation was performed on a capillary RSLC C18 column (75 µm x 15 cm, 1.7 µm) (Thermo Fisher) using a 0.1% formic acid (A) aqueous solution and CH_3CN containing 0.1% formic acid (B) as the mobile phase, with a linear gradient from 5% to 50% in 60 minutes at a flow rate of 300 nl·min^{-1}. Mass spectra were acquired in the m/z range 375-1500. Protein identification was performed using the Proteome Discoverer (PD) software (Thermo Fisher Scientific).

2.3.17.2 Genome sequencing of S. mutans evolved strain

DNA was purified using the MagAttract HMW DNA Kit (Qiagen, Hilden, Germany). Genomic DNA was extracted from both wild type and evolved strains using a standard phenol-chloroform protocol followed by ethanol precipitation from 0.75 mL of overnight BHI cultures inoculated from the freezer stocks. DNA quality and integrity were assessed by agarose gel electrophoresis, while concentration and purity were determined spectrophotometrically (NanoDrop, Thermo Fisher Scientific). Only high-quality DNA samples (A260/A280 ratio between 1.8 and 2.0) were used for sequencing. To prepare 500 bp paired end libraries of all isolates, the Nextera XT DNA Library Preparation kit (Illumina, Eindhoven, The Netherlands) was used. Libraries were sequenced on the Illumina NextSeq 500 sequencing platform using v2 (300 cycles) sequencing chemistry. Briefly, genomic DNA was fragmented, end-repaired and ligated to indexed adapters. Libraries were quantified by Qubit fluorometry and quality-checked using a Bioanalyzer (Agilent Technologies). Paired-end sequencing was performed on an Illumina platform (e.g., NextSeq or NovaSeq), generating reads with a length of 150 bp. Raw sequencing data were processed using FastQC for quality control and Trimmomatic for adapter removal and quality trimming. High-quality reads were aligned to the *S. mutans* reference genome using BWA-MEM. Variant calling was performed with GATK, and structural variations were identified using Delly. Genome assemblies were further analysed with Prokka for annotation.

Comparative genomic analysis between the wild type and evolved strains was carried out to identify mutations, deletions and gene rearrangements. Candidate mutations and deletions identified in the evolved strain were validated by PCR amplification followed by Sanger sequencing.

2.3 Results and discussion

2.3.1 MIC and growth curves

To identify the molecular target of a manool, experimental conditions had to be optimized in order to allow interaction between the compound and its target while minimizing effects on the overall physiology of the treated cells. As a first step in this process, the Minimal Inhibitory Concentration (MIC) of manool against *S. mutans* was determined using the serial dilution method, following the CLSI protocol (2009). Bacterial cultures were incubated with several concentrations of manool (ranging from 2.5 µM to 40 µM) or vehicle as a control at 37°C for 24 hours (Figure 9). Bacterial growth was assessed spectrophotometrically at 600 nm by measuring the optical density (OD) of the medium.

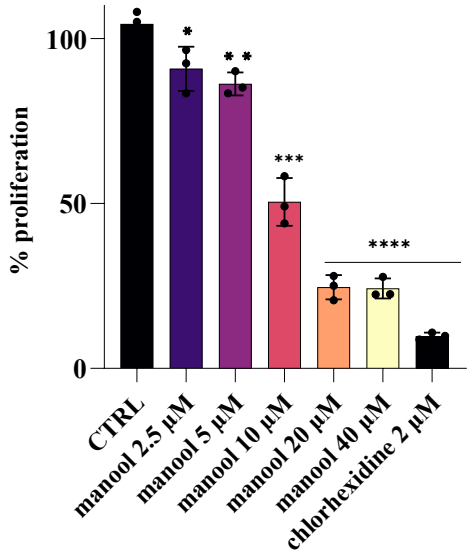

Figure 9. *Determination of the minimal inhibitory concentration (MIC) of manool against S. mutans. Bacterial cultures were incubated for 24 hours at 37°C in the presence of increasing concentrations of manool (2.5–40 µM) or vehicle control. Bacterial growth was evaluated by measuring the optical density of the medium at 600 nm (OD_{600}). (****p-value< 0.0001; ***p-value< 0.001; **p-value< 0.005).*

The results showed that at 10 µM manool, approximately 40% of the bacteria survived, whereas at 20 µM, complete bacterial growth inhibition was observed (MIC_{100}). To further investigate manool's impact on *S. mutans* proliferation, bacterial growth was monitored over 660 minutes starting from an initial OD of 0.05, in the absence or presence of manool at concentrations of 2.5 µM, 5 µM, and 10 µM. In the control condition, a typical sigmoidal growth curve was observed (Figure 10-A), with a lag phase of approximately 200 minutes, followed by a 200-minutes exponential phase reaching a maximum OD of ~1.6,

and then a stationary phase. No decline in cell viability was noted under these conditions. In contrast, manool-treated cultures exhibited a prolonged lag phase: ~300 minutes at 2.5 μM, ~650 minutes at 5 μM, and beyond 660 minutes at 10 μM. Additionally, the slope of the exponential phase decreased proportionally with increasing manool concentration, indicating a dose-dependent inhibitory effect. Since manool appeared to primarily affect the lag phase, its impact when added during the exponential phase was estimated. After overnight cultures, *S. mutans* was inoculated at an OD of 0.1 and allowed to grow until reaching an OD of 0.5, at which point manool was introduced at the same concentrations as before. Under these conditions, growth parameters between treated and untreated cultures were nearly identical (Figure 10-B), suggesting that manool's inhibitory effect is most pronounced when administered prior to the onset of exponential growth.

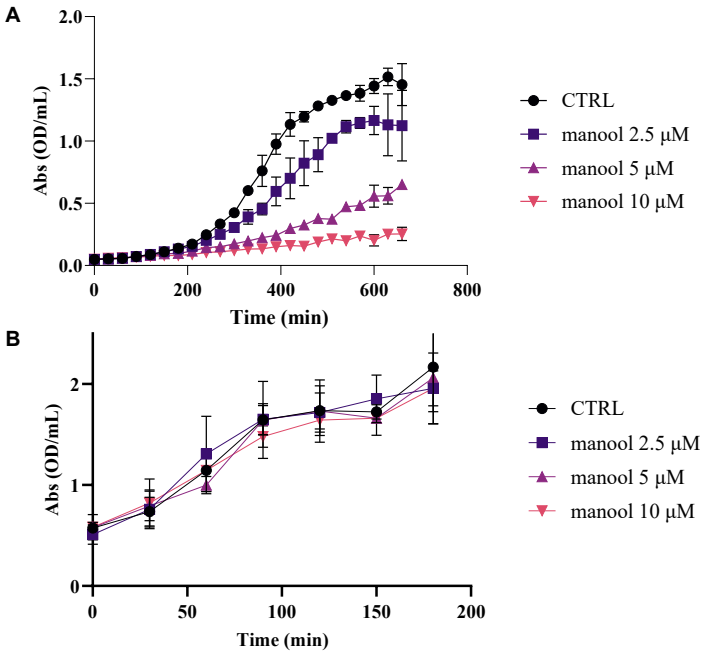

Figure 10. *Growth curve of S. mutans in BHI broth with supplementation of manool (0, 2.5, 5, 10 µM). OD 600 nm measured every 30 mins (A) Effect of manool on S. mutans growth when added during the exponential phase of growth. At 0.5 OD manool was added at concentrations of 2.5, 5, and 10 µM.(B) Bacterial proliferation was monitored by measuring the* OD_{600} *every 30 minutes for 660 minutes. All data calculated from the average of three independent experiments with error bars representing Standard Deviation (SD).*

Based on the results of the growth curves, the activity of manool was tested against different clinical strains of other Gram-positive bacteria and Table 1 shows the bacteria sensitive to manool treatment. As Figure 11 and Figure A9 in appendix 2.5 show, manool is able to interfere in the early phases of the growth of *Bacillus safensis* and *Streptococcus epidermidis*. Regardless of the different dose required to exert a sensible effect, the consequences of incubation with manool for the two

bacteria were similar to those observed for *S. mutans*. This result supports the hypothesis that manool mainly exerts its antimicrobial activity during the lag phase, regardless of the bacteria treated and the amount of terpenoid used. These results could evidence that manool can reduce proliferation by forcing bacteria to adapt to the pressure of the diterpene during the lag phase.

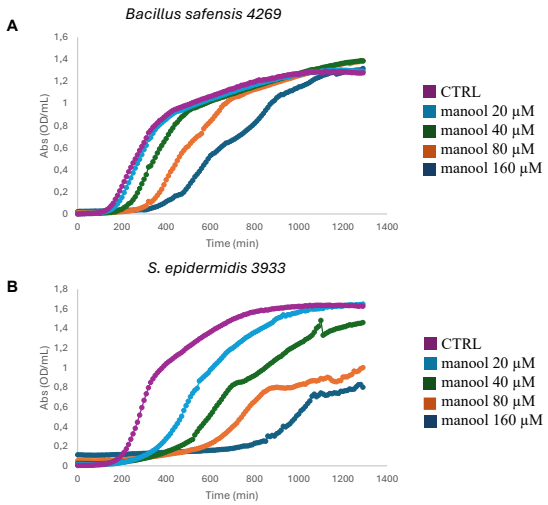

Figure 11. *Growth curve of Bacillus safensis and Streptococcus epidermidis in BHI broth with supplementation of manool (10, 20, 40 and 60 µM). OD 600 nm measured every 10 mins.*

Table 1. *Bacteria strains sensitive to manool.*

STRAINS	ACTIVITY	STRAINS	ACTIVITY
E. faecalis strain 1	+	*S. epidermidis strain 1*	-
E. faecalis strain 2	+	*S. epidermidis strain 2*	+
E. faecalis strain 3	+	*S. condimenti strain 1*	+
E. faecalis strain 4	+	*S. condimenti strain 2*	+
E. faecalis strain 5	+	*B. cereus*	+
E. faecalis strain 6	+	*B. subtilis*	+
S. aureus strain 1	-	*B. safensis*	-
S. aureus strain 2	-	*S. warnieri*	-
S. aureus strain 3	-	*S. lugdunensis*	-
S. aureus strain 4	-	*E. avium*	+
S. aureus strain 5	+	*E. faecium strain 1*	+
B. pumilus strain 1	+	*E. faecium strain 2*	+
B. pumilus strain 2	+		

2.3.2 Metabolomics studies of S. mutans exposed to manool by NMR

Glycolysis represents one of the principal catabolic pathways in *S. mutans*, playing a central role in energy production and metabolic regulation. To explore how this pathway is affected by the presence of manool, an NMR-based metabolomic study was conducted to monitor changes in glucose fermentation process. *S. mutans* cultures were exposed to increasing

concentrations of manool (2.5 µM, 5 µM, and 10 µM) and samples were collected at regular time intervals over an 11-hour incubation period, with measurements taken every 30 minutes. The analysis focused on evalueting glucose consumption and the accumulation of key fermentative metabolites using ^1H NMR spectroscopy. For spectral integration, distinct and well-resolved signals were selected: the doublet at 5.24 ppm (J = 3.7 Hz) corresponding to glucose; the multiplet at 4.12 ppm for lactic acid; the doublet at 1.38 ppm (J = 6.8 Hz) for acetoin; and the doublet at 1.13 ppm (J = 5.8 Hz) for 2,3-butanediol. These metabolites were chosen as representative markers of the glycolytic and fermentative activity of *S. mutans*. The results revealed a dose-dependent reduction in glucose uptake in cultures treated with manool compared to the untreated control group (Figure 12-A). In contrast, the control group exhibited a progressive increase in the production of lactic acid, acetoin and 2,3-butanediol over time, consistent with active fermentation and metabolic turnover (Figure 12-B, C, D). Overall, manool exerts a measurable impact on the metabolic activity of *S. mutans*, reducing glucose fermentation in a concentration-dependent manner. The use of NMR spectroscopy provided a powerful and non-invasive tool to monitor these changes in real time, offering valuable insights into the metabolic consequences of antimicrobial treatment and highlighting the potential of manool as a candidate for therapeutic development targeting bacterial energy metabolism. From a causal point of view, these results

cannot be interpreted unambiguously. On the one hand, the variations observed in glucose consumption are related to the decrease in bacterial proliferation, as they depend on differences in the number of bacterial cells under different conditions. On the other hand, the possibility cannot be ruled out that the reduction in glycolysis may be caused by a decrease in the availability of glucose for the bacteria, which is somehow dependent on treatment with manool.

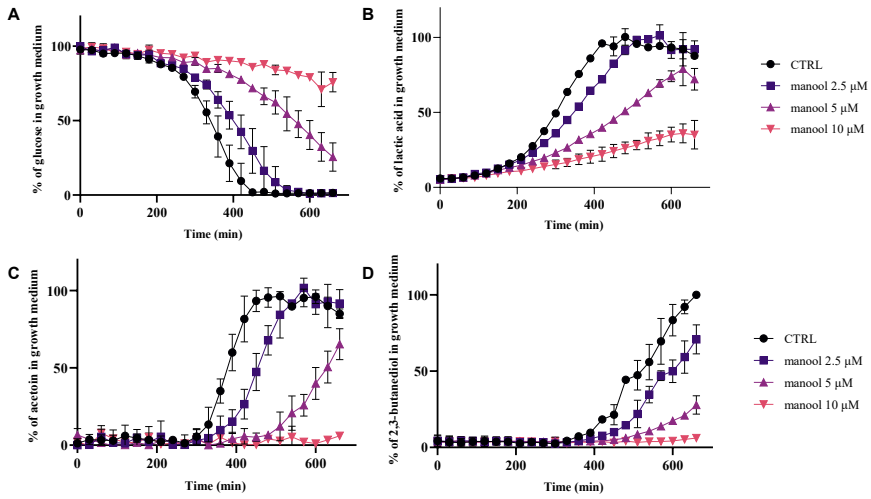

Figure 12. *Impact of manool on glucose metabolism and production of fermentative end-products in S. mutans. Glucose (A) levels in the growth medium for the control and the treatments with manool at 2.5, 5 and 10 µM. Results are expressed as a percentage, with 100 indicating the area of the glucose signal in the control group at 0 minutes. Lactic acid (B), acetoin (C) and 2,3-butanediol (D) in the growth medium in the control group and the treatments with manool at 10, 5 and 2.5 µM. Data, after blank (BHI medium) subtraction are expressed as a percentage, indicating 100 as the area of the metabolite signals in the control group in the exponential phase. Data calculated from the average of two independent experiments with error bars representing SD.*

In order to go further on these data, the NMR-based monitoring of the metabolism of *S. mutans* was performed again, but incubating *S. mutans* bacteria with different concentration of manool during their exponential growing phase. The results reported in Figure 13 showed that the curves obtained using this approach were very similar to those reported in Figure 10b. This result, on the one hand confirmed that NMR spectroscopy is a useful technique to monitor the metabolic changes of glucose (Figure 13-A) and lactic acid (Figure 13-B) in real time, on the other hand suggested that the observed changes were mainly induced by the variation of living bacteria, regardless of the nutrients availability.

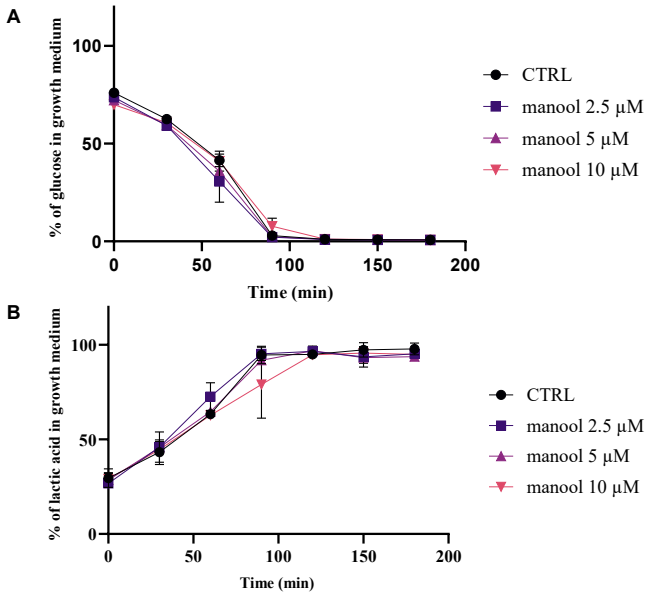

Figure 13. *Impact of manool on glucose metabolism and lactic acid production in S. mutans exponential phase. Glucose (A) and lactic acid (B) levels in the growth medium for the control and the treatments with manool at 2.5, 5 and 10 µM. Results are expressed as a percentage, with 100 indicating the area of the glucose signal in the control group at 0 minutes. Data, after blank (BHI medium) subtraction are expressed as a percentage, indicating 100 as the area of the metabolite signals in the control group in the exponential phase. Data calculated from the average of two independent experiments with error bars representing SD.*

2.3.3 Drug Affinity Responsive Target Stability Assay (DARTS) results

To identify the potential molecular targets of manool responsible for its biological activity in *S. mutans*, two types of DARTS (Drug Affinity Responsive Target Stability) experiments were conducted: one using bacterial protein extracts (pe-DARTS) and the other using live bacterial cells (bc-DARTS). The pe-DARTS approach, which relies on direct chemical

interaction and structural compatibility, was essential for identify the proteins potentially capable to interact with manool. In contrast, the cell-based bc-DARTS assay provided insights into the cellular permeability of manool and its ability to reach intracellular targets. Additionally, this method allowed to correlate potential interaction targets with bacterial growth phases and the corresponding proteomic profiles.

2.3.3.1 DARTS on protein extract (pe-DARTS) and DARTS on bacterial cells (bc-DARTS)

The pe-DARTS experiments were conducted incubating protein lysates of *S. mutans* with manool at the concentration of 20 μM, selected based on the proliferation studies. Results led to the identification of approximately 20 proteins (Table 2), most of which are involved in the transmembrane transport of essential metabolites such as sugars, amino acids and ions. Notably, two major protein families emerged: the ATP-binding cassette (ABC) superfamily and the phosphotransferase system (PTS) family, both crucial for nutrient uptake and bacterial growth. Furthermore, the gamma subunit of the ATP synthase complex was identified, thus supporting the interaction between this complex and manool that was previously hypothesized (Bisio, A., et al., 2020).

Table 2. *Proteins identified by pe-DARTS assay*

Accession	Mass	Description	Sum PEP Score	Coverage [%]	# Peptides	# PSMs	# Unique Peptides	# AAs	Score Sequest HT: Sequest HT
Q8DT62	29,9	Putative ABC transporter, glutamine binding protein	36,95	30	8	46	8	270	61,65
Q8DW32	28,3	Putative ABC transporter, ATP-binding protein	44,797	38	8	48	8	256	92,22
Q8DU84	45	Putative ABC transporter, ATP-binding protein, proline/glycine betaine transport system	40,009	25	11	37	11	404	31,93
Q00751	31,6	Multiple sugar-binding transport system permease protein MsmG	100,082	49	19	232	15	377	359,64
Q00750	31,9	Multiple sugar-binding transport system permease protein MsmF	20,19	9	3	7	3	277	17,7
Q8DW36	27,6	Putative ABC transporter, ATP-binding protein amino acid transport system	31,751	23	6	36	6	246	59,37
Q8DTB0	35,9	ABC transporter substrate-binding protein	72,724	45	14	71	14	333	104,38
Q8DSC5	17,3	ABC transporter permease	16,646	19	3	13	3	156	25,37
Q8DSU1	30,7	Putative branched chain amino acid ABC transporter, permease protein	7,204	4	1	3	1	289	4,8
Q8DTY2	23,8	Putative amino acid ABC transporter, permease protein	36,54	30	7	32	7	267	59,48
I6L8X6	52,6	Putative PTS system, membrane component possible ribulose-monophosphate	5,9	4	1	6	1	485	9,64

Q8DWF7	30,3	PTS pathway enzyme IIC Putative PTS system, IID component	20,731	12	7	23	7	273	24,01
Q8DUI0	45,2	ATP-dependent Clp protease ATP-binding subunit ClpX	14,376	10	4	27	4	410	29,14
P95788	32,3	ATP synthase gamma chain	24,106	25	6	29	6	292	23,77
Q93D93	32,7	Protease HtpX homolog	4,986	4	1	1	1	299	2,69
Q8DTK0	28,9	Putative alpha/beta superfamily hydrolase	8,406	7	3	8	3	249	6,16
Q8DVH1	38	PDZ domain-containing protein	7,358	7	2	6	2	346	7,93

To adapt the DARTS protocol for live bacterial cells, it was necessary to account for the significant biological and structural differences between prokaryotic and eukaryotic systems. A critical challenge was minimizing changes in *S. mutans* proteome during manool incubation, as such changes, whether due to compound uptake or bacterial growth, could confound the interpretation of proteolytic protection. Specifically, it would be difficult to determine whether increased levels of undigested proteins were due to manool binding or upregulated expression. To address this, *S. mutans* cells in the exponential growth phase were centrifuged and resuspended in minimal M9 medium supplemented with 0.4% glucose. This setup allows to maintain cell viability while significantly slowing their metabolism and protein turnover. The schematic representation

of the bc-DARTS protocol, adapted to make DARTS suitable for application in live bacterial, is shown in Figure 14.

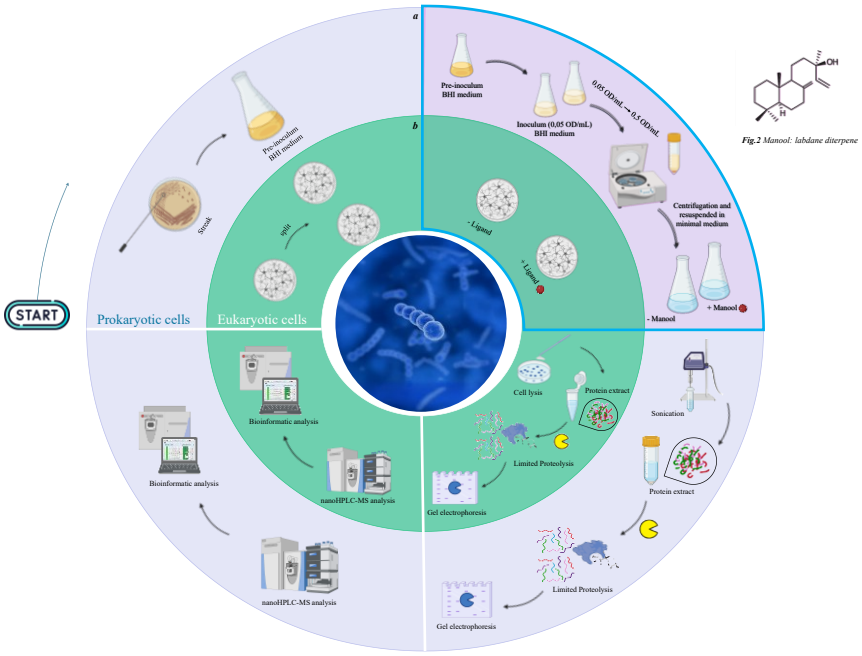

Figure 14. *Schematic overview illustrating the differences between the novel DARTS method applied to live bacterial cells (a) and the standard DARTS protocol used in eukaryotic systems (b)*

This diagram illustrates the key experimental steps and specific modifications implemented to ensure compatibility with bacterial cell physiology, as well as the results of these modifications. Moreover, the classical protocol used in eukaryotic cells is also shown. Briefly, manool was added at sub-MIC concentrations (5 and 10 µM) and incubated for 90 minutes at 37°C while shaking. Following incubation, cells were lysed, and protein identification was performed via mass

spectrometry under the same conditions used for pe-DARTS. Strikingly, all proteins identified in the bc-DARTS assay (Table 3) belonged to the same families observed in pe-DARTS: ABC transporters, PTS proteins and components of the ATP synthase complex. A comparative analysis of both datasets revealed a strong overlap, reinforcing the consistency of the findings, suggesting that the identified proteins are actual manool targets.

Table 3. *Proteins identified by DARTS assay on bacterial cells.*

Accession	Mass	Description	Sum PEP Score	Coverage [%]	# Peptides	# PSMs	# Unique Peptides	# AAs	Score Sequest HT: Sequest HT
Q8DT25	42,3	Putative ABC transporter, ATP-binding protein, MsmK-like protein	17,17	17	5	24	2	377	12,41
Q8CM14	25,9	Putative ABC transporter ATP-binding protein	14,82	15	3	13	3	233	8,33
Q8DUD7	37,7	Putative ABC transporter, periplasmic ferrichrome-binding protein	44,706	44	13	53	13	340	19,86
Q8DT62	29,9	Putative ABC transporter, glutamine binding protein	24,059	30	7	28	7	270	3,51
Q8DUT1	29	Putative amino acid transporter, amino acid-binding protein	23,762	26	7	19	7	271	7,72
Q8DW22	39,1	Putative oligopeptide ABC transporter, ATP-binding protein OppD	7,913	7	2	6	2	350	1,62
Q8DRU8	43,4	Putative osmoprotectant amino acid ABC transporter, ATP-binding protein	21,786	17	7	16	7	383	1,82

Q8DW31	46,1	Putative ABC transporter, membrane protein	24,845	14	6	51	6	420	8,38
Q8DUS9	29,3	Putative amino acid transporter, amino acid-binding protein	9,407	9	2	5	2	271	4,31
Q8DSC4	35,5	PTS system mannose-specific EIIAB component	18,324	13	4	34	4	330	1,89
Q8DSC3	28,1	Putative PTS system, mannose-specific component IIC	5,33	10	2	3	2	272	3,2
Q8DWF7	30,3	Putative PTS system, IID component	13,951	16	5	12	5	273	3,95
P95786	20,4	ATP synthase subunit delta	16,871	24	5	9	5	178	5,57

However, these results also have a second implication of great interest. Given the reliability of non-targeted proteomic approaches when applied to both cell lysates and intact cells, one objective of this project was to establish experimental conditions that would allow DARTS to be applied directly to living bacterial cells. This would represent a significant advance over previous studies, which typically employed DARTS only on bacterial lysates (Chen et al., 2024). The results obtained confirmed the effectiveness of the bc-DARTS protocol developed, demonstrating that the use of a minimal medium allows for accurate and biologically relevant analysis of protein-ligand interactions, as it preserves the physiological integrity of the bacteria while reducing their metabolic activity. This upgraded approach offers a versatile assay that can be extended to various classes of pathogenic bacteria, potentially revolutionizing the identification of therapeutic targets of old

and new antibacterial drugs. It opens new avenues for antimicrobial drug discovery by enabling the direct observation of molecular interactions in their native cellular context, which is crucial for understanding the dynamics of drug action and resistance mechanisms. A merge between the data obtained by pe- and bc-DARTS strongly suggested that manool is able to interact with multiple membrane-associated transport proteins responsible for the translocation of solutes, ions and xenobiotics. In particular, several members of the ATP-binding cassette (ABC) transporter family were detected, highlighting them as putative key targets of manool. These transporters are integral membrane proteins that utilize the energy from ATP hydrolysis to actively transport a wide range of substrates across cellular membranes (Figure 15).

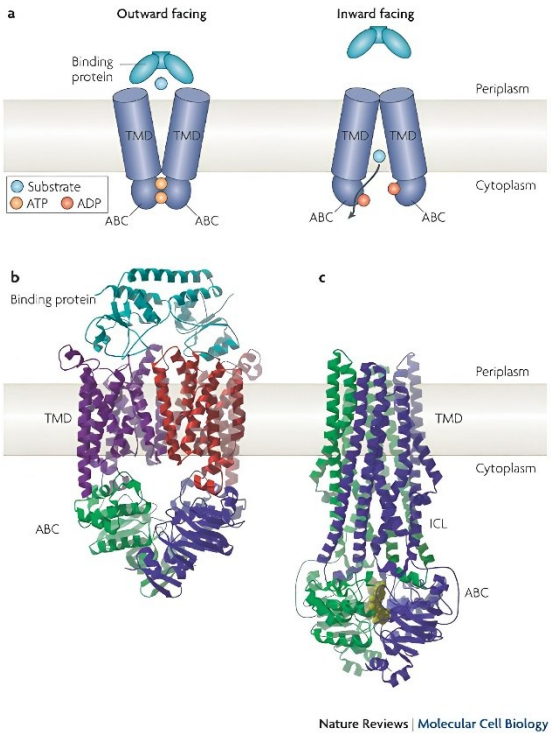

Figure 15. *The figure shows the typical ABC transporters, with the transmembrane and cytoplasmic ATP-binding domains. It compares how the structures are organized and the direction of substrate transport in importers and exporters (Rees, Johnson & Lewinson 2009)*

In bacteria, ABC transporters play a dual role: they mediate the uptake of essential nutrients such as amino acids, sugars and metal ions, and moreover contribute to the efflux of toxic compounds, including antibiotics and metabolic waste products. This dual functionality makes them critical for bacterial survival and a strategic target for antimicrobial intervention. The identification of ABC transporters as potential targets of manool suggests that this compound may interfere with key transport mechanisms, thereby compromising

bacterial homeostasis and viability. These findings not only validate the effectiveness of live-cell DARTS protocol but also highlight manool's potential as a lead compound for the development of new antibacterial agents aimed at disrupting nutrient acquisition and drug resistance pathways in pathogenic bacteria.

2.3.4 Evaluation of manool effects on efflux pumps activity

Various membrane-associated channel proteins, also including some ABC transporters, are grouped under the name efflux pumps (EPs). These are proteins composed of a single unit or multiple components, ubiquitously present in both Gram-positive and Gram-negative bacteria (Figure 16). These transport systems play a crucial role in maintaining cellular homeostasis by actively exporting a wide range of substrates including antibiotics, metabolic by-products, toxic compounds and signalling molecules out of the bacterial cell. Through this mechanism, bacteria are able to regulate their internal environment, preserve membrane potential and mitigate the effects of toxic agents (Soto 2013). One of the primary strategies by which bacteria develop resistance to antimicrobial agents involves the progressive acquisition and expression of diverse enzymes and transport systems, including efflux pumps. These pumps are a defensive barrier, preventing the intracellular accumulation of antibiotics and thereby reducing their efficacy (Pérez et al., 2012). Notably, natural compounds, such as diterpenes, have been reported to possess efflux pump

inhibitory properties. Such inhibition can enhance the intracellular retention of antibiotics, often resulting in a synergistic effect that restores bacterial susceptibility to previously ineffective drugs (Seukep et al., 2022).

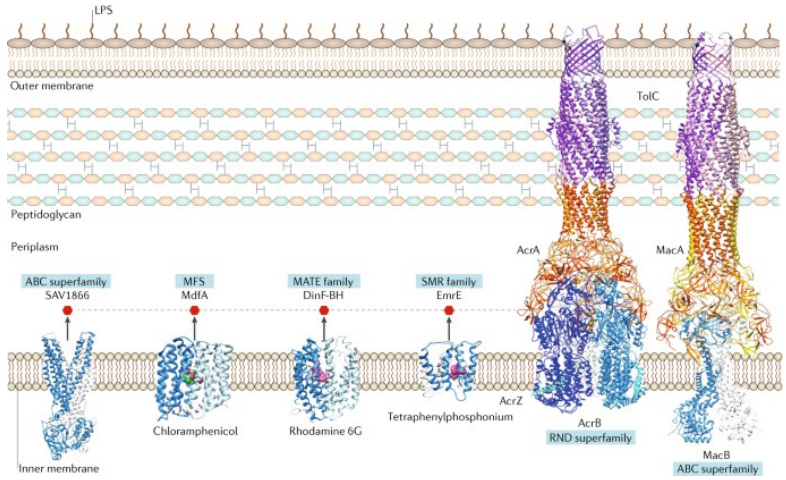

Figure 16. *The structure and organization of drug transporters in the Gram-negative bacterial envelope. All transporters are located in the inner membrane and belong to one of five families: ABC, MFS, MATE, SMR and RND. ABC transporters use ATP, whereas the others use electrochemical gradients. RND transporters form tripartite pumps (e.g. AcrAB-TolC and MacAB-TolC) that expel substrates from the cell, while others act as single inner membrane units. Interactions with the peptidoglycan are speculative (Du et al., 2018).*

Based on both DARTS results, ABC transporters emerged as main putative target of manool in *S. mutans*. Some ABC transporters can extrude xenobiotic from bacteria, working like efflux pumps. This characteristic gives to these family of proteins a key role in antibiotic resistance. In order to investigate whether manool exerts an inhibitory effect on efflux pump activity in *S. mutans*, a fluorometric assay based on

ethidium bromide (EtBr) accumulation was employed. EtBr is a fluorescent dye that serves as a substrate for bacterial efflux systems; its intracellular accumulation is inversely proportional to efflux pump activity. In this assay, *S. mutans* cells were treated with increasing concentrations of manool and fluorescence intensity was measured over time to assess EtBr retention. The results showed a dose-dependent increase in EtBr fluorescence within the bacterial cells upon treatment with manool, indicating a reduction in bacteria efflux activity (Figure 17). This result confirms that manool interferes with the function of efflux pumps, maybe enhancing the intracellular accumulation of EtBr. This result supports the hypothesis that manool may act as a modulator of bacterial transport systems.

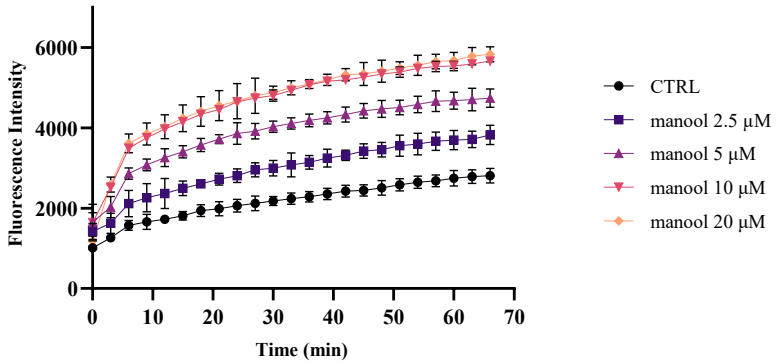

Figure 17. *An ethidium bromide (EtBr) accumulation assay was performed to evaluate the impact of manool on efflux pump (EP) activity in S. mutans. EtBr fluorescence intensity was measured in the presence of three concentrations of manool (2.5, 5, and 10 µM).*

By inhibiting efflux pumps, manool could potentiate the activity of conventional antibiotics, especially in strains of *S. mutans* that exhibit multidrug resistance. This opens promising avenues for the development of combination therapies with natural compounds to overcome bacterial defence mechanisms and restore antibiotic efficacy.

2.3.4 Modulation of ABC exporters enhance antibiotic susceptibility by LC-MS analysis

Numerous studies have demonstrated that ABC (ATP-binding cassette) transporters are involved in the translocation of a wide array of substrates across cellular membranes, extending beyond nutrient uptake to include detoxification processes. These transporters play a pivotal role in bacterial physiology by contributing to the extrusion of toxic compounds, including antibiotics, influencing bacterial susceptibility to antimicrobial agents. Given this functional versatility, it is plausible that inhibition of ABC transporters could enhance the efficacy of antibiotic treatments. Manool has shown potential in modulating transporter activity. In this context, Nagayama et al. (2014) conducted functional analyses on ABC transporters in *S. mutans*, generating isogenic mutant strains through targeted inactivation of ABC efflux systems. These mutants exhibited increased sensitivity to several antibiotics, particularly aminoglycosides and tetracyclines, suggesting a direct correlation between ABC transporter activity and antibiotic resistance mechanisms in *S. mutans*. To further investigate this

hypothesis, combination assays were conducted to evaluate the interaction between manool and kanamycin, an aminoglycoside antibiotic. In Figure 18 are represented the MIC of kanamycin alone (Figure 18-A) and the MIC of kanamycin in combination with 10 µM of manool (Figure 18-B).

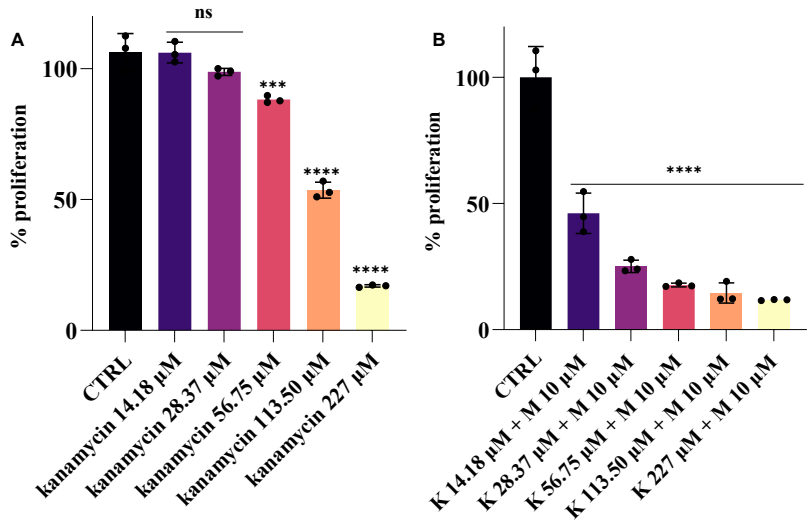

Figure 18. *Determination of the MIC_{100} of kanamycin alone against S. mutans by serial dilution (range: 14.2–227 µM), establishing a baseline inhibitory concentration of 227 µM. (A) Evaluation of the synergistic antibacterial effect of kanamycin and manool. Kanamycin was tested at sub-MIC concentrations in the presence of 10 µM manool (the MIC_{50} of the diterpene). After a 24-hour incubation period at 37 °C, bacterial growth inhibition was measured spectrophotometrically at 600 nm in a 96 well plate. A borderline synergistic pharmacological interaction was indicated by the fractional inhibitory concentration index (FICI) (B).*

Results showed that the MIC of kanamycin is drastically reduced when in combination with manool. Moreover, the fractional inhibitory concentration index (FICI) was calculated

to determine the nature of the interaction between kanamycin and manool (Table 4). Kanamycin alone exhibited a MIC_{100} of 227 µM against *S. mutans* but, when combined with 10 µM of manool, the MIC_{100} dropped significantly to 28.37 µM, indicating a strongly enhanced antibacterial activity. Accordingly, to the criteria established by Lewis, a synergistic effect is defined by FICI < 0.5, an additive effect by 0.5 < FICI < 1, an indifferent effect by 1 ≤ FICI ≤ 4, and an antagonistic effect by FICI > 4. In the case of kanamycin and manool, the calculated FICI value of 0.62 that indicates an additive effect, confirming that manool enhances the action of kanamycin without inducing antagonism.

Table 4. *Fractional Inhibitory Concentration Index (FICI) of manool in combination with kanamycin*

Molecules	MIC_{100} (alone) µM	MIC_{100} (combination) µM	FICI value
Kanamycin	227	28.37	0.62
Manool	20	10	

Based on these results and the data obtained by the EPs assay, it can be supposed that manool could reduce the antibiotic resistance of kanamycin in *S. mutans* mediated by ABC-exporters. To validate this hypothesis, a time-course analysis using was conducted. *S. mutans* bacteria were incubated with kanamycin at 28.37 µM or 56.75 µM, both alone and in combination with 10 µM manool. From the different incubation mixtures, samples of supernatants were collected at various

time points (0 to 120 minutes) and subjected to LC-MS/MS with multiple reaction monitoring (MRM) to measure the amount of kanamycin. The quantitative analysis revealed that the presence of manool significantly reduced the extracellular concentration of kanamycin over time (Figure 19), compatible with a decrease efficacy of the bacterial efflux systems. These results support the hypothesis that manool interferes with ABC transporter-mediated extrusion of kanamycin, increasing its intracellular retention and antibacterial potency. This finding underscores the potential of manool as an adjuvant compound capable of modulating drug resistance mechanisms in *S. mutans* by targeting efflux systems.

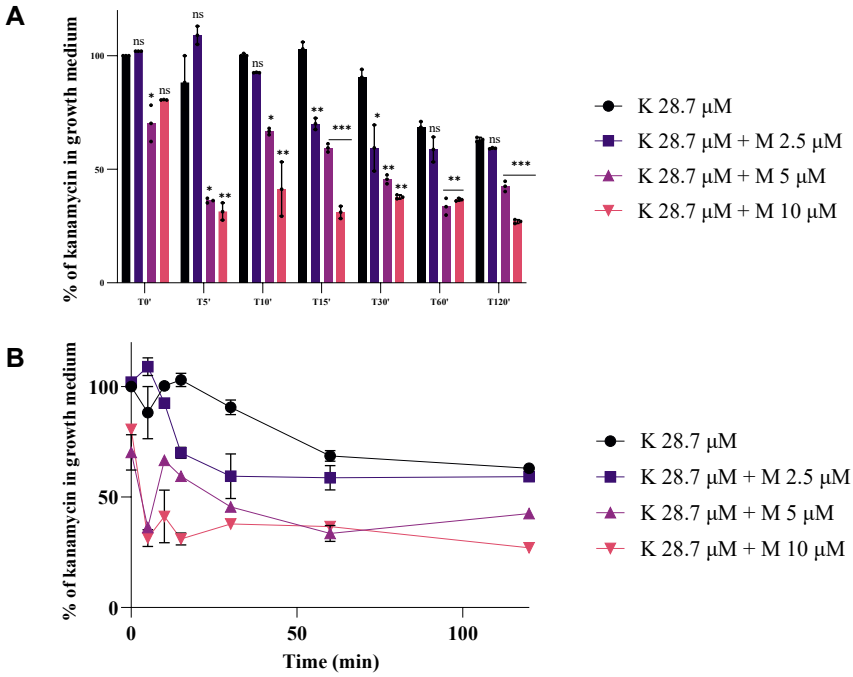

Figure 19. *Two different representations of extracellular kanamycin concentrations in the growth medium over 120 minutes of incubation with S. mutans and kanamycin (28.375 µM), either alone or in combination with increasing concentrations of manool (2.5, 5 and 10 µM). The residual kanamycin concentration in the culture supernatant was quantified by LC-MS/MS. Data calculated from the average of two independent experiments with error bars representing SD. (ns, not significant, ****p-value< 0,0001, ***p-value< 0,001, **p-value < 0,005, *p-value<0,01).*

2.3.5 LC MS-based analysis of amino acids uptake

As previously discussed, in bacterial cells ABC transporters are not only involved in the efflux of toxic compounds and antibiotics but also play a crucial role in the uptake of essential nutrients, including amino acids (AAs). To further validate the findings obtained through the DARTS approach, the impact of manool treatment on nutrient trafficking in *S. mutans* was investigated, with a particular focus on amino acid uptake.

Indeed, several ABC proteins identified via DARTS analysis are known to mediate transmembrane transport of amino acids. To assess whether manool interferes with this process, the concentration of specific AAs was monitored in the culture medium of *S. mutans* during bacterial growth in the presence of three sub-inhibitory concentrations of manool (2.5 μM, 5 μM, and 10 μM), as well as in a control medium without manool. As showed in Figure 20, time-course measurements revealed that in the untreated control medium there was a marked decrease in the concentration of amino acids within the first 150 minutes of incubation. After this initial phase, amino acids levels remained relatively constant. Notably, the AAs level reduction was noted during the lag phase of *S. mutans* growth, suggesting that the inhibition of their uptake occurs before exponential proliferation. In contrast, cultures treated with manool showed no significant reduction in the concentration of most monitored amino acids over the same period, indicating that manool effectively inhibits AA uptake mainly during lag phase (Figure 20-Arg, Glu, Phe). This supports the hypothesis that manool interferes with ABC transporter-mediated nutrient acquisition, thereby potentially impairing bacterial growth and metabolism. Interestingly, glutamine levels remained comparable between treated and untreated samples throughout the experiment (Figure 20-Gln). Glutamine plays a unique and central role in bacterial nitrogen metabolism, serving as both a nitrogen donor and a precursor for biosynthetic pathways. Due to its metabolic importance,

bacterial cells possess multiple transport systems specifically dedicated to glutamine uptake. The unaffected glutamine levels suggest that while manool inhibits general AA transport, it may not significantly impact specialized systems dedicated to glutamine, highlighting the specificity and complexity of ABC transporter regulation.

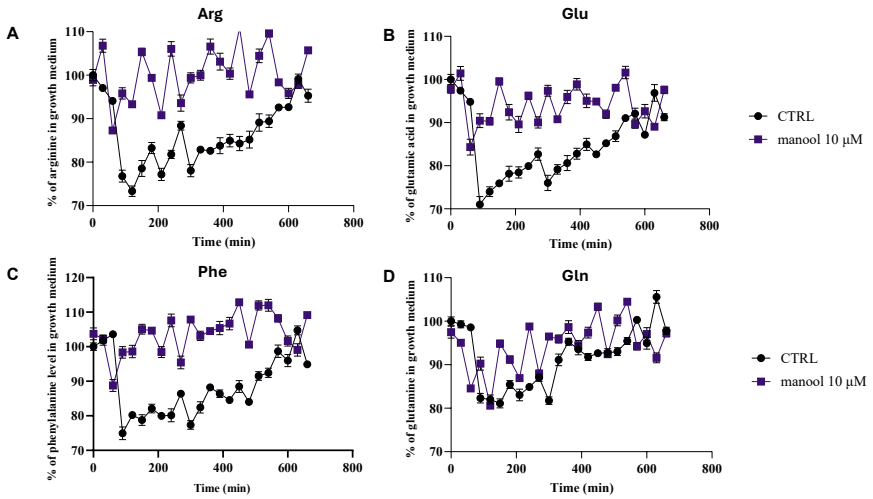

Figure 20. *Manool reduces amino acid uptake in S. mutans by interfering with the import of nutrients via the ABC transporter. Time course analysis of the concentrations of amino acids (AAs) in the culture medium of S. mutans grown in the absence (black line) or presence (purple line) of a sub-MIC concentration of Manool (10 µM). AA levels were measured by LC-MS at multiple time points over 150 minutes. (A) Arginine (B) Glutamic acid (C) Phenylalanine (D) Glutamine. Data represent the average of two independent experiments; error bars indicate standard deviation.*

Taken together, these findings reinforce the notion that manool disrupts ABC transporter function in *S. mutans*, not only by impairing efflux mechanisms but also by limiting nutrient import. This dual interference could contribute to the compound's

antimicrobial activity and supports its potential as a lead molecule for the development of novel strategies targeting bacterial transport systems.

2.3.6 Computational studies for the identification of manool binding mode to ABCs

The results obtained so far indicated a pleiotropic capacity of manool to inhibit different ABC proteins, thus suggesting the possibility of the diterpene to interact with different binding sites in multiple proteins or, more likely, with a pocket conserved in different proteins. Furthermore, previous studies demonstrated the structural compatibility of manool with the ATP binding site of human ATP-synthase (Bisio et al., 2020). Therefore, we evaluated through computational approaches the ability of manool to bind the ATPase subunits of ABCs, which play a key role in regulating the activity of these proteins. We focused on the multiple sugar-binding transport ATP-binding protein from *S. mutans* serotype c (strain ATCC 700610 / UA159) as our model (Q00752), one of the few ATP binding domains of *S. mutans* ABC whose structure has been elucidated. A dimeric model was created based on the starting template. This model was then refined through a simulated annealing protocol to improve its structural accuracy. The best-scoring structure from this process was further optimized through energy minimization, and its backbone conformation was carefully assessed using a Ramachandran plot analysis. The results confirmed that all residues adopted allowed geometries,

indicating a reliable and well-refined model (see Figure A10). The 3D multiple sugar-binding protein model was then refined by means of a 400 ns of molecular dynamics (MD) simulation to gain further insights into the stability and dynamics of this protein. Analysing the root mean square deviation (RMSD) of all the α carbons of the protein from the starting multiple sugar-binding protein model structure, we observed that, despite an initial increase, in the last 350 ns in which there were no constraints on the structure (see Experimental section for more details) the RMSD after 150 ns remained around 4.0 Å (see Figure A11), suggesting that the system was fairly stable during the entire remaining time of MD simulation. During the final 200 ns of the MD simulation, a protein structure snapshot was recorded every nanosecond, resulting in a set of 200 distinct protein conformations. To account for the inherent flexibility of residues within the binding site, manool was docked across all 200 multiple sugar-binding protein conformations using Autodock-GPU software (Santos-Martins 2021). For each docking calculation, both the best-ranked solution and a representative structure of the most populated cluster were identified, yielding a total of 400 docking solutions for manool. These docking poses were subsequently clustered, and only clusters containing at least 40 poses (corresponding to the 10% of the docking results) were considered for further analysis. An RMSD threshold of 2.0 Å was applied to determine cluster membership. Ultimately, four significant clusters of docking poses were identified (see Figure A12). To gain deeper insight

into the potential binding modes of manool, these four clusters were each subjected to an additional 400 ns of MD simulation. As illustrated in Figure A13, the analysis of the binding mode stability highlighted that the docking poses associated with clusters 2 and 4 were relatively unstable, exhibiting an average RMSD of approximately 8.3 and 6.5 Å, respectively. In contrast, the binding modes represented by clusters 1 and 3 demonstrated greater stability, with an average RMSD around 3.0 and 2.3 Å, respectively, thereby supporting the reliability of these latter two docking arrangements. To more accurately evaluate the reliability of the four different ligand–protein complexes, the binding free energies were calculated using MD coordinates obtained from the final 350 ns of the simulation. The Molecular Mechanics-Poisson Boltzmann Surface Area (MM-PBSA) method was employed for these calculations (see the Experimental section for detailed methodology). This approach involves analysing snapshots from the MD simulation to compute the contributions of both gas-phase and solvation free energies for the unbound ligand, unbound protein, and the bound complex. As presented in Table 5, the analysis identified cluster 3 as the most reliable binding mode for manool. This was evidenced by its superior binding energy (ΔPBSA = -17.0 kcal/mol), which was 7.9 kcal/mol more favourable than the interaction energies observed for the second-best pose. These results suggest stronger and more stable interaction for the cluster 4 binding configuration, thereby supporting its potential as the preferred binding mode for manool.

Table 5. *MM-PBSA results for the analyzed protein-manool complexes. ΔPBSA is the sum of the van der Waals (VDW), electrostatic (ELE), as well as polar (EPB) and non-polar (ENPOLAR) solvation free energy. Data are expressed as kcal·mol^{-1}.*

Cpd01	VDW	ELE	EPB	ENPOLAR	EDISPER	ΔPBSA
CL01	-39.05	-1.54	8.14	-31.07	53.94	-10.42
CL02	-38.34	-3.02	10.37	-30.81	53.12	-9.11
CL03	-42.55	-4.17	7.59	-31.12	53.62	-17.02
CL04	-35.01	-3.86	8.27	-30.11	52.91	-7.91

Figure 21 presents the predicted binding mode of manool, derived from cluster 3. The analysis reveals that the trimethyldecahydronaphthalene moiety is positioned within a hydrophobic pocket of the binding site, where it is surrounded by several key lipophilic residues. This positioning facilitates efficient interactions with Y13, P14, T46, and I221 of monomer A, likely contributing to the stabilization of the ligand within the binding pocket and enhancing its binding affinity. Meanwhile, the hydroxyl group establishes two stable hydrogen bonds: one with the backbone nitrogen of K213 and another via a water-mediated interaction with the side chain of the same residue (K213). These interactions likely play a role in further anchoring the ligand within the pocket, reinforcing its stability. Interestingly, the second monomer of the dimeric system does not appear to engage in direct stabilizing interactions with the ligand. However, its presence may contribute to the overall binding mode by providing structural constraints that help maintain the proper orientation of the ligand within the binding

site. This suggests that while direct contacts are absent, the dimeric architecture might still influence ligand positioning and possibly its functional activity. As highlighted by the MM-PBSA analysis, a comparison of the interaction energy of this binding mode with alternative configurations indicates that both hydrophobic and electrostatic interactions play a crucial role in ligand stabilization. The combination of hydrophobic contacts and hydrogen bonding interactions allows manool to effectively fit within the binding site, suggesting a favourable and stable interaction pattern that could be relevant for its biological activity.

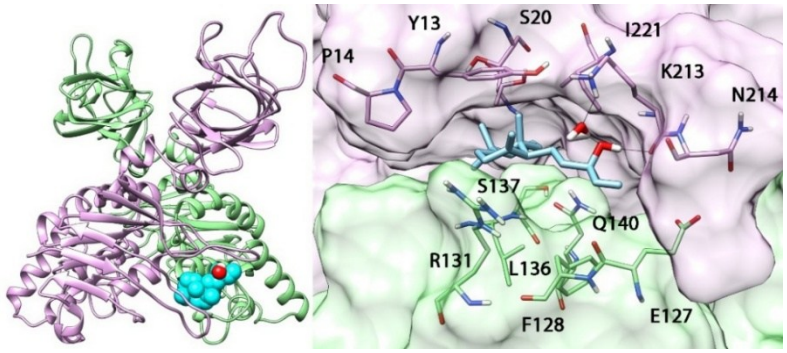

Figure 21. *Minimized average structures of manool (sky blue) in complex with multiple sugar-binding transport ATP-binding protein. General overview (left) and ligand-binding site interaction analysis (right). The two monomers are colored pink (monomer A) and green (monomer B). In the general overview, the ligand is shown in green CPK representation. In the binding site view, the protein residues surrounding the ligand, forming the binding site, are shown as pink (monomer A) and green (monomer B) sticks, while hydrogen bonds are represented as black lines.*

2.3.7 Connecting molecular targeting to cellular response

ABC transporters were indicated as putative molecular targets of manool. The subsequent experimental strategy was designed to determine how this interaction translates into functional effects on *S. mutans* physiology and virulence. For this reason, several complementary assays were performed to elucidate the downstream consequences of ABC transporter modulation, including proteomic profiling, transcriptomic analysis of stress-response regulators and host pathogen interaction studies. This integrated approach enabled the characterization of the cellular pathways influenced by manool. It provided a mechanistic framework. This framework links target action with alterations in bacterial stress adaptation, membrane transport, and virulence-associated traits.

2.3.8 Proteomic studies

Proteomics represents a powerful tool for understanding bacterial physiology, adaptation and pathogenicity at the molecular level. In pathogenic bacteria, proteomic profiling is particularly valuable for revealing mechanisms of antibiotic resistance, virulence factor regulation and metabolic adaptation to hostile environments. Based on this knowledge, proteomic analysis was performed to investigate the molecular response of *S. mutans* to manool treatment across different phases of its growth curve. Bacterial cultures were exposed to manool during the lag, exponential and stationary phases, and protein

expression was analysed using LC-MS. As Figure 22 (C) reported, during the early phases of the growth, proteomics results showed that the level of several proteins involved in nutrients uptake was decreased, in particular that of ABC-transporters required for the amino acid trafficking and proteins belonging to bacteria regulatory proteins family. This could depend on an abnormal degradation of these proteins, possibly as a consequence of the binding of manool. Moreover, on the other hand, during the late phases of the growth (Figure 22-A-B), results revealed an overexpression of ABC transporter proteins. This suggests a compensatory upregulation of membrane transport systems in response to manool-induced inhibition. Additionally, a significant increase in the expression of stress-related proteins and DNA repair enzymes was observed, particularly during the exponential phase (Figure 22). These proteins are typically associated with oxidative stress management, membrane integrity maintenance and genomic stability. The combined upregulation of ABC transporters and stress-response elements indicates that manool exerts pressure on both membrane transport and DNA integrity, triggering adaptive responses that reflect its antimicrobial potential.

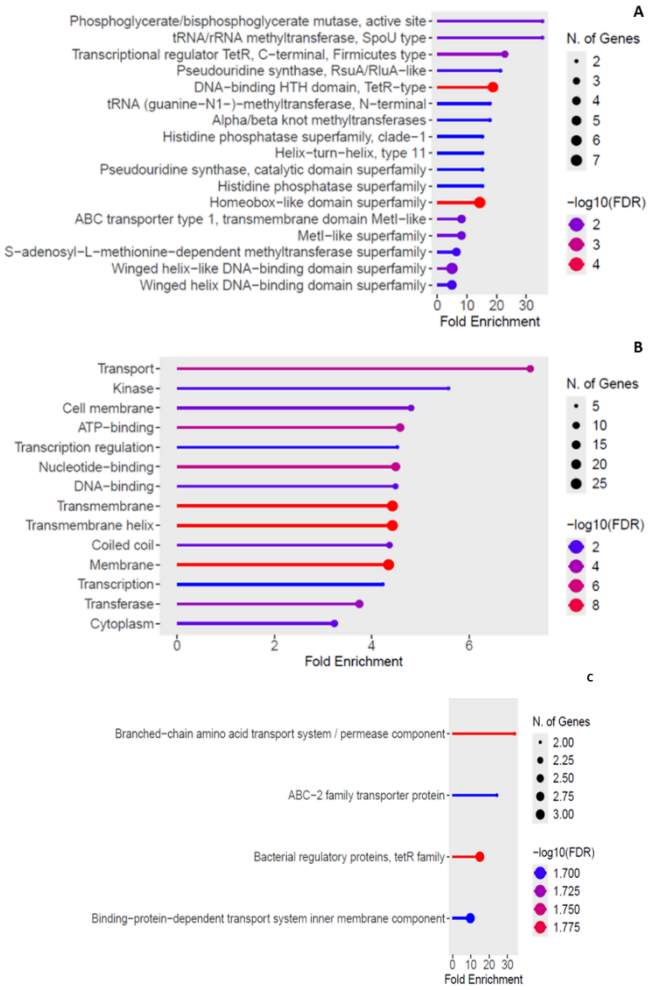

Figure 22. *Proteomic changes in S. mutans following manool treatment across different growth phases (A–B): During the exponential and stationary phases, manool exposure resulted in the upregulation of several ABC transporters, together with proteins involved in stress response and DNA repair. (C) During the lag phase, downregulation of proteins associated with nutrient uptake was observed, particularly amino acid-related ABC transporters and members of bacterial regulatory protein families.*

2.3.9 Manool regulation of stress response kinase VicKR

Based on proteomics results and literature knowledge, stress responses genes were quantified using real-time PCR. In particular, we focused on genes involved in the two-component signal transduction systems (TCSTSs), through which bacteria can detect transient environmental changes, such as fluctuations in pH, temperature and nutrient levels. These systems comprise a membrane-bound histidine kinase and an intracellular response regulator. The key roles of TCSTSs are to sense changes in the environment and alter the expression of specific sets of genes. This enables them to mount coordinated responses to environmental stimuli, thus playing important roles in bacterial adaptation, survival and virulence. TCSTSs send signals via phosphotransferase between histidine sensor kinases and their respective response regulators (Senadheera et al., 2009). This triggers the response regulators to dimerize and bind to conserved DNA motifs, ultimately adjusting cellular functions such as biofilm formation, stress tolerance and nutrient uptake. In particular, ComDE, LevRS, VicRK and the orphan CovR regulator have been studied in detail and have been shown to coordinate the expression of several virulence attributes. The LevRS system is important for the management of carbohydrate metabolism, in contrast, the ComDE system is involved in the regulation of bacteriocin production and competence. VicRK influences acid and oxidative stress responses, as well as competence and is the only TCSTS that is essential in *S. mutans* (Senadheera et

al., 2009). In deeper, as showed in Figure 23, the VicRK two-component system, particularly the sensor kinase VicK, is a pivotal regulator of environmental adaptation and virulence in *S. mutans*. Upon exposure to stress-inducing agents, such as antimicrobial molecules, VicK becomes activated and initiates a transcriptional cascade that enhances bacterial survival. This includes upregulation of genes involved in biofilm formation, exopolysaccharide synthesis and oxidative stress tolerance (Senadheera, D. B., et al, 2012). Several studies have proposed phosphotransferase cross talk between VicRK and the LiaFSR TCSTS, which contributes to surface adhesion, mutacin production and the ability to tolerate environmental stresses, including cell envelope damage and heat shock.

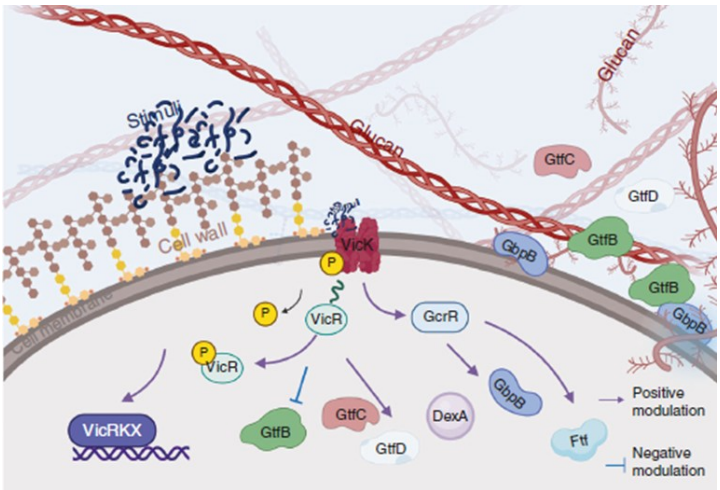

Figure 23. *The mechanisms of sensor kinase VicK in S. mutans stress responses*

To evaluate the impact of manool on the virulence of *S. mutans* from a transcriptomic perspective, quantitative real-time PCR

of *vick* mRNA was used. To this end, *S. mutans* was cultured to the late lag phase and exponential phase, then incubated with manool at 2.5, 5, and 10 μM for 30 minutes. After treatment, cells were collected, RNA was isolated, purified and RT-qPCR was carried out. Quantitative real-time PCR analysis of *S. mutans* treated with manool showed a decrease in the mRNA level expression of *vick* gene, in particular during the late lag phase (Figure 24-A). Interestingly, during exponential phase, RT-qPCR revealed a two-phase expression pattern of the *vicK* gene (Figure 24-B). At low concentrations of manool, *vicK* expression was downregulated, thus suggesting that the VicRK signalling pathway was suppressed, possibly due to reduced stress perception or partial inhibition of bacterial metabolism. In contrast, at higher concentrations, *vicK* expression was upregulated, indicating the activation of the stress response machinery. This increase may be an adaptive mechanism by which *S. mutans* tries to counteract intensified antimicrobial pressure by increasing the transcription of genes involved in biofilm formation, exopolysaccharide synthesis and oxidative stress tolerance. The concentration-dependent modulation of *vicK* expression highlights its role as a dynamic sensor in the bacterial response to environmental stress and antimicrobial challenge.

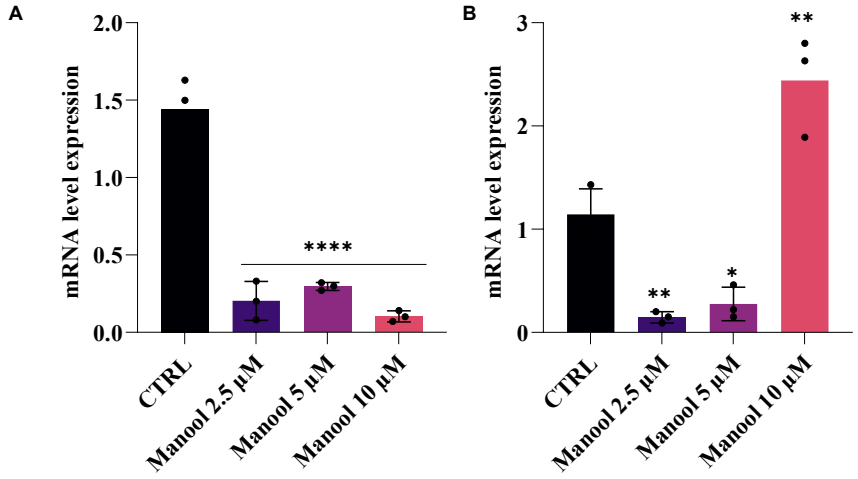

Figure 24. *Quantitative real time PCR of vick mRNA levels in Streptococcus mutans after incubation with manool at the concentration of 2.5, 5 and 10 µM. vick mRNA levels in Streptococcus mutans treated with manool during late lag phase (A) and during exponential phase (B). All data were normalized to housekeeping gene. (n=3) (ns, not significant, ****p-value< 0,0001, ***p-value< 0,001, **p-value < 0,005, *p-value<0,01).*

2.3.10 Invasion and adhesion experiments

Adhesion and invasion experiments are essential for understanding the interactions between bacterial pathogens and eukaryotic host cells. These assays typically involve incubating bacterial strains with cultured eukaryotic cells, such as epithelial or endothelial cell lines, to evaluate the ability of bacteria to adhere to and penetrate the host cell surface (Frutos-Grilo et al., 2023). Adhesion is assessed by quantifying the number of bacteria that remain attached to the cell membrane after washing, while invasion is measured by determining the number of bacteria that successfully enter the

host cells, often using antibiotic protection assays to eliminate extracellular bacteria. These experiments provide critical insights into the virulence mechanisms of pathogens, including the role of surface proteins, secretion systems and host cell receptors. Such studies are fundamental for identifying potential therapeutic targets and for developing strategies to prevent bacterial colonization and infection. Several studies have explored the interaction between *S. mutans* and human gingival fibroblast (HGF-1) cells to better understand its virulence mechanisms. One notable study demonstrated that both planktonic and biofilm forms of *S. mutans* and *S. sobrinus* can adhere to and invade HGF-1 cells, with biofilm-associated bacteria showing significantly greater efficiency in both adhesion and invasion. This suggests that the biofilm lifestyle enhances the bacterium's ability to colonize and persist in soft tissues of the oral cavity, not just on hard surfaces like teeth (Berlutti et al., 2010). The adhesion process is mediated by bacterial surface adhesins that recognize and bind to host cell receptors. Once adhered, *S. mutans* can trigger host cell signaling pathways that facilitate bacterial internalization. Moreover, Vick is a key modulator of biofilm architecture and surface adhesin expression, its activity directly affects the ability of *S. mutans* to colonize and penetrate host tissues. VicK-deficient strains show reduced biofilm formation and diminished invasion capacity, underscoring the kinase's role in coordinating environmental sensing with host cell interaction (Deng et al., 2021). Taken together, these findings position VicK

as a central node in the regulatory network that governs stress adaptation and host cell invasion. Based on proteomics and RT-qPCR results on *vick* gene after manool incubation, adhesion and invasion experiments were performed to fully understand the impact of manool on the virulence of *S. mutans* (Jiang et al., 2019). In Figure 25, the protocol applied for invasion experiment was illustrated.

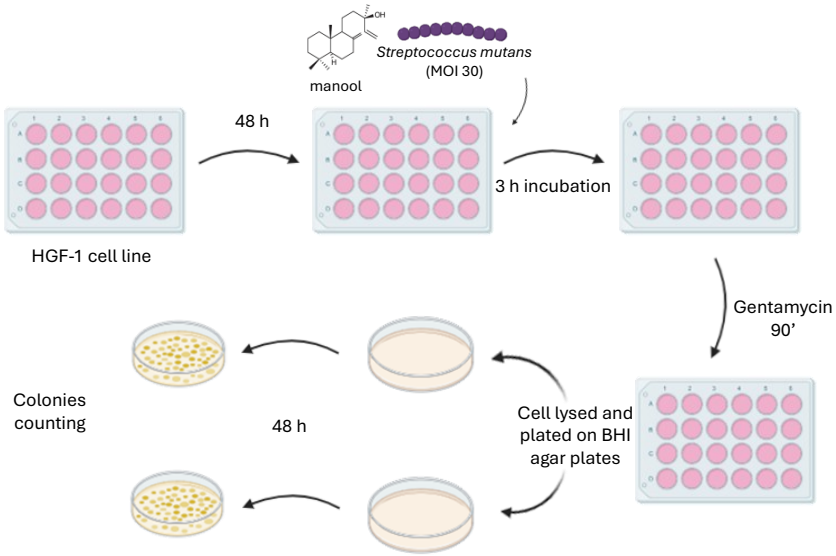

Figure 25. *Representation of invasion experiment. Human Gingival Fibroblasts were infected with S. mutans (MOI 30). After 3 h of infection, ycin was added in order to kill all extracellular bacteria. Finally, intracellular bacteria were plated on BHI agar and after 48 h colonies were counted.*

Invasion and adhesion assays were performed to evaluate the interaction between *S. mutans* and the human gingival fibroblast cell line HGF-1 and to assess the modulatory effect

of manool. The results demonstrated that *S. mutans* can adhere to and invade HGF-1 cells, confirming its potential to colonize soft tissues in the oral cavity. Interestingly, treatment with manool led to a dose-dependent reduction in bacterial invasion (Figure 26-A), with higher concentrations significantly decreasing the number of internalized bacteria. However, no notable changes were observed in bacterial adhesion across all tested concentrations (Figure 26-B), indicating that manool selectively interferes with the invasion process without affecting the initial attachment of *S. mutans* to host cells. These findings suggest that manool may impair intracellular entry mechanisms, possibly by targeting bacterial virulence factors or host cell signaling pathways while leaving surface-level interactions unchanged.

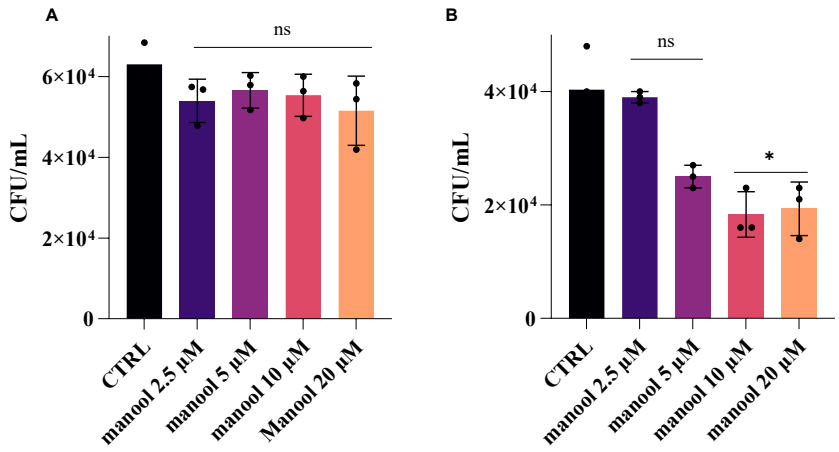

Figure 26. *Effect of manool in adhesion (A) and invasion (B) of S. mutans in Human Gingival Fibroblasts (*p-value< 0,01).*

2.3.11 Evolution experiment

Evolution is an on-going process, and it can be studied experimentally in organisms with rapid generations (Figure 27). The success of any therapeutic agent is limited by the development of tolerance or resistance to that compound from the time it is first used. This is true for agents used to treat bacterial, fungal, parasitic, and viral infections, and for treating chronic diseases such as cancer and diabetes. It applies to ailments caused or suffered by any living organism. A wide range of biochemical and physiological mechanisms may be responsible for resistance. In the case of antimicrobial agents, the processes that contribute to emergence and dissemination of resistance are complex, and the lack of basic knowledge on these topics is one of the primary reasons that there has been so little significant achievement in the effective prevention and control of resistance development. The tracking of mutations underlying phenotypic changes offers the opportunity for detailed molecular analyses of novel phenotypes. This provides a breadth of information on diverse biological systems and may retrace key past events of natural history (Davies, J., & Davies, D., 2010). To investigate the long-term adaptive response of *S. mutans* to manool exposure, an evolution experiment was conducted. Bacterial cultures were continuously incubated with sub-inhibitory concentrations of manool over an 8-week period, simulating prolonged environmental pressure.

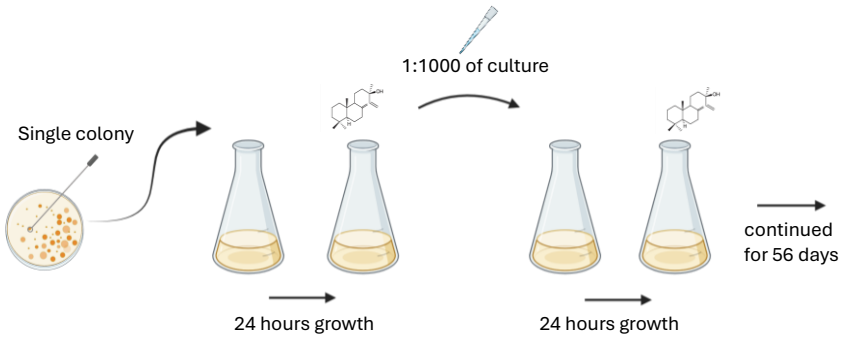

Figure 27. *Workflow of Evolution Experiment. S. mutans was continuously incubated with manool for eight weeks. Every week manool concentration was increased, starting from a concentration of manool of 2.5 µM until week 8 with a final concentration of manool of 30 µM.*

The results show a change in manool MIC towards *S. mutans* after 8 weeks. Indeed, following thin incubation time bacterial growth is not inhibited at a concentration of 20 µM (Figure 28). This data is not surprising since, as previously reported, the introduction of antibiotics as antimicrobial agents, the MIC baselines for many commonly used antibiotics have risen significantly. Examples of this “MIC creep” include vancomycin (60-fold MIC increase in 16 years), erythromycin (250-fold MIC increase in 5 years), ciprofloxacin (120-fold MIC increase in 19 years) and tobramycin (8-fold MIC increase in 17 years) (Sandoval-Motta & Aldana 2016).

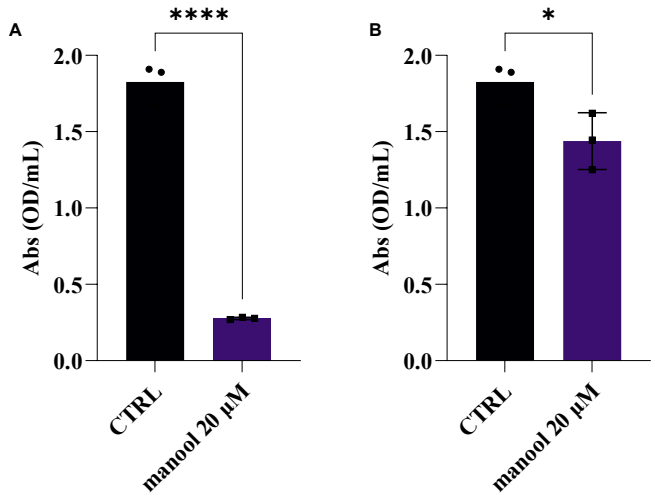

Figure 28. *Streptococcus mutans incubated with 20 µM of manool at week 1 (A). Streptococcus mutans was exposed to increasing concentrations of manool every week, until week 8. After long exposition to manool S. mutans was incubated with manool at 20 µM (B).*

Further information was obtained by monitoring the growth curves obtained treating with increasing concentration of manool bacteria exposed for 1 and 8 weeks to the compound. In the first case, the resulting curves demonstrated that 1 week exposure generated negligible resistance effect on *S. mutans*. Conversely, for the strain at week 8 it can be seen that up to 10 µM manool the growth phases were almost unperturbed, while at 20 µM some effects can be observed (Figure 29). It is therefore evident that prolonged exposure to manool led to the selection of a resistant strain of the bacterium that was named S. *mutans* evolved strain. At the end of the incubation period, cell aliquots were cryopreserved and subsequently analysed using both genomic and proteomic approaches.

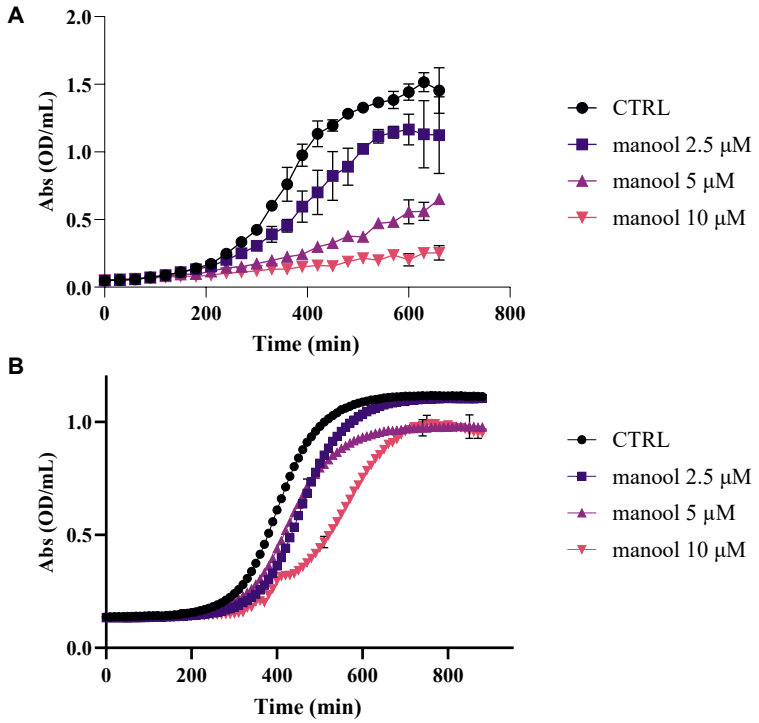

Figure 29. *Growth curve of S. mutans in BHI broth with supplementation of manool (0, 2.5, 5, 10 µM). OD 600 nm measured every 30 mins (A). Effect of manool on S. mutans evolved strain growth at the same concentrations of the diterpene (B). All data calculated from the average of three independent experiments with error bars representing Standard Deviation (SD).*

2.3.11.1 Proteomic analysis of evolved strain

Based on previous results, which showed a significant difference in the response of *S. mutans* wild type and *S. mutans* evolved strain after incubation with manool, proteomic studies were performed to investigate at a molecular level the main differences between the proteomes of the evolved strain and

wild type strain. Proteomic investigation revealed substantial differences in the distribution of proteins, as clearly emerged from the reported Venn diagram (Figure 30) were the number of proteins detected specifically in each strain as well as the shared core proteome is shown.

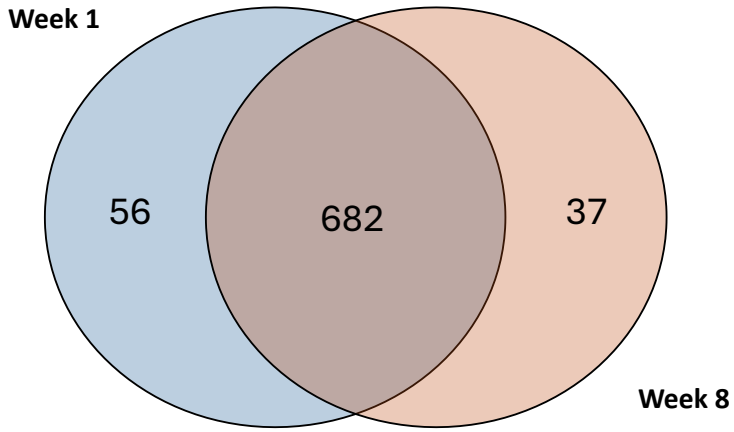

Figure 30. *Venn Diagram of proteins belonging to S. mutans wild type proteome (blue) and S. mutans evolved strain proteome (pink).*

These results were then subjected to a gene ontology enrichment analysis. Results shown in Figure 31, revealed that in the evolved strain an overexpression of proteins involved in the transport of substrates can be observed.

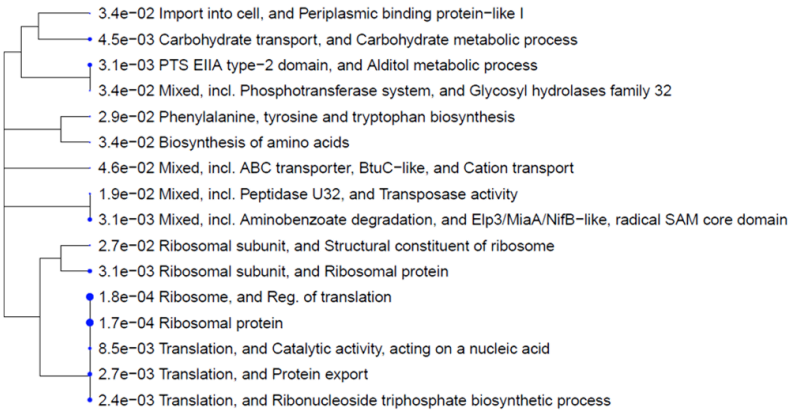

Figure 31. *Proteomic analysis of Evolution Experiments. Enrichment of proteins belong to week 8 after exposition of increasing concentrations of manool in S. mutans.*

This finding suggested that an adaptative shift in cellular processes occurred, allowing the bacterium to reduce the effects of manool by using enhancing the efficiency of pathways alternative to those affected by the diterpene. The literature clearly shows that one of the most common and widespread adaptive responses to prolonged exposure to antimicrobial stressors including antibiotics and other potentially toxic compounds is the activation of multidrug efflux systems together with a stricter control of cellular permeability (Sandoval-Motta & Aldana 2016). Prolonged exposure to the manool molecule therefore induced a stress response in the bacterium, increasing the protein classes shown in the Figure 31, which coincides with the data in the literature.

2.3.11.2 Genome sequencing analysis of evolved strain

Whole-genome sequencing of the evolved *S. mutans* revealed the emergence of three high-impact mutations, all classified as stop-gained variants. The occurrence of these mutations indicates selective pressure caused by prolonged exposure to manool.

Table 6. *Gene mutation emerged from sequencing of evolved S. mutans genome.*

Gene	Product	Count
rpoZ	DNA-directed RNA polymerase subunit omega	stop_gained c.157G>T p.Glu53*
rpoZ	DNA-directed RNA polymerase subunit omega	stop_gained c.47C>A p.Ser16*
irvR	LexA repressor	stop_gained c.621C>G p.Tyr207*

Two independent premature stop mutations were identified in *rpoZ*, which encodes the omega-subunit of the DNA-directed RNA polymerase (variants c.157G>T, p.Glu53* and c.47C>A, p.Ser16*). While RpoZ is not essential for catalytic activity, it plays a significant role in RNA polymerase stability, assembly, and transcriptional accuracy. It has also been associated with global transcriptional regulation under stress conditions. Experiments involving antibiotics and other stressors have reported loss-of-function mutations in *rpoZ*. Alterations to transcriptional dynamics, increased tolerance and reprogramming of stress-response pathways can result from truncation of the ω-subunit. The role of the *rpoZ* gene in *S. mutans* is not well understood. A study by Mathew et al. (2006)

(Mathew et al., 2006) examined the consequences of deleting *rpoZ* in *Mycobacterium smegmatis*. In this work, the authors generated a *rpoZ* knockout mutant. They demonstrated that loss of the ω subunit leads to pleiotropic surface-related phenotypes. These include altered colony morphology, reduced sliding motility, and defective biofilm formation. It was revealed through microscopy analyses that these defects arise from an impaired ability to produce extracellular matrix, while it was shown through lipid profiling that the mutant fails to synthesize the short-chain mycolic acids normally associated with biofilm growth. Complementation with a wild-type copy of *rpoZ* restored all phenotypes, confirming a direct role for the subunit in these processes. Although its functions in *S. mutans* are not yet clear, the study suggests that *rpoZ* may influence surface adaptation and biofilm behaviour beyond its structural role in RNA polymerase. A third stop-gained mutation was detected in *irvR* (c.621C>G, p.Tyr207*) which is a gene that codes for the LexA-like repressor that regulates the IrvR/IrvA system. This system is known to control competence, stress survival and cell envelope remodelling in *S. mutans.* Inactivation of *irvR* is expected to derepress its regulon, which could enhance global stress tolerance and contribute to the increased robustness observed in the evolved strain (Niu et al., 2010). The results of genomics and proteomics studies suggest an adaptive strategy: continued exposure to manool leads to changes in global regulation rather than specific target resistance. The combined inactivation of *rpoZ* and *irvR* likely shifts the

transcriptional landscape toward a phenotype characterised by strengthened cell envelope integrity, enhanced efflux capacity, reduced intracellular accumulation of toxic molecules and activation of general stress pathways. This global shift correlates well with the observed increase in the minimal inhibitory concentration (MIC) and the absence of inhibition at 20 µM after 8 weeks, reflecting a typical pattern of adaptive resistance widely documented for many antimicrobial compounds.

2.4 Conclusions

For the first time, a DARTS protocol has been successfully optimised and applied directly to living bacterial cells. This represents a significant methodological advancement over previous approaches, which relied solely on cell lysates. This innovation allows for the identification of protein targets within their native physiological context, offering more accurate and biologically relevant information about interactions between compounds and proteins. A specific interaction with membrane-associated proteins was revealed by this in vivo DARTS (bc-DARTS) approach using *Streptococcus mutans* and the plant-derived compound manool, which was not detectable through proteome extract-based DARTS (pe-DARTS) alone. Most importantly, bc-DARTS identified ATP-binding cassette (ABC) transporters as the principal molecular targets of manool in *S. mutans*. ABC proteins are known to play pivotal roles in bacterial physiology, including nutrient uptake, virulence

regulation and antibiotic resistance. By interfering with these transporters, manool disrupts nutrient acquisition pathways, thus reducing the ability of *S. mutans* to obtain essential resources for growth and survival. This effect directly compromises bacterial fitness and pathogenic potential. Furthermore, quantitative monitoring of kanamycin concentrations by LC-MS demonstrated that manool reduces the antibiotic resistance of *S. mutans* to kanamycin, specifically by inhibiting ABC exporter activity. This dual mechanism, impairing nutrient uptake while sensitizing the bacterium to antibiotic treatment, highlights the therapeutic relevance of manool as a natural compound with antimicrobial potential. Complementary proteomic analyses provided deeper insights into the downstream cellular responses of *S. mutans* following treatment to manool. These studies revealed alterations in pathways associated with virulence, invasiveness and stress adaptation, thus improving understanding of about manool pleiotropic effects. Collectively demonstrate the potential of manool as a modulator of both nutrient acquisition and antibiotic resistance in *S. mutans*. Finally, prolonged exposure of *S. mutans* to manool over an eight-week period facilitated the characterization of an evolved strain through integrated proteomic and genomic analyses. The proteomic data revealed a pronounced overexpression of transporter proteins, consistent with an adaptive mechanism aimed at counteracting the inhibitory effects of manool on nutrient uptake and antibiotic resistance. Complementary genome sequencing further

demonstrated the deletion of the *irvR* and *rpoZ* genes, indicating that sustained selective pressure by manool not only by protein expression but also drives stable genetic alterations affecting regulatory and stress-response pathways. Taken together, these findings underscore the multifaceted impact of manool on *S. mutans*, encompassing both immediate physiological modulation and long-term evolutionary adaptation. The identification of transporter overexpression and gene deletion highlights the capacity of natural compounds to exert profound selective forces on bacterial populations, thus influencing their fitness, virulence and resistance mechanisms. This Chapter of this PhD project establishes a foundation for future investigations into the evolutionary mechanisms of bacterial pathogens under prolonged exposure to bioactive plant metabolites and reinforces the potential of manool as a candidate for antimicrobial development. Together, these findings highlight the dual impact of manool on *S. mutans*, combining proteomic reprogramming with genomic modifications and underscore its potential to modulate bacterial physiology in a lasting and multifaceted manner.

2.5 Appendix

Figure A1. *Monitoring of amino acids uptake by LC-MS.*

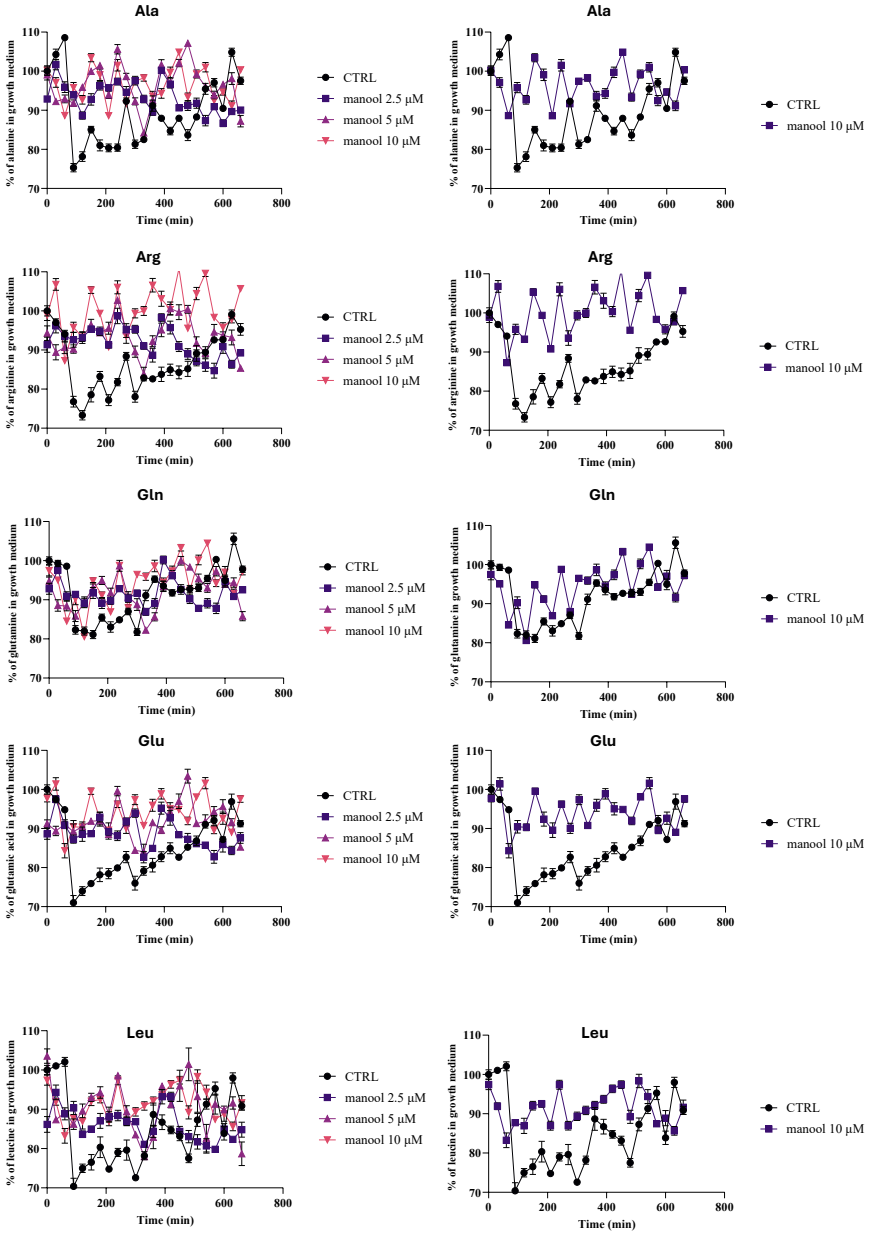

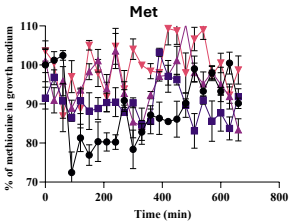
Met
% of methionine in growth medium
Time (min)

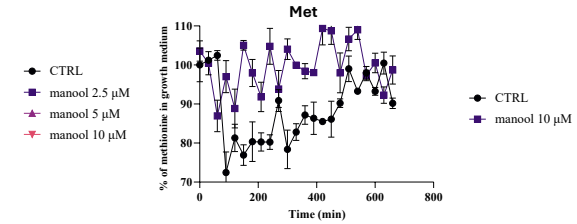
CTRL
manool 2.5 µM
manool 5 µM
manool 10 µM

Met
% of methionine in growth medium
Time (min)

CTRL
manool 10 µM

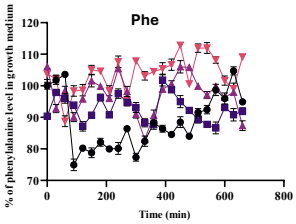
Phe
% of phenylalanine level in growth medium
Time (min)


CTRL
manool 2.5 µM
manool 5 µM
manool 10 µM

Phe
% of phenylalanine level in growth medium
Time (min)

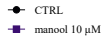
CTRL
manool 10 µM

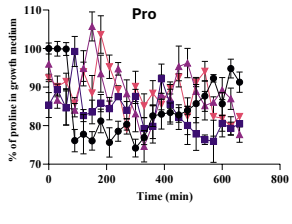
Pro
% of proline in growth medium
Time (min)


CTRL
manool 2.5 µM
manool 5 µM
manool 10 µM

Pro
% of proline level in growth medium
Time (min)

CTRL
manool 10 µM

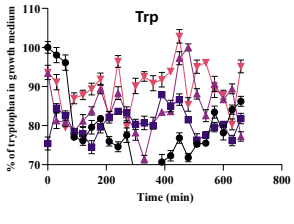
Trp
% of tryptophan in growth medium
Time (min)


CTRL
manool 2.5 µM
manool 5 µM
manool 10 µM

Trp
% of tryptophan in growth medium
Time (min)

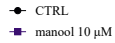
CTRL
manool 10 µM

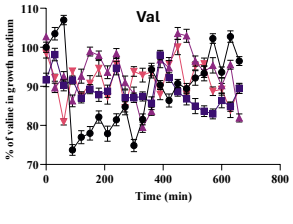
Val
% of valine in growth medium
Time (min)


CTRL
manool 2.5 µM
manool 5 µM
manool 10 µM

Val
% of valine in growth medium
Time (min)

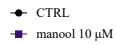
CTRL
manool 10 µM

***Figure A2**. Proteomic analysis: up-regulated proteins, exponential phase.*

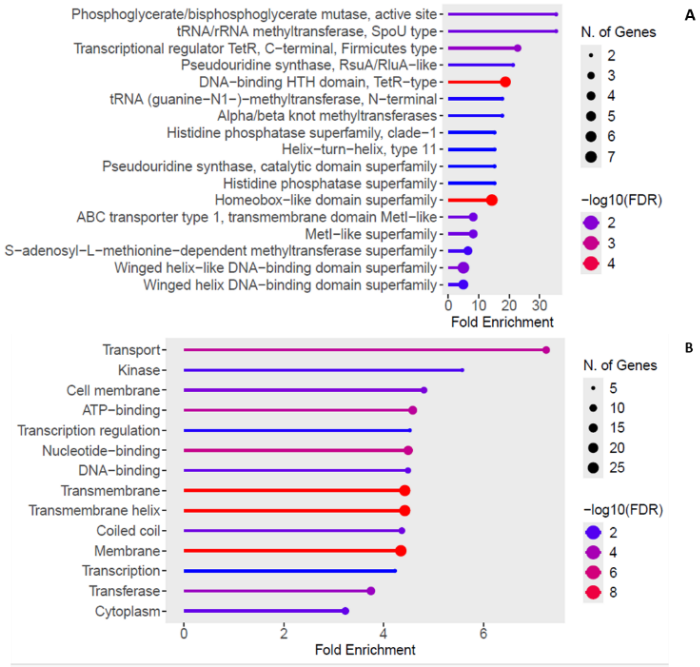

***Figure A3**. Proteomic analysis: up-regulated proteins, lag phase phase.*

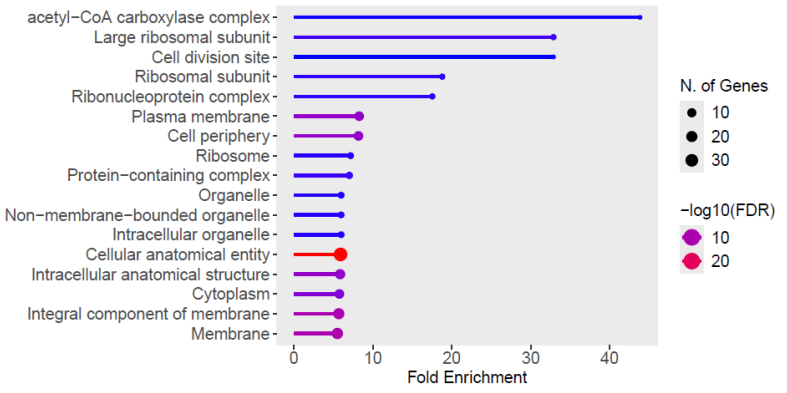

Figure A4. *Proteomic analysis: down-regulated proteins, exponential phase.*

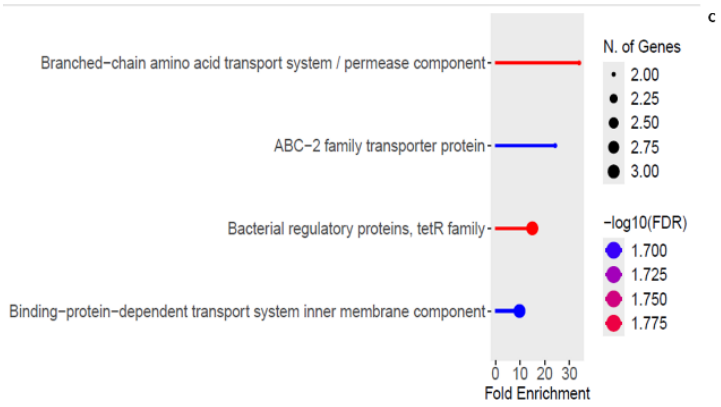

Figure A5. *Proteomic analysis: down-regulated proteins, lag phase phase.*

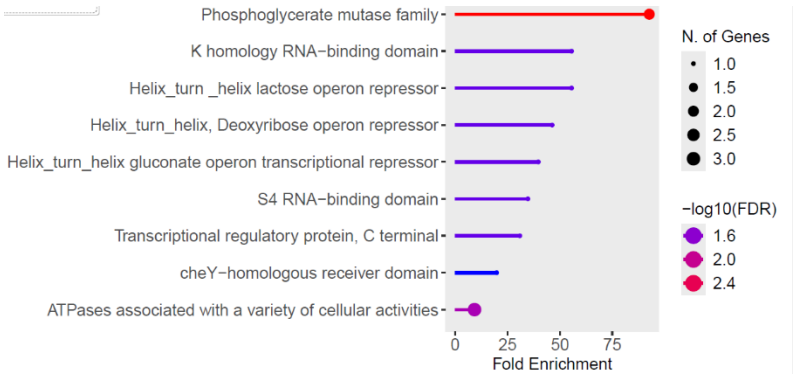

Figure A6. *MTT assay of Human Immortalized Keratinocytes (HaCaT) after 24 hours of incubation with increasing concentrations of manool.*

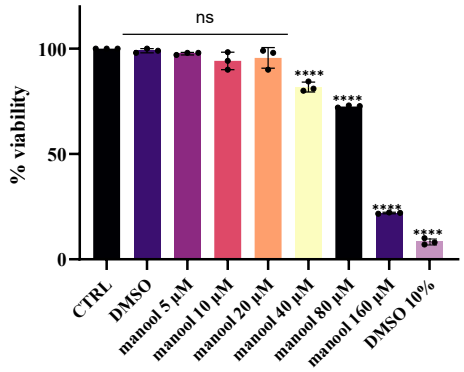

Figure A7. *Alamar blue results: % Alamar blue reduction over the time (24 hours) (A); % metabolic activity of HGF-1 cell line after 24 hours of incubation with increasing concentrations of manool (B).*

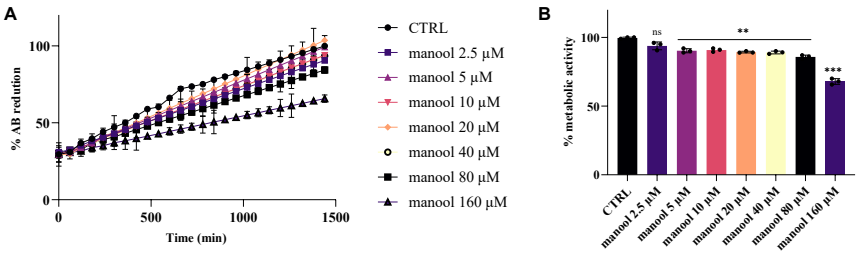

***Figure A8**. Evolution experiment: CFU/mL of S. mutans plated every week before manool increasing concentration.*

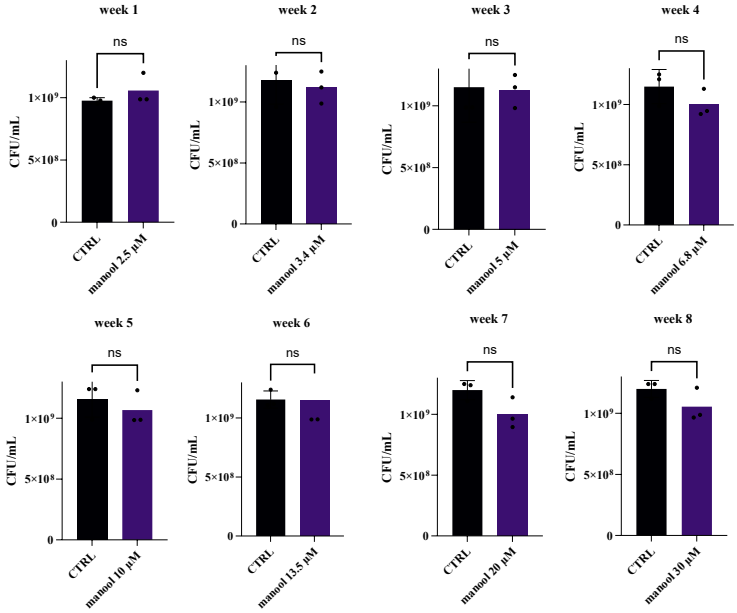

***Figure A9**. Manool activity against different clinical strains.*

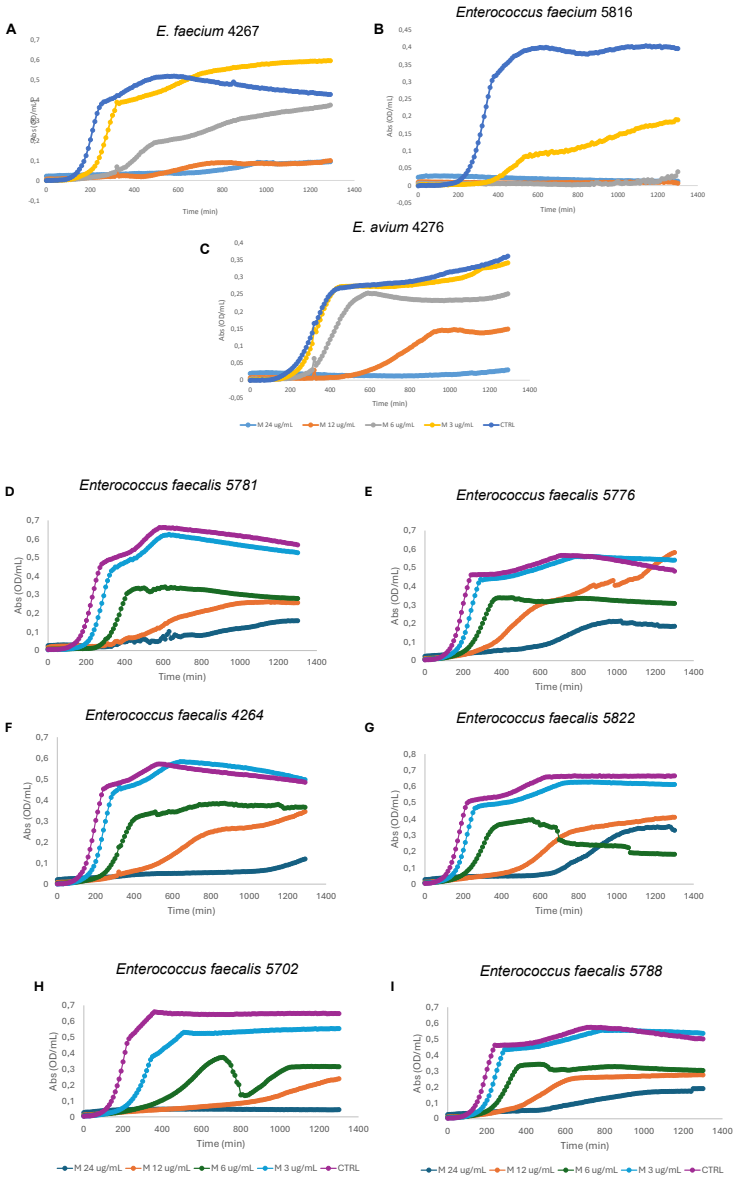

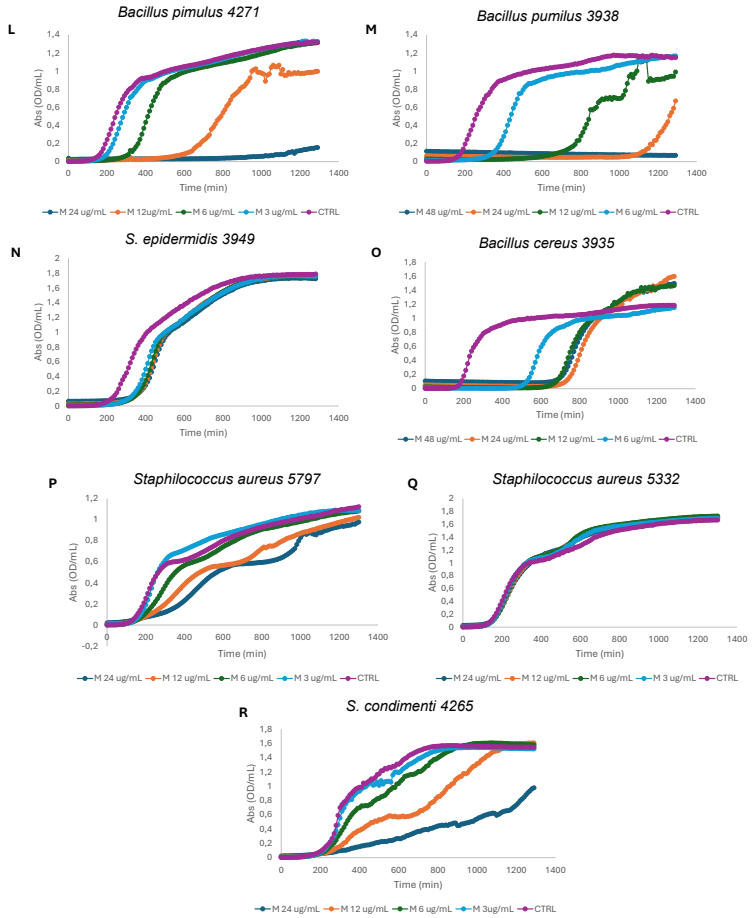

Figure A10. *Root-mean-square deviation (RMSD) of Cα atoms with respect to the starting model during the 400 ns of the MD simulation. The RMSD reaches a stable plateau, indicating that the protein structure remains conformationally stable over the analyzed time window.*

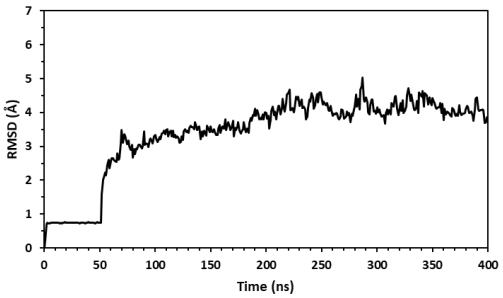

Figure A11. *Distribution of* ***cpd01*** *docking poses across different clusters. The x-axis represents the number of poses within each cluster, while the y-axis indicates the identified docking pose clusters. Clusters are sorted based on the similarity of the docking poses, highlighting the most populated binding modes. The red dashed line indicates the number of poses threshold used for selecting the most representative clusters.*

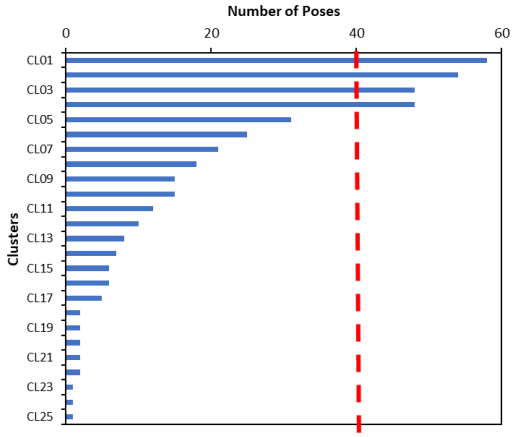

Figure A12. *Molecular dynamics analysis of the different protein–* ***cpd01*** *complexes. RMSD analysis of the* ***cpd01*** *binding pose was performed to assess the structural stability of the protein–ligand interactions throughout the simulation time.*

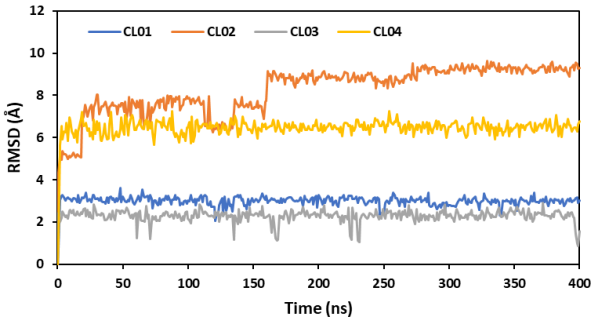

Figure A13. *Ramachandran plot of the minimized model of the multiple sugar-binding protein obtained from Modeller. The distribution of φ and ψ backbone dihedral angles shows that the majority of residues fall within the most favored and additionally allowed regions, indicating good stereochemical quality of the homology model after energy minimization.*

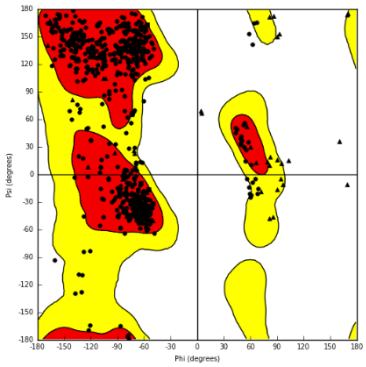

Figure A14. *^{1}H NMR spectra of manool acquired in methanol-d4*

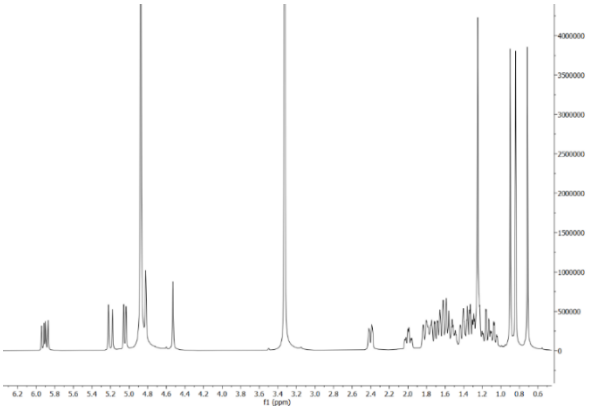

Figure A15. *Rapresentative COSY (A), HSQC (B) and HMBC (C) spectra of the supernatant collected after 420 minutes for the control group.*

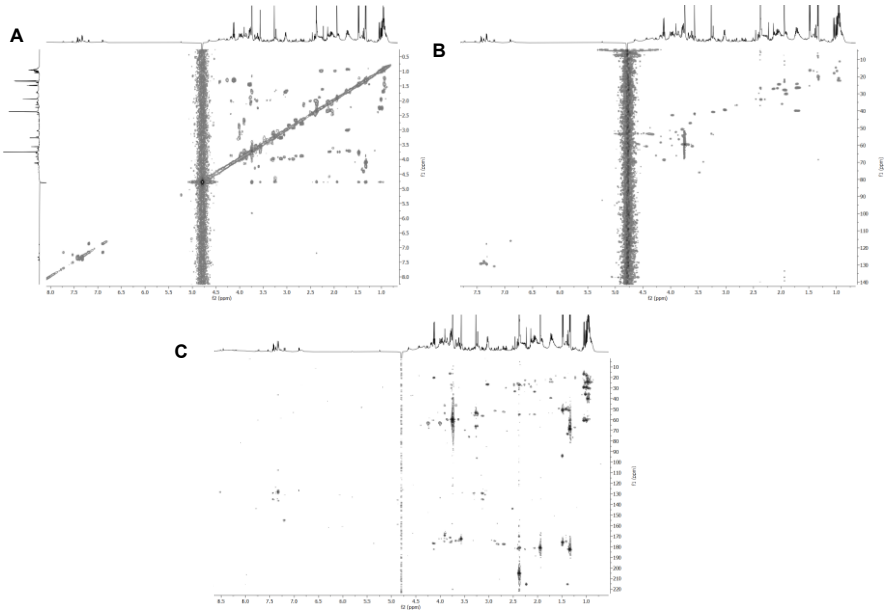

Figure A16. *Rapresentative ^{1}H NMR spectra of supernatants showing the decrease of glucose (doublets at 5.24 and 4.65 ppm, panel A) and the increase of lactic acid (doublet at 1.34 ppm, panel B) over the time.*

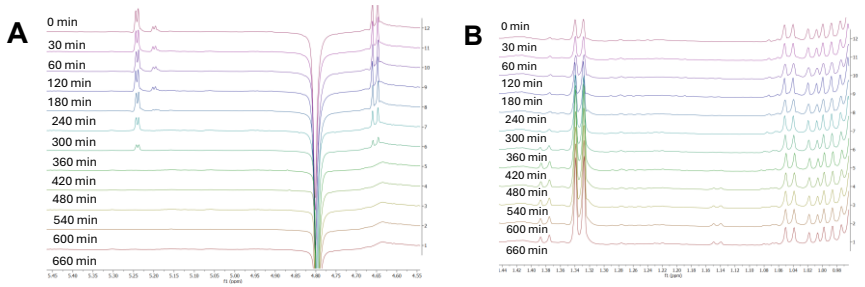

Figure A17. *Representative ^{1}H nuclear magnetic resonance (NMR) spectra (A and B) showing identified metabolites, as well as glucose (C) and lactic acid (D) spikes.*

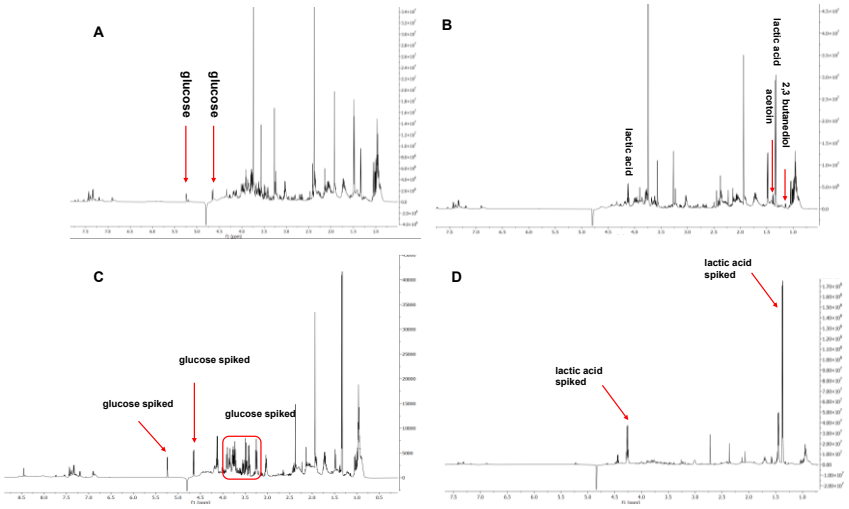

Figure A18. *The selected amino acid transitions using the MRM method were as follows: L-alanine 90 m/z ->44 m/z ; L-proline 116 m/z ->70 m/z ; L-valine 118 m/z ->55 m/z ; L-leucine/isoleucine 132 m/z ->86 m/z ; L-aspartic acid 134 m/z ->74 m/z ; L-glutamic acid 148 m/z ->84 m/z ; L-methione 150 m/z ->104 m/z; L-phenylalanine 166 m/z->103 m/z; L-arginine 175 m/z->70 m/z; L-tryptophan 203 m/z ->116 m/z*

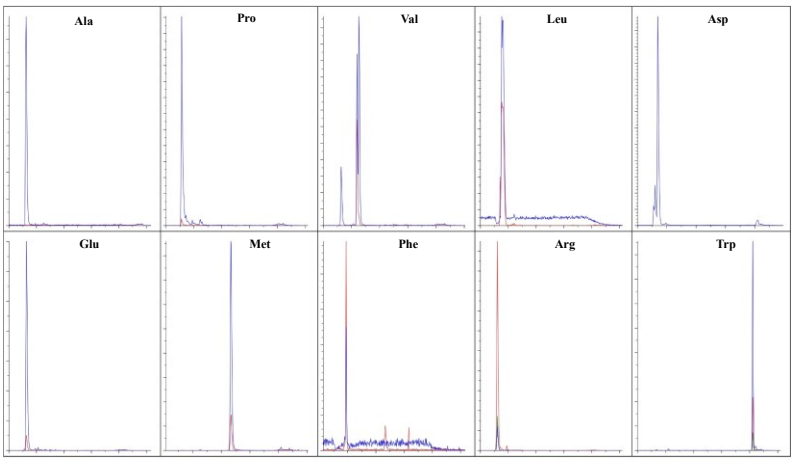

Figure A19. *Kanamycin transitions using the MRM method was as follows:485 m/z -> 163 m/z*

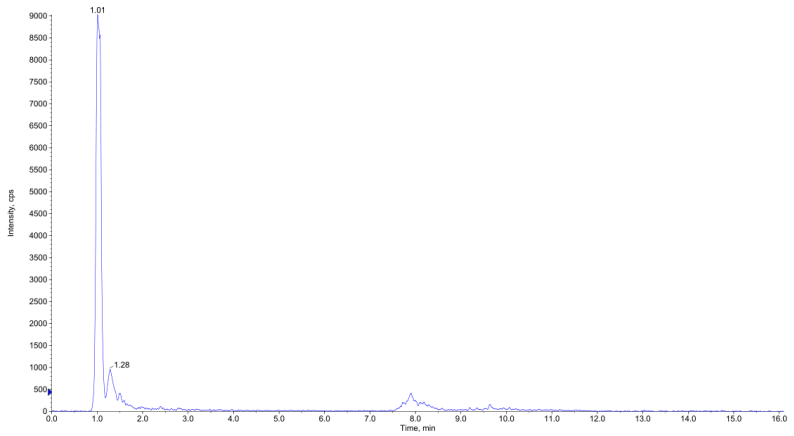

Chapter 3

Application of the new DARTS approach to bacterial cells: a tool for studying the effect of ammoresinol on *Listeria monocytogenes*

3.1 Introduction

3.1.1 Application of the bc-DARTS protocol to identify the molecular targets of ammoresinol in Listeria monocytogenes

As a part of a research strategy that aims to identify plant-derived antimicrobial compounds and elucidate their mechanisms of action through a standardised experimental workflow, the bc-DARTS (Drug Affinity Responsive Target Stability) approach described above was applied to investigate the molecular interactions of ammoresinol, a plant-derived compound with demonstrated antibacterial activity against *Listeria monocytogenes*. This project relayed on the same workflow previously developed and validated in the study of *Streptococcus mutans* and the diterpene manool. It involved selecting a bioactive plant species, identifying and structurally characterising the most active compound and then applying a proteomic approach to identify targets. This strategy was applied to the gum resin of *Ferula ammoniacum*. The crude extract was tested using a disk diffusion assay and was found to exhibit significant antimicrobial activity against the Gram-positive pathogen *Listeria monocytogenes*. The extract was then fractionated and MIC was determined for each fraction. The most active fraction was then analysed by nuclear magnetic resonance (NMR) spectroscopy, leading to the identification of a single pure compound: ammoresinol. The final goal was the identification of the main bacterial proteins

interacting with the compound using a compound-centric proteomic approach based on DARTS combined with mass spectrometry. For that purpose, the protocol previously optimized for the identification of protein targets in living *S. mutans* cells was exploited (Figure 32), thus using intact bacterial cells for the identification of protein targets in conditions that closely reproduce the physiological ones. This strategy offers key advantages over conventional lysate-based methods; among the others, it allows preserving membrane integrity and protein conformation as well as the protein-protein complexes. This is essential for detecting interactions with membrane-associated proteins. It is also essential for detecting other structurally sensitive targets. The bc-DARTS protocol was used in an attempt to identify putative protein targets that are potentially responsible for the antimicrobial activity of ammoresinol towards *L. monocytogenes*. These targets were subsequently validated using multiple strategies, as described in the following sections, to assess their functional relevance and explore the compound's potential mechanisms of action.

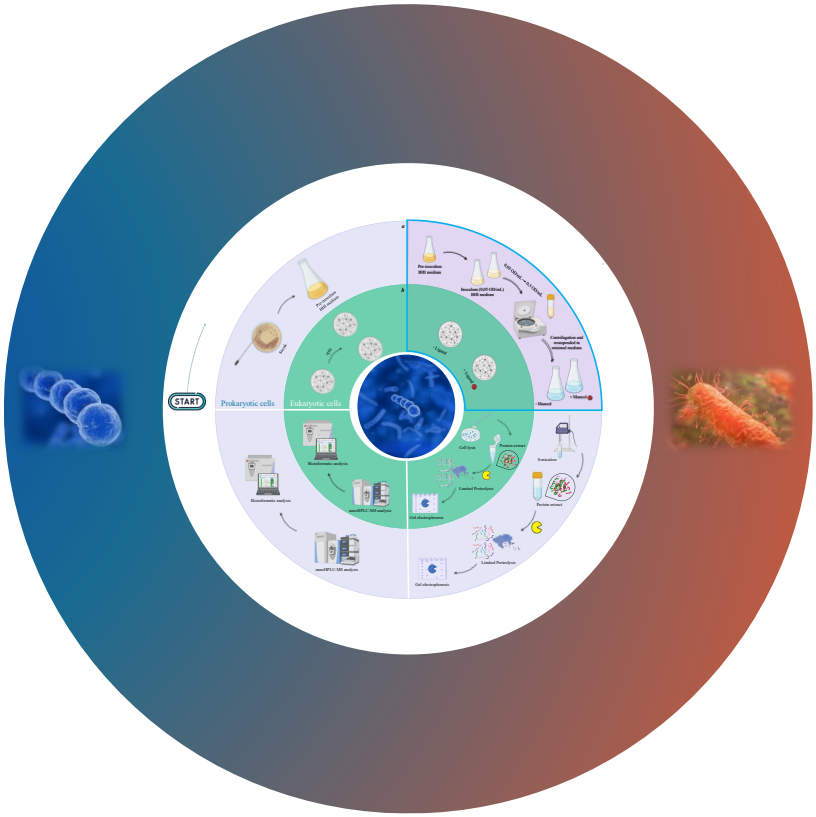

Figure 32. *Know-how transfer: the new approach bc-DARTS from S. mutans to L. monocytogenes.*

3.1.2 Ferula ammoniacum

Ferula ammoniacum (D.Don) Spalik, M.Panahi, Piwczyński & Puchałka, previousely known as *Dorema ammoniacum*, is a perennial plant that grows to 1–2 meters and from spring to early summer contains a milky juice (Figure 33-A) (Abedini et al., 2014). This plant is native to Iran, Afghanistan and central Asia. This is considered as a key medicinal species in Iran's arid and semi-arid regions, including Yazd, Isfahan and Semnan provinces (Adhami et al., 2013). Gum ammoniacum is recognized as "Ushaq" and "Vasha" in Iranian Traditional

Medicine; “Ushuk”, and “Kandar in Ayurveda; (Ahmadi et al., 2022) and "Persian ammoniacum" in Greek and Latin medicinal literatures (Alanis 2005) (Figure 33-B). It is an oleogum resin acquired as an exudate from the stem and leaf of flowering and fruiting plants of *F. ammoniacum* (Alekshun & Levy 2007). Traditionally, it is used in the treatment of catarrh, asthma, (Murray et al., 2022) (Alruways 2023) cystitis, colics, furuncles, indolent tumours, infected wound, digestive disorders, chronic bronchitis (Behpour et al., 2011). It is also used as anthelmintic agents, anticonvulsant, diapharetic, expectorant, carminative, mild diuretic, stimulant, emmenagogue and documented in the British Pharmacopoeia for its antispasmodic and expectorant properties (Alruways 2023). Additionally, gum ammoniacum has other wide range uses in food productions, confectionary, paint manufacturing, production of the detergents and mainly in production of special glues for jewellery (Ahmadi et al., 2022). Previous phytochemical investigations of gum ammoniacum exhibited the presence of sesquiterpene chromandione, sesquiterpene coumarin and sesquiterpene derivatives (Byun & Kim 2023). Several biological activities attributed to these compounds including antioxidant, antibacterial, (Calixto 2000) and antiacethylcholinesterase (Alekshun & Levy 2007).

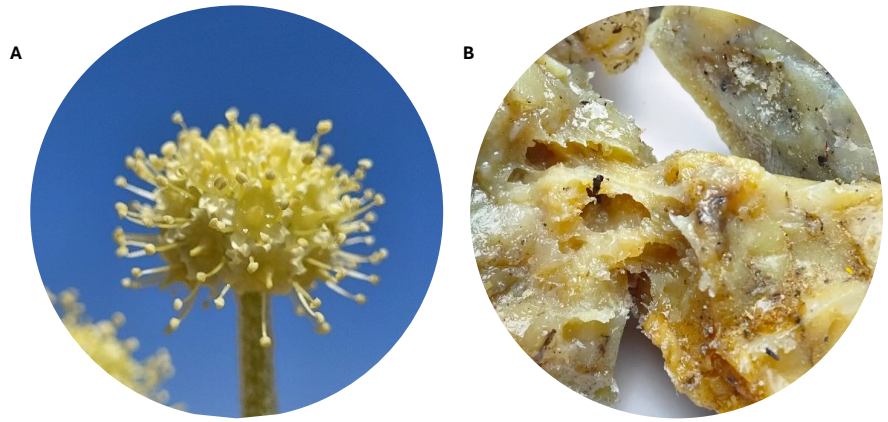

Figure 33. *Ferula ammoniacum (D.Don) Spalik, M.Panahi, Piwczyński & Puchałka, previousely known as Dorema ammoniacum (A); Gum ammoniacum (B).*

3.1.3 Ammoresinol: A Specialized Metabolite

Sesquiterpenoid coumarins represent a distinctive group of natural products predominantly isolated from various plant species, particularly within the genera *Ferula* (Apiaceae), *Daucus* (Apiaceae), *Artemisia* (Asteraceae), *Achillea* (Asteraceae), *Jatropha* (Euphorbiaceae), and *Aegle* (Rutaceae). Structurally, these compounds are characterized by the conjugation of a sesquiterpenoid moiety with a coumarin nucleus (Figure 34). The coumarin component typically derives from umbelliferone, scopoletin, or isofraxidin, while the terpenoid portion may consist of either acyclic or cyclic sesquiterpenes, contributing to a high degree of structural diversity within the class.

This structural complexity is closely linked to a wide range of biological activities exhibited by sesquiterpenoid coumarins. Numerous studies have reported their pharmacological properties, including anticancer, anti-inflammatory, antibacterial, antiviral, antiparasitic, antioxidant, and gastroprotective effects (Hussain et al., 2019). Their multifunctional bioactivity is thought to arise from their ability to interact with diverse cellular targets, often involving modulation of enzyme activity, interference with signalling pathways, or direct interaction with microbial or cancer cell membranes.

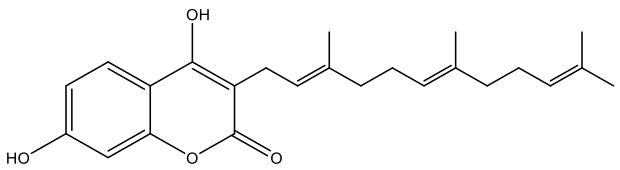

Figure 34. *Chemical structure of ammoresinol, a sesquiterpenoid coumarin ($C_{24}H_{30}O_4$).*

3.1.4 Listeria monocytogenes

Listeria monocytogenes is one of six species in the Listeria genus, belonging to the Clostridium sub-branch. It is a small, Gram-positive, rod-shaped, non-spore-forming facultative anaerobe and intracellular pathogen (Figure 35). It is acid-tolerant and psychrotolerant, meaning it can grow at low temperatures, and it is also resistant to high salt concentrations

(Cole, Jones & Holyoak 1990). It is motile at 24–28 °C due to peritrichous flagella, but becomes non-motile above 30 °C. Its widespread presence in soil and water makes it a major foodborne pathogen that causes listeriosis, a severe gastrointestinal infection. Optimal growth occurs at temperatures between 30 and 37 °C, although the bacterium can grow within a wide temperature range (1–45 °C), in up to 20% NaCl, at pH values between 4.6 and 9.5 and at water activity values (aw) as low as 0.90 (Ravindhiran et al., 2023). A key survival mechanism of *L. monocytogenes* is its ability to form biofilms, which protect the bacteria from antimicrobial treatments and physical cleaning methods while promoting adaptive and cross-protective responses (Byun & Kim, 2023).

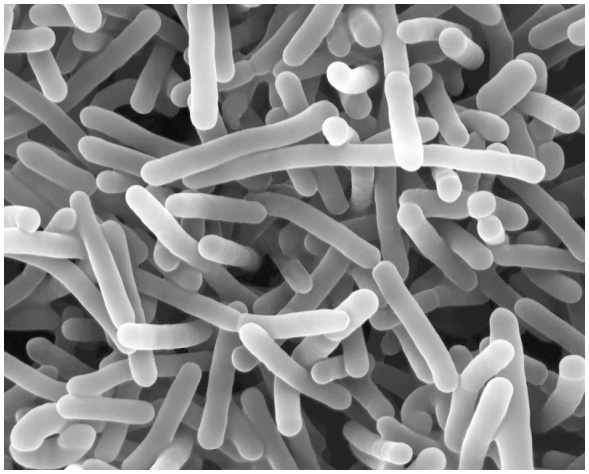

Figure 35. *Scanning Electron Microscope (SEM) image of Listeria monocytogenes. (Science Photo Library).*

3.1.4.1 Cell Wall Structure

The cell wall of Gram-positive bacteria provides protection against both mechanical and osmotic forces, while also functioning as a framework for surface proteins that are involved in sensing the environment. It also plays a role in permeability, adhesion and surface hydrophobicity (Neuhaus & Baddiley 2003). The wall is primarily composed of a thick layer of peptidoglycan, which contains alternating units of N-acetylglucosamine (NAG) and N-acetylmuramic acid (NAM) that are cross-linked to provide rigidity. Additional components include teichoic acids, lipoteichoic acids and polyphosphates (Figure 36). Peptidoglycan biosynthesis occurs in three stages, namely cytoplasmic synthesis of UDP-linked precursors, membrane-associated formation of lipid intermediates (Lipid I

and II) involving the carrier bactoprenol, and extracellular polymerization and crosslinking. Key enzymes in these processes include MurA, MurF and MurG (Scheffers & Pinho 2005).

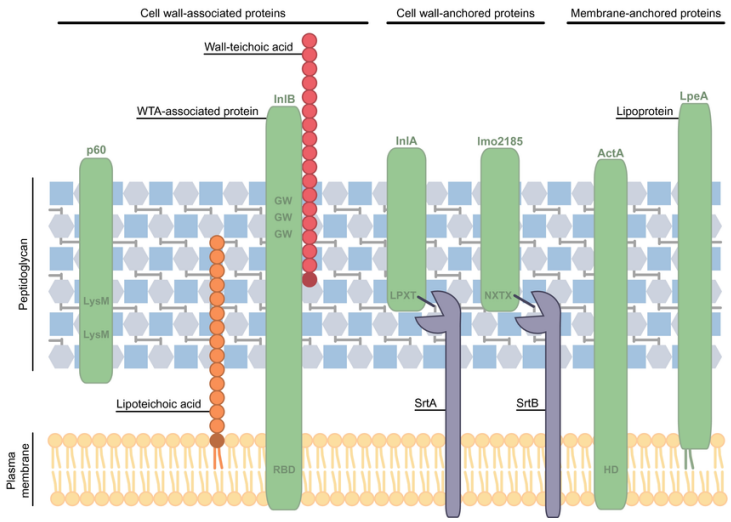

Figure 36. *Cell wall structure of L. monocytogenes, illustrating the main structural components and surface molecules that contribute to bacteria virulence (Sumrall et al., 2020).*

3.1.4.2 Virulence Factors

L. monocytogenes can invade both phagocytic (e.g., macrophages) and non-phagocytic (e.g., epithelial) cells. After internalization, the bacterium escapes from the phagosome to replicate in the host cytosol, using a cluster of virulence genes. Central to this process is the transcriptional regulator PrfA

(Figure 37), which activates genes required for invasion, intracellular survival and cell-to-cell spread, including *hly*, *plcA*, *plcB*, *actA*, *mpl* and *mprF* (Portnoy et al., 1992). Listeriolysin O (LLO), encoded by *hly*, is a pore-forming toxin essential for phagosomal escape; Phospholipases PlcA and PlcB and the metalloprotease Mpl, support vacuole disruption and spread between cells; ActA enables intracellular motility by hijacking the host actin cytoskeleton (Pizarro-Cerdá & Cossart 2006); MprF, a membrane-associated protein, contributes to resistance against cationic antimicrobial peptides (CAMPs) by modifying the membrane with lysyl-phosphatidylglycerol, reducing its negative charge and increasing resistance to host defences and certain antibiotics such as vancomycin. This sophisticated arsenal of virulence factors allows *L. monocytogenes* to persist in hostile environments, evade immune responses and cause systemic infections.

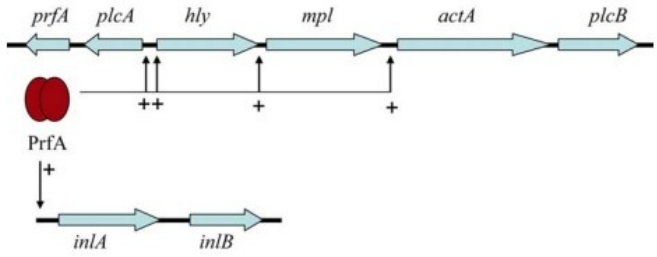

Figure 37. *Representation of the L. monocytogenes pathogenicity island which encodes the central virulence regulator prfA and associated genes essential for intracellular survival and pathogenicity. The island includes factors involved in host cell invasion and escape from the phagosome highlighting the pivotal role in the virulence of L. monocytogenes (Vázquez-Boland et al., 2001).*

3.2 Material and Methods

3.2.1 Plant Material

Gum ammoniacum was purchased from an herbal medicine shop in Shahroud in September 2017. The plant and its gum were sourced from their natural habitat and authenticated by the expert botanist Dr. A. Sonboli. A voucher specimen (MPH-2945) was deposited at the Herbarium of the Medicinal Plants and Drugs Research Institute, Shahid Beheshti University, Tehran, Iran.

3.2.2 Extraction and Purification

Gum ammoniacum (2.0 kg) was ground and then subjected to maceration using ethyl acetate (3 × 10 L, with each maceration lasting 48 hours). The extract was evaporated under vacuum, yielding 890 g of a brown gum. The amount of 800 g was separated via silica gel column chromatography (10 cm diameter, 70−230 mesh, 2 kg) using a gradient elution from *n*-hexane to ethyl acetate (100:0 → 0:100), followed by a stepwise increase of methanol (up to 40%) in ethyl acetate. All 400 collected fractions (250 mL each) were monitored by TLC [UV 254 nm; $Ce(SO_4)_2$-H_2SO_4 visualization] and pooled into 16 combined fractions F_1− F_{16} (Figure 38).

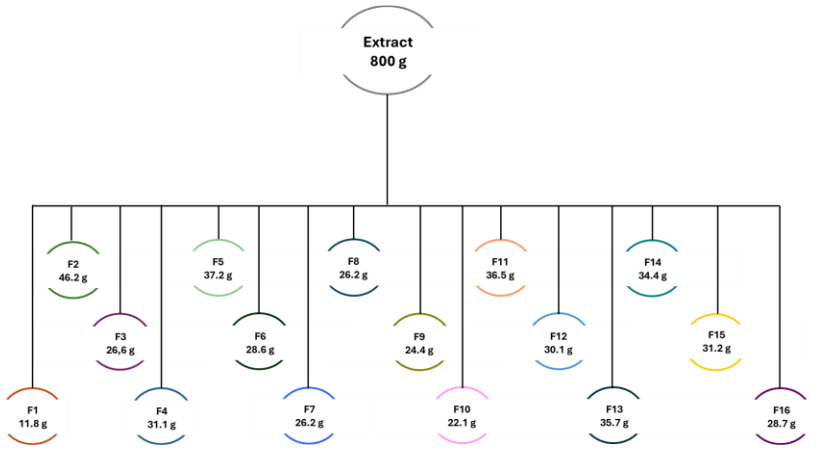

Figure 38. *Extract separation diagram.*

Ammoresinol (30 mg) was was purified as colorless crystals (> 98% purity) by recrystallizing a part (100 mg) of fraction F9 in *n*-hexane (Figure 39).

Figure 39. *Fraction F9 after recrystallization and Ammoresinol*

Its structure was confirmed by extensive 1D and 2D-NMR spectroscopic data, including ^{1}H NMR, ^{13}C NMR, DEPT-90, DEPT-135, ^{1}H- ^{1}H COSY, HSQC, and HMBC (Figure 40).

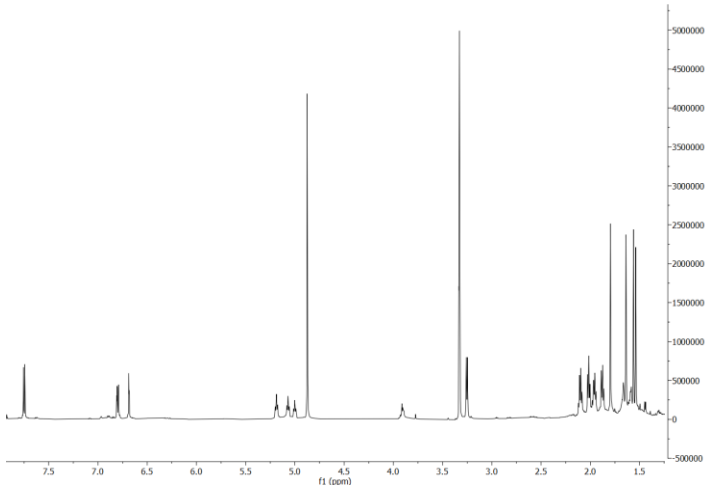

Figure 40. *^{1}H NMR spectra of ammoresinol acquired in methanol-d4*

3.2.3 Disk Diffusion Assay

The first screening of potential antimicrobial activity of (gum ammoniacum) was evaluated using the disk diffusion method (Hombach et al., 2015). The bacterial strains tested included *Escherichia coli*, *Staphylococcus aureus*, *Klebsiella spp.*, *Streptococcus mutans*, *Citrobacter spp.*, *Salmonella spp.*, *Bacillus subtilis*, *Shigella spp.*, *Enterococcus faecalis*, *Bacillus clausii*, *Pseudomonas aeruginosa*, *Acinetobacter baumannii*, *Streptococcus epidermidis*, and *Listeria monocytogenes*. Briefly, fresh colonies were used to prepare an inoculum at 0.5 McFarland turbidity. Suspensions of the tested microorganisms

were prepared in Brain Hearth Infusion (BHI) medium. After 24 h the cells were adjusted to 0.5 McFarland standard turbidity (0.08-0.1 OD/mL) and were spread on solid media plates. Sterile filter paper discs (Ø=6 mm) were placed on inoculated media with light pressure and impregnated with 10 µL of the *Ferula ammoniacum* extract. Ampicillin (20 µg) was used as a standard antimicrobial drug. A sterilized disc containing BHI (5 µL) with 1% MetOH was used as a negative control sample. Plates were incubated at 37 °C for 24 h. The diameter of the inhibition zones (mm) was measured. and the results were expressed as positive or negative effect on bacteria strains.

3.2.4 Minimal Inhibitory Concentration (MIC) and Growth curve of Listeria monocytogenes

Samples were dissolved in 100% Methanol (MeOH) at different concentrations (fractions: from 50 to 6.25 µg/mL), added to each well and bacterial suspensions (0.5×10^5 CFU/mL), and then incubated at 37 °C for 24 h (for experimental detailed see section 2.2.4). The growth curves of *L. monocytogenes* were performed in flasks with and without ammoresinol (for experimental detailed see section 2.2.5). Ammoresinol was added to three of the four flasks at concentrations of 5 µg/mL, 10 µg/mL and 20 µg/mL, respectively. The flasks were then left to incubate at 37°C, with constant agitation. The first sample was taken after 60 minutes, and subsequent samples were taken at regular intervals of 10 minutes. Growth was quantified using a spectrophotometer at a wavelength of 600 nm. The

change in absorbance of each flask was monitored for 900 minutes.

3.2.5 Drug Affinity Responsive Target Stability Assay on protein extract (pe-DARTS) and on bacterial cells (bc-DARTS)

The DARTS assay was initially performed by incubating ammoresinol with a protein extract (pe-DARTS) from *L. monocytogenes*, followed by limited proteolysis, SDS-PAGE analysis of digestion products, and proteomic identification of the separated proteins. *L. monocytogenes* cells from inoculum were centrifuged at 3000 rpm for 10 minutes; the pellets were then resuspended in 25 mM MOPS buffer to a density of 50 OD/ml. Next, 50 OD of cells were lysed by sonication at an amplitude of 10 for 30 minutes, with 10 seconds ON and 10 seconds OFF. The lysates were centrifuged at 15,000 rpm for 20 minutes, and the supernatant was transferred into sterile Eppendorf tubes. The protein content of the supernatant was quantified using the Bradford method. For the DARTS assay, 50 µg of proteins were aliquoted for both control and treated samples. The treated sample for the pe-DARTS assay was incubated with ammoresinol (20 µg/mL) for 30 minutes at 4°C. The lysates were then digested with subtilisin (enzyme:protein ratio of 1:2000) at 37°C for 30 minutes. The resulting protein mixtures were separated by one-dimensional polyacrylamide gel electrophoresis (SDS-PAGE). The gel bands were then analyzed by LC-MS/MS using an Orbitrap Q-Exactive mass

spectrometer (Thermo Fisher Scientific), equipped with a nano-ESI source, coupled to an UHPLC nanoUltimate 3000 system (Thermo Fisher).

The bc-DARTS assay involved the incubation of ammoresinol with *L. monocytogenes* bacterial cells, followed by proteolysis, SDS-PAGE analysis and LC-MS. The *L. monocytogenes* overnight inoculum was centrifuged at 3000 rpm for 15 minutes and the cells were resuspended in BHI medium to a density of 0.05 OD/ml. The cells were incubated at 37°C and cultured to the established optical densities (0.5 OD/ml and 1 OD/ml). Then cells were centrifuged at 3000 rpm for 15 minutes. After discarding the supernatant, the pellet was resuspended in M9 minimal medium 1X supplemented with 0.4% glucose for both control and treated samples, at a density of 0,5 OD/ml and 1 OD/mL. The treated samples were incubated with ammoresinol at 1 µg/mL, 5 µg/mL and 10 µg/mL for 90 minutes. The samples were then centrifuged at 3000 rpm for 10 minutes. After discarding the supernatant, the pellets were resuspended in 25 mM MOPS buffer. The cells were then lysed by sonication at an amplitude of 10 for 30 minutes, with 10 seconds ON and 10 seconds OFF. The lysates were centrifuged at 15,000 rpm for 20 minutes, and the supernatant was transferred into sterile Eppendorf tubes. The protein content of the supernatant was quantified using the Bradford method. For the DARTS assay, 50 µg of proteins were aliquoted for control and treated samples. The lysates were then digested with subtilisin (enzyme:protein ratio of 1:2000) at 37°C for 30 minutes. The

resulting protein mixtures were separated by SDS-PAGE. The gel bands were digested following the previously described protocol and subsequently analyzed by LC-MS under the same conditions.

3.2.6 Western Blot

pe-DARTS and bc-DARTS samples were also subjected to western blot analyses. proteins samples (20 µg) underwent DARTS protocol were fractionated on SDS-PAGE and transferred into nitrocellulose membranes. After electro transferring, the nitrocellulose membrane was coloured with Red Ponceau, to verify the transferring and then the nitrocellulose membrane was blocked with 10% non-fat dry milk for 2 h at room temperature and then immunoblotted with appropriate primary antibodies, against prfA (Invitrogen), O/N at 4 °C. The signals were visualized with the appropriate horseradish peroxidase-conjugated secondary antibody and enhanced chemiluminescence (Amersham Biosciences-GE Healthcare, NY, USA).

3.3 Result and Discussion

3.3.1 Evaluation of the antibiotic action of the F. ammoniacum extract

3.3.1.1 Disk diffusion assay

The antimicrobial efficacy of *F. ammoniacum* extract against several bacterial strains was evaluated using the inhibition zone

method, a microbiological technique. This method involves observing the formation of an area free of bacterial growth around a disc soaked with the extract. The screened strains included both Gram-positive and Gram-negative bacteria (see Materials and Methods). The extract obtained from the gum resin was tested at a concentration of 500 µg/mL and exhibited significant activity against *L. monocytogenes*, as determined by the diameter (mm) of the inhibition zone formed. The observed antibacterial activity in the extract may be related to its complex composition or may mainly depend on individual molecules with antimicrobial properties. To investigate this further, the extract was separated into different fractions, whose antimicrobial activity was measured to identify those responsible for the observed effects.

3.3.1.2 Minimal Inhibitory Concentration and growth curve

The analysis of antibacterial activity of the fractions, obtained following a bio-guided chromatographic separation, was carried out in BHI for *L. monocytogenes*. The samples were dissolved in 100% Methanol (MeOH) at different concentrations (fractions: from 50 to 6.25 µg/mL), added to each well and bacterial suspensions (0.5×10^5 CFU/mL), and then incubated at 37 °C for 24h (Table 7).

Table 7. *The minimal Inhibitory concentration of most promising Fractions against L. monocytogenes*

Fractions	MIC_{100} (µg/mL)
F6	-
F7	50
F8	>50
F9	<25
F10	>50

As showed in Table 7, F9 exerted the most promising activity against *L. monocytogenes*. Spectroscopic and spectrometric analyses revealed that this fraction contains as largely prominent component ammoresinol. Subsequentially, F9 was subjected to recrystallization to obtain the pure compound. Consequently, the minimal inhibitory concentration of ammoresinol towards *L. monocytogenes* was determinate. As showed in Figure 41, 20 µg/mL is the MIC of ammoresinol for *L. monocytogenes.*

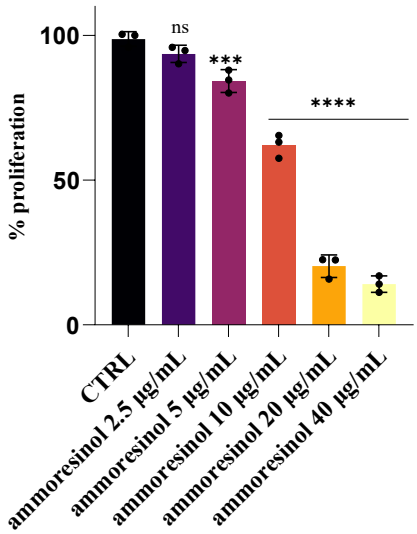

Figure 41. *Determination of the minimal inhibitory concentration (MIC) of ammoresinol against L. monocytogenes. Bacterial cultures were incubated for 24 hours at 37°C in the presence of increasing concentrations of ammoresinol (2.5–40 µg/mL) or vehicle control. Bacterial growth was evaluated by measuring the optical density of the medium at 600 nm (OD_{600}).*

To evaluate the effects of ammoresinol on *L. monocytogenes* proliferation, the bacterial growth was monitored for 900 min, starting from a bacteria-containing medium with a 0.05 OD/ml in the absence of the compound and in the presence of four concentrations of ammoresinol (2.5 µg/mL, 5 µg/mL, 10 µg/mL and 20 µg/mL) (Figure 42). The results showed a significant decrease in the slope of the exponential phase when *L. monocytogenes* was incubated with ammoresinol. Interestingly, although some prolongation of the lag phase was observed, in this case it was clearly less drastic than in the case of *S. mutans* treated with manool.

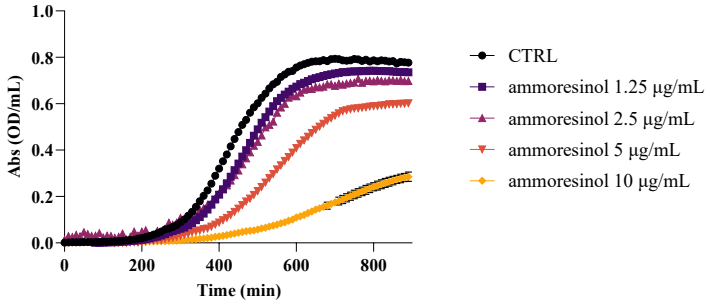

Figure 42. *Growth curve of L. monocytogenes in BHI broth with supplementation of ammoresinol (0, 1.25, 2.5, 5, 10 µg/mL). Bacterial proliferation was monitored by measuring the* OD_{600} *every 10 minutes for 900 minutes.*

By analysing changes in metabolic pathways and protein expression profiles, it would be possible to identify specific cellular processes that are affected by ammoresinol. Such studies could provide insights into the mechanisms behind the prolonged lag phase, revealing how the compound impacts bacterial metabolism, stress response and cell division under a molecular point of view.

3.3.3 Target proteins identified using the DARTS (Drug Affinity Responsive Target Assay) assay

Given the efficacy and the reliability of bc-DARTS approach implemented in the research of manool targets in *S. mutans*, the same method was used here. Indeed, form the one hand this could lead to the identification of ammoresinol intracellular targets, on the other hand this could provide a further validation of the protocol, demonstrating that its applicability is not limited to a single bacterial species. The combination of in vitro (pe-

DARTS) and in vivo (bc-DARTS) analyses enabled the identification of a set of putative protein targets of ammoresinol in *L. monocytogenes* (Table 8). Merging the results from both approaches generated a shortlist of the most reliable interactors, strengthening confidence in the specificity and biological relevance of these interactions. The identified proteins cover several functional categories, including key components of the bacterial cell wall biosynthesis machinery such as MurA1, MurA2, MurE, MurF, MurG, MurI and MreC. The presence of these targets suggests that ammoresinol may impair cell wall formation, ultimately affecting bacterial proliferation. Additionally, proteins involved in virulence regulation (PrfA), stress response (GrpE) and immune evasion (PlcA, MprF and Iap) were detected, suggesting that ammoresinol may interfere with multiple critical cellular processes for bacterial survival and pathogenicity. Several of these proteins are notably membrane-associated or peripherally exposed, which supports the hypothesis that ammoresinol primarily interacts at the bacterial envelope level, as observed in bc-DARTS experiments. The findings emphasise the effectiveness of the dual DARTS approach in identifying significant molecular targets, confirming it as a valuable asset for pinpointing antimicrobial targets, especially for natural substances with intricate or until now unexplained mechanisms of action.

Table 8. *Putative ammoresinol protein targets identified by DARTS assays*

Gene ID	Molecular Weight (kDa)	Description
P34024	36.32	PlcA protein. Synthesizes phosphatidylinositol-specific phospholipase C, which disrupts phagosomal vacuoles, enabling immune evasion.
P0DJM3	21.91	GrpE protein. Involved in the cellular response to hyperosmotic stress and heat shock.
P22262	27.30	PrfA protein. Transcriptional regulator of virulence factors.
Q8Y4H1	37.00	NamA dehydrogenase. Catalyzes the reduction of nitro groups in nitroesters and nitroaromatic compounds; potentially involved in detoxification processes.
Q8Y6I9	97.60	MprF protein. Confers resistance to cationic antimicrobial peptides produced by the host immune system.
Q8Y5L9	53.74	MurE protein. Catalyzes the addition of meso-diaminopimelic acid to the UDP-N-acetylmuramoyl-L-alanyl-D-glutamate precursor in peptidoglycan biosynthesis.
Q8Y4C4	45.97	MurA1 protein. Involved in the early steps of bacterial cell wall biosynthesis.
Q8Y4A2	45.10	MurA2 protein. Involved in the early steps of bacterial cell wall biosynthesis.
Q8Y7N7	29.16	MurI protein. Supplies D-glutamate required for cell wall biosynthesis.
Q8Y8P0	50.46	MurF protein. Catalyzes the final step in the formation of the UDP-MurNAc-pentapeptide precursor for peptidoglycan synthesis.
Q8Y5M2	39.01	MurG protein. Catalyzes the synthesis of lipid I and lipid II intermediates in peptidoglycan biosynthesis.
Q8Y6Y4	32.09	MreC protein. Plays a key role in maintaining cell shape and is involved in peptidoglycan synthesis.
P21171	50.58	Iap protein. Encodes a murein hydrolase associated with cell invasion; essential for proper cell division.

3.3.4 Validation of PrfA as ammoresinol target

Most virulence genes of *L. monocytogenes* are activated by the transcriptional regulator PrfA. Previous studies have shown that environmental parameters, such as temperature, pH, stress conditions and medium composition, affect the expression of PrfA and PrfA-dependent proteins. PrfA is the major regulator of virulence genes in *L. monocytogenes*

(Renzoni, Cossart & Dramsi 1999). Given the critical role played by this protein DARTS results were validated. Therefore, protein samples obtained from the pe/bc DARTS assay were analyzed by Western blotting using a specific antibody against prfA. This protein has emerged as an ammoresinol putative target since in DARTS assay a protection from proteolysis upon treatment with ammoresinol was detected. Indeed, according to the DARTS principle, binding a small molecule to a target protein can induce conformational stabilisation, resulting in increased resistance to proteolytic degradation. The results of WB analysis clearly showed a differential pattern of prfA digestion between treated and untreated samples (Figure 43). In the control condition, where no ammoresinol was added, prfA was completely degraded, as evidenced by the absence of detectable bands on the blot. Conversely, for pe-DARTS and bc-DARTS samples incubated with ammoresinol a strong and intact band of prfA was observed, indicating a protection against subtilisin digestion.

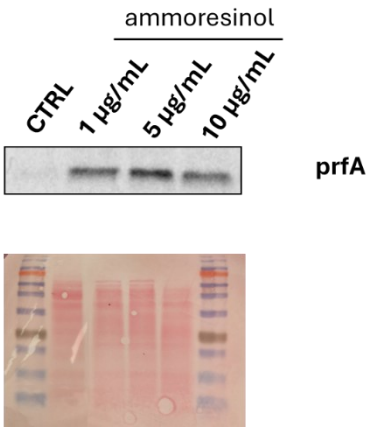

Figure 43. *Western blot analysis. L. monocytogenes was treated with 1 µg/mL, 5 µg/mL and 10 µg/mL of ammoresinol in a minimal media following the new bc-DARTS approach. Subsequentially, proteins were digested with subtilisin in a ratio of 1:2000. A WB-based measurement of prfA following the different treatments was performed. The results of the resulting bands, compared to Red Ponceau intensity are reported.*

This result confirms that ammoresinol by binding prfA, led to a stabilization of prfA structure by protecting this latter to protease hydrolysis. Moreover, the observed protection is consistent with a ligand-induced conformational change that enhances protein stability, thus confirming the specificity of the binding event.

3.4 Conclusion

The study of *Ferula ammoniacum* as a source of new bioactive compounds led to discover the potential of *F. ammoniacum* extract against *L. monocytogenes.* Subsequentially, the isolation and purification of ammoresinol, a sesquiterpenoid coumarin was performed. Antimicrobial assays, such as the

Minimal Inhibitory Concentration (MIC) and growth studies showed the significant activity of ammoresinol against *L. monocytogenes.* In order to investigate the target of ammoresinol in *L. monocytogenes* and even more to validate the new approach on live bacterial cells, DARTS experiments were carried out. The new bc-DARTS applied in live bacterial cells has proven affective not only in original application but also when extended to different systems. In more detail, it enabled the study of another target in a different bacterium using a distinct molecule. This finding highlights the versatility of the new methodology, opening avenues for further investigations across diverse bacteria and compounds. Moreover, the results obtained by DARTS assay and subsequent western blot analysis provide strong evidence of a direct interaction between ammoresinol and prfA, encompassing to the pathogenicity island of *L. monocytogenes*. The partial protection of the protein from protease degradation in the presence of ammoresinol indicates a ligand-induced stabilization, corresponding to specific binding. This result is particularly significant given the established role of proteins encoded by *Listeria* pathogenicity island in mediating virulence (Coelho et al., 2019). In fact, proteins within this genomic region, such as listeryolisin O, phospholipases and other virulence factors, are essential for bacterial survival and dissemination within the host (Kayal & Charbit 2006). These proteins allow Listeria to escape from phagosome, promote intracellular replication and facilitate cell-

to-cell spread, thus contributing to systemic infection. The binding with ammoresinol suggests that its functional activity could modulates, with potential consequences for the pathogenic process (Lee, S., 2020). If ammoresinol interferes with virulence proteins, it may attenuate *L. monocytogenes* ability to invade host tissues and establish infection. These findings highlight the therapeutic potential of targeting virulence factors. By impairing the activity of proteins encoded within the pathogenicity island it could be possible to reduce the severity of infection while minimizing selective pressure for resistance.

Chapter 4

Conclusions and future prospectives

Conclusions and future prospective

This PhD thesis has provided new insights into the mechanisms of antibiotic resistance and the potential of natural molecules as modulators of bacterial physiology. By optimizing and applying Drug Affinity Responsive Target Stability (DARTS) directly to bacterial cells using a minimal medium for the first time in these conditions, this project has established a methodological framework that significantly advances the study of small molecule-proteins interactions in living bacterial cells. DARTS assay performed under these novel experimental conditions have enabled the identification of protein targets in their native physiological context, thus overcoming the limitations of lysate-based approaches. The use of natural compounds as investigative tools has revealed their capacity not only to interfere with essential bacterial processes but also to reduce the antibiotic resistance to conventional antibiotics, thus suggesting a role of the natural products also as a coadjutant of conventional antibiotics. Moreover, this thesis underscores the value of combining innovative proteomic methodologies with natural product research to in deeper understand antibiotic resistance mechanisms. The results could not only contribute to the fundamental knowledge of bacterial adaptation but even more they could be important for the development of novel antimicrobial strategies. In conclusion, this PhD project establishes a methodological and conceptual framework that connects proteomic innovation with natural product research. This work makes two important

contributions. Firstly, it enables direct identification of protein targets in living bacterial cells. Secondly, it demonstrates the modulatory potential of natural molecules. This means it helps both fundamental microbiology and applied antimicrobial discovery. The perspectives outlined here highlight the potential for future studies to expand these findings towards translational applications, which, ultimately, could support the development of effective and sustainable strategies to combat antibiotic resistance, one of the most pressing challenges in global health.

References

Abedini, A., Roumy, V., Mahieux, S., Gohari, A., Farimani, M. M., Rivière, C., ... & Hennebelle, T. (2014). Antimicrobial activity of selected Iranian medicinal plants against a broad spectrum of pathogenic and drug multiresistant micro-organisms. Letters in applied microbiology, 59(4), 412-421.

Adhami, H. R., Lutz, J., Kählig, H., Zehl, M., & Krenn, L. (2013). Compounds from gum ammoniacum with acetylcholinesterase inhibitory activity. Scientia pharmaceutica, 81(3), 793.

Ahmadi, E., Rezadoost, H., Alilou, M., Stuppner, H., & Farimani, M. M. (2022). Purification, structural characterization and antioxidant activity of a new arabinogalactan from Dorema ammoniacum gum. International Journal of Biological Macromolecules, 194, 1019-1028.

Ajdić, D., McShan, W. M., McLaughlin, R. E., Savić, G., Chang, J., Carson, M. B., ... & Ferretti, J. J. (2002). Genome sequence of Streptococcus mutans UA159, a cariogenic dental pathogen. Proceedings of the National Academy of Sciences, 99(22), 14434-14439.

Alanis, A. J. (2005). Resistance to antibiotics: are we in the post-antibiotic era?. Archives of medical research, 36(6), 697-705.

Alekshun, M. N., & Levy, S. B. (2007). Molecular mechanisms of antibacterial multidrug resistance. Cell, 128(6), 1037-1050.

Alruways, M. W. (2023). Antimicrobial effects of Ferula species-an herbal tactic for management of infectious diseases. Journal of King Saud University-Science, 35(7), 102806.

Anagnostou, M., Tomou, E. M., Krigas, N., & Skaltsa, H. (2025). Phenolic constituents of Greek native Salvia species: a comprehensive review. Phytochemistry Reviews, 1-81.

Avato, P., Fortunato, I. M., Ruta, C., & D'Elia, R. (2005). Glandular hairs and essential oils in micropropagated plants of Salvia officinalis L. Plant Science, 169(1), 29-36.

Banyal, A., Tiwari, S., Sharma, A., Chanana, I., Patel, S. K. S., Kulshrestha, S., & Kumar, P. (2023). Vinca alkaloids as a potential cancer

therapeutics: recent update and future challenges. *3 Biotech*, *13*(6), 211.

Behpour, M., Ghoreishi, S. M., Khayatkashani, M., & Soltani, N. (2011). The effect of two oleo-gum resin exudate from Ferula assa-foetida and Dorema ammoniacum on mild steel corrosion in acidic media. Corrosion science, 53(8), 2489-2501.

Ben Farhat, M., Jordán, M. J., Chaouech-Hamada, R., Landoulsi, A., & Sotomayor, J. A. (2009). Variations in essential oil, phenolic compounds, and antioxidant activity of tunisian cultivated Salvia officinalis L. Journal of Agricultural and Food Chemistry, 57(21), 10349-10356.

Berlutti, F., Catizone, A., Ricci, G., Frioni, A., Natalizi, T., Valenti, P., & Polimeni, A. (2010). Streptococcus mutans and Streptococcus sobrinus are able to adhere and invade human gingival fibroblast cell line. International Journal of Immunopathology and Pharmacology, 23(4), 1253-1260.

Birhanu, A. G. (2023). Mass spectrometry-based proteomics as an emerging tool in clinical laboratories. Clinical proteomics, 20(1), 32.

Bisio, A., Schito, A. M., Pedrelli, F., Danton, O., Reinhardt, J. K., Poli, G., ... & De Tommasi, N. (2020). Antibacterial and ATP synthesis modulating compounds from Salvia tingitana. Journal of natural products, 83(4), 1027-1042.

Bobate, S., Mahalle, S., Dafale, N. A., & Bajaj, A. (2023). Emergence of environmental antibiotic resistance: Mechanism, monitoring and management. Environmental Advances, 13, 100409.

Borris, R. P. (1996). Natural products research: perspectives from a major pharmaceutical company. Journal of ethnopharmacology, 51(1-3), 29-38.

Botelho, M. G. (2000). Fractional inhibitory concentration index of combinations of antibacterial agents against cariogenic organisms. Journal of Dentistry, 28(8), 565-570.

Brooker, S. G., Cambie, R. C., & Cooper, R. C. (1989). Economic native plants of New Zealand. Economic Botany, 43(1), 79-106.

Byun, K. H., & Kim, H. J. (2023). Survival strategies of Listeria monocytogenes to environmental hostile stress: biofilm formation and stress responses. Food Science and Biotechnology, 32(12), 1631-1651.

Calixto, J. B. (2000). Efficacy, safety, quality control, marketing and regulatory guidelines for herbal medicines (phytotherapeutic agents). Brazilian Journal of medical and Biological research, 33, 179-189.

Case, D. A., Aktulga, H. M., Belfon, K., Ben-Shalom, I. Y., Berryman, J. T., Brozell, S. R., ... & Kollman, P. A. (2023). Amber 2023. University of California, San Francisco.

Chaachouay, N., & Zidane, L. (2024). Plant-derived natural products: a source for drug discovery and development. *Drugs and Drug Candidates*, *3*(1), 184-207.

Chen, X., Niu, X., Li, L., Chen, K., Song, D., Chen, B., ... & Wu, Z. (2024). Design, Synthesis, and Target Identification of Novel Phenylalanine Derivatives by Drug Affinity Responsive Target Stability (DARTS) in Xanthomonas oryzae pv Oryzae. Journal of Agricultural and Food Chemistry, 72(7), 3436-3444.

Cho, S. M., Farrokh, S., Whitman, G., Bleck, T. P., & Geocadin, R. G. (2019). Neurocritical care for extracorporeal membrane oxygenation patients. Critical care medicine, 47(12), 1773-1781.

Coculescu, B. I. (2009). Antimicrobial resistance induced by genetic changes. Journal of medicine and life, 2(2), 114.

Coelho, C., Brown, L., Maryam, M., Vij, R., Smith, D. F., Burnet, M. C., ... & Casadevall, A. (2019). Listeria monocytogenes virulence factors, including listeriolysin O, are secreted in biologically active extracellular vesicles. Journal of Biological Chemistry, 294(4), 1202-1217.

Cole, M. B., Jones, M. V., & Holyoak, C. (1990). The effect of pH, salt concentration and temperature on the survival and growth of Listeria monocytogenes. Journal of Applied Microbiology, 69(1), 63-72.

Cossart, P., & Dramsi, S. (1999). PrfA, the transcriptional activator of virulence genes, is upregulated during interaction of Listeria monocytogenes with mammalian cells and in eukaryotic cell extracts. Molecular microbiology, 34(3), 552-561.

Cotton, A. D., Wells, J. A., & Seiple, I. B. (2021). Biotin as a reactive handle to selectively label proteins and DNA with small molecules. ACS Chemical Biology, 17(12), 3270-3275.

Dal Piaz, F., Vera Saltos, M. B., Franceschelli, S., Forte, G., Marzocco, S., Tuccinardi, T., ... & Braca, A. (2016). Drug affinity responsive target

stability (DARTS) identifies laurifolioside as a new clathrin heavy chain modulator. Journal of natural products, 79(10), 2681-2692.

Darby, E. M., Trampari, E., Siasat, P., Gaya, M. S., Alav, I., Webber, M. A., & Blair, J. M. (2023). Molecular mechanisms of antibiotic resistance revisited. Nature Reviews Microbiology, 21(5), 280-295.

Davies, J., & Davies, D. (2010). Origins and evolution of antibiotic resistance. Microbiology and molecular biology reviews, 74(3), 417-433.

Demetzos, C., & Dimas, K. S. (2001). Labdane-type diterpenes: Chemistry and biological activity. Studies in Natural Products Chemistry, 25, 235-292.

Deng, Y., Yang, Y., Zhang, B., Chen, H., Lu, Y., Ren, S., ... & Hu, T. (2021). The vicK gene of Streptococcus mutans mediates its cariogenicity via exopolysaccharides metabolism. International Journal of Oral Science, 13(1), 45.

Du, D., Wang-Kan, X., Neuberger, A., Van Veen, H. W., Pos, K. M., Piddock, L. J., & Luisi, B. F. (2018). Multidrug efflux pumps: structure, function and regulation. Nature Reviews Microbiology, 16(9), 523-539.

Dudai, N., Larkov, O., Chaimovitsh, D., Lewinsohn, E., Freiman, L., & Ravid, U. (2003). Essential oil compounds of Origanum dayi Post. Flavour and fragrance journal, 18(4), 334-337.

Eberhardt, J., Santos-Martins, D., Tillack, A. F., & Forli, S. (2021). AutoDock Vina 1.2. 0: new docking methods, expanded force field, and python bindings. Journal of chemical information and modeling, 61(8), 3891-3898.

El-Saadony, M. T., Saad, A. M., Mohammed, D. M., Alkafaas, S. S., Ghosh, S., Negm, S. H., ... & El-Tarabily, K. A. (2025). Curcumin, an active component of turmeric: biological activities, nutritional aspects, immunological, bioavailability, and human health benefits-a comprehensive review. *Frontiers in immunology*, *16*, 1603018.

Fischbach, M. A., & Walsh, C. T. (2009). Antibiotics for emerging pathogens. Science, 325(5944), 1089-1093.

Frutos-Grilo, E., Kreling, V., Hensel, A., & Campoy, S. (2023). Host-pathogen interaction: Enterobacter cloacae exerts different adhesion and invasion capacities against different host cell types. Plos one, 18(10), e0289334.

Galgano, M., Pellegrini, F., Catalano, E., Capozzi, L., Del Sambro, L., Sposato, A., ... & Capozza, P. (2025). Acquired bacterial resistance to antibiotics and resistance genes: from past to future. Antibiotics, 14(3), 222.

Gaurav, A., Bakht, P., Saini, M., Pandey, S., & Pathania, R. (2023). Role of bacterial efflux pumps inantibiotic resistance, virulence, and strategies to discover novel efflux pump inhibitors. Microbiology, 169(5), 001333.

Ghorbani, A., & Esmaeilizadeh, M. (2017). Pharmacological properties of Salvia officinalis and its components. Journal of traditional and complementary medicine, 7(4), 433-440.

Grimaldi, M., Palisi, A., Marino, C., Montoro, P., Capasso, A., Novi, S., ... & D'Ursi, A. M. (2020). NMR-based metabolomic profile of hypercholesterolemic human sera: Relationship with in vitro gene expression?. PLoS One, 15(4), e0231506.

Ha, J., Park, H., Park, J., & Park, S. B. (2021). Recent advances in identifying protein targets in drug discovery. Cell chemical biology, 28(3), 394-423.

Hedl, T. J., San Gil, R., Cheng, F., Rayner, S. L., Davidson, J. M., De Luca, A., ... & Lee, A. (2019). Proteomics approaches for biomarker and drug target discovery in ALS and FTD. Frontiers in Neuroscience, 13, 548.

Hombach, M., Maurer, F. P., Pfiffner, T., Böttger, E. C., & Furrer, R. (2015). Standardization of operator-dependent variables affecting precision and accuracy of the disk diffusion method for antibiotic susceptibility testing. Journal of clinical microbiology, 53(12), 3864-3869.

Humphries, R. M., Ambler, J., Mitchell, S. L., Castanheira, M., Dingle, T., Hindler, J. A., ... & Sei, K. (2018). CLSI methods development and standardization working group best practices for evaluation of antimicrobial susceptibility tests. Journal of clinical microbiology, 56(4), 10-1128.

Hussain, M. I., Syed, Q. A., Khattak, M. N. K., Hafez, B., Reigosa, M. J., & El-Keblawy, A. (2019). Natural product coumarins: biological and pharmacological perspectives. Biologia, 74(7), 863-888.

Iobbi, V., Brun, P., Bernabé, G., Dougue Kentsop, R. A., Donadio, G., Ruffoni, B., ... & De Tommasi, N. (2021). Labdane diterpenoids from Salvia tingitana Etl. synergize with clindamycin against methicillin-resistant Staphylococcus aureus. Molecules, 26(21), 6681.

Iobbi, V., Parisi, V., Bernabè, G., De Tommasi, N., Bisio, A., & Brun, P. (2023). Anti-biofilm activity of carnosic acid from Salvia rosmarinus against methicillin-resistant Staphylococcus aureus. Plants, 12(21), 3679.

Jacob, D., Deborde, C., Lefebvre, M., Maucourt, M. & Moing, A. NMRProcFlow: a graphical and interactive tool dedicated to 1D spectra processing for NMR-based metabolomics. Metabolomics 13, 1–5 (2017).

Jiang, Q., Zhou, X., Cheng, L., & Li, M. (2019). The adhesion and invasion mechanisms of Streptococci. Current Issues in Molecular Biology, 32(1), 521-560.

Jiang, X., Shon, K., Li, X., Cui, G., Wu, Y., Wei, Z., ... & Lu, Y. (2024). Recent advances in identifying protein targets of bioactive natural products. Heliyon, 10(13).

Kayal, S., & Charbit, A. (2006). Listeriolysin O: a key protein of Listeria monocytogenes with multiple functions. FEMS microbiology reviews, 30(4), 514-529.

Kopec, K. K., Bozyczko-Coyne, D., & Williams, M. (2005). Target identification and validation in drug discovery: the role of proteomics. Biochemical Pharmacology, 69(8), 1133-1139.

Lane, C. S. Rapid LC-MS/MS Analysis of Free Amino Acids in Extracellular Matrix Quantitative, Fast, Sensitive and Robust Analysis of Free Amino Acids on the QTRAP ® 6500+ System. (2015).

Lee, S. (2020). Bacteriocins of Listeria monocytogenes and their potential as a virulence factor. Toxins, 12(2), 103.

Lemos, J. A., & Burne, R. A. (2008). A model of efficiency: stress tolerance by Streptococcus mutans. Microbiology, 154(11), 3247-3255.

Lemos, J. A., Palmer, S. R., Zeng, L., Wen, Z. T., Kajfasz, J. K., Freires, I. A., ... & Brady, L. J. (2019). The biology of Streptococcus mutans. Microbiology spectrum, 7(1), 10-1128.

Lemos, J. A., Quivey Jr, R. G., Koo, H., & Abranches, J. (2013). Streptococcus mutans: a new Gram-positive paradigm?. Microbiology, 159(Pt_3), 436-445.

Liao, L. X., Song, X. M., Wang, L. C., Lv, H. N., Chen, J. F., Liu, D., ... & Tu, P. F. (2017). Highly selective inhibition of IMPDH2 provides the basis of antineuroinflammation therapy. Proceedings of the National Academy of Sciences, 114(29), E5986-E5994.

Lomenick, B., Hao, R., Jonai, N., Chin, R. M., Aghajan, M., Warburton, S., ... & Huang, J. (2009). Target identification using drug affinity responsive target stability (DARTS). Proceedings of the National Academy of Sciences, 106(51), 21984-21989.

Mathew, R., Mukherjee, R., Balachandar, R., & Chatterji, D. (2006). Deletion of the rpoZ gene, encoding the ω subunit of RNA polymerase, results in pleiotropic surface-related phenotypes in Mycobacterium smegmatis. Microbiology, 152(6), 1741-1750.

Mendoza, A. M. B., Maliñana, S. A. A., Maravillas, S. I. D., Moniva, K. C., & Jazul, J. P. (2025). Relationship of self-medication and antimicrobial resistance (AMR) in low-and middle-income countries (LMICs): a scoping review. Journal of Public Health and Emergency, 9.

Mohammadi, T., Moazzeni, H., Pirani, A., Vaezi, J., Motahhari, K., Joharchi, M. R., & Bussmann, R. W. (2023). Ethnobotany of plants used by indigenous communities in Birjand, a dry region with rich local traditional knowledge in eastern Iran. Ethnobotany Research and Applications, 26, 1-40.

Moreira, M. R., Souza, A. B., Moreira, M. A., Bianchi, T. C., Carneiro, L. J., Estrela, F. T., ... & Veneziani, R. C. (2013). RP-HPLC analysis of manool-rich Salvia officinalis extract and its antimicrobial activity against bacteria associated with dental caries. Revista Brasileira de Farmacognosia, 23(6), 870-876.

Morteza-Semnani, K., & Saeedi, M. (2004). Essential oils composition of Nepeta cataria L. and Nepeta crassifolia Boiss. and Buhse from Iran. Journal of Essential Oil Bearing Plants, 7(2), 120-124.

Murale, D. P., Hong, S. C., Haque, M. M., & Lee, J. S. (2016). Photo-affinity labeling (PAL) in chemical proteomics: a handy tool to investigate protein-protein interactions (PPIs). Proteome Science, 15(1), 14.

Murray, C. J., Ikuta, K. S., Sharara, F., Swetschinski, L., Aguilar, G. R., Gray, A., ... & Tasak, N. (2022). Global burden of bacterial antimicrobial resistance in 2019: a systematic analysis. The lancet, 399(10325), 629-655.

Muteeb, G., Rehman, M. T., Shahwan, M., & Aatif, M. (2023). Origin of antibiotics and antibiotic resistance, and their impacts on drug development: A narrative review. Pharmaceuticals, 16(11), 1615.

Nagayama, K., Fujita, K., Takashima, Y., Ardin, A. C., Ooshima, T., & Matsumoto-Nakano, M. (2014). Role of ABC transporter proteins in stress responses of Streptococcus mutans. Oral health and dental management, 13(2), 359-365.

Naghavi, M., Vollset, S. E., Ikuta, K. S., Swetschinski, L. R., Gray, A. P., Wool, E. E., ... & Dekker, D. M. (2024). Global burden of bacterial antimicrobial resistance 1990–2021: a systematic analysis with forecasts to 2050. The Lancet, 404(10459), 1199-1226.

Nakano, K., & Ooshima, T. (2009). Serotype classification of Streptococcus mutans and its detection outside the oral cavity. Future microbiology, 4(7), 891-902.

Nazir, A., Nazir, A., Zuhair, V., Aman, S., Sadiq, S. U. R., Hasan, A. H., ... & Bulimbe, D. B. (2025). The Global Challenge of Antimicrobial Resistance: Mechanisms, Case Studies, and Mitigation Approaches. Health Science Reports, 8(7), e71077.

Neuhaus, F. C., & Baddiley, J. (2003). A continuum of anionic charge: structures and functions of D-alanyl-teichoic acids in gram-positive bacteria. Microbiology and molecular biology reviews, 67(4), 686-723.

Nishino, K., Yamasaki, S., Nakashima, R., Zwama, M., & Hayashi-Nishino, M. (2021). Function and inhibitory mechanisms of multidrug efflux pumps. Frontiers in Microbiology, 12, 737288.

Niu, G., Okinaga, T., Qi, F., & Merritt, J. (2010). The Streptococcus mutans IrvR repressor is a CI-like regulator that functions through autocleavage and Clp-dependent proteolysis. Journal of bacteriology, 192(6), 1586-1595.

Oliveira, M., Antunes, W., Mota, S., Madureira-Carvalho, Á., Dinis-Oliveira, R. J., & Dias da Silva, D. (2024). An overview of the recent advances in antimicrobial resistance. Microorganisms, 12(9), 1920.

Palama, T. L., Canard, I., Rautureau, G. J., Mirande, C., Chatellier, S., & Elena-Herrmann, B. (2016). Identification of bacterial species by untargeted NMR spectroscopy of the exo-metabolome. Analyst, 141(15), 4558-4561.

Parham, S., Kharazi, A. Z., Bakhsheshi-Rad, H. R., Nur, H., Ismail, A. F., Sharif, S., ... & Berto, F. (2020). Antioxidant, antimicrobial and antiviral properties of herbal materials. *Antioxidants*, *9*(12), 1309.

Pérez, A., Poza, M., Fernández, A., del Carmen Fernández, M., Mallo, S., Merino, M., ... & Bou, G. (2012). Involvement of the AcrAB-TolC efflux pump in the resistance, fitness, and virulence of Enterobacter cloacae. Antimicrobial agents and chemotherapy, 56(4), 2084-2090.

Pérez-Flores, J. G., García-Curiel, L., Pérez-Escalante, E., Contreras-López, E., Aguilar-Lira, G. Y., Ángel-Jijón, C., ... & Portillo-Torres, L. A. (2025). Plant antimicrobial compounds and their mechanisms of action on spoilage and pathogenic bacteria: A bibliometric study and literature review. *Applied Sciences*, *15*(7), 3516.

Pfeifer, Y., Cullik, A., & Witte, W. (2010). Resistance to cephalosporins and carbapenems in Gram-negative bacterial pathogens. International journal of medical microbiology, 300(6), 371-379.

Pizarro-Cerdá, J., & Cossart, P. (2006). Subversion of cellular functions by Listeria monocytogenes. The Journal of Pathology: A Journal of the Pathological Society of Great Britain and Ireland, 208(2), 215-223.

Portnoy, D. A., Chakraborty, T., Goebel, W., & Cossart, P. (1992). Molecular determinants of Listeria monocytogenes pathogenesis. Infection and immunity, 60(4), 1263-1267.

Ravindhiran, R., Sivarajan, K., Sekar, J. N., Murugesan, R., & Dhandapani, K. (2023). Listeria monocytogenes an emerging pathogen: a comprehensive overview on listeriosis, virulence determinants, detection, and anti-listerial interventions. Microbial Ecology, 86(4), 2231-2251.

Rees, D. C., Johnson, E., & Lewinson, O. (2009). ABC transporters: the power to change. Nature reviews Molecular cell biology, 10(3), 218-227.

Ren, Y. S., Li, H. L., Piao, X. H., Yang, Z. Y., Wang, S. M., & Ge, Y. W. (2021). Drug affinity responsive target stability (DARTS) accelerated small molecules target discovery: Principles and application. Biochemical pharmacology, 194, 114798.

Renzoni, A., Cossart, P., & Dramsi, S. (1999). PrfA, the transcriptional activator of virulence genes, is upregulated during interaction of Listeria monocytogenes with mammalian cells and in eukaryotic cell extracts. *Molecular microbiology*, *34*(3), 552-561.

Reygaert, W. C. (2018). An overview of the antimicrobial resistance mechanisms of bacteria. AIMS microbiology, 4(3), 482.

Rich Moravec, B. S., & Riss, T. (2003). The Celltiter-Blue™ Cell Viability Assay: Monitoring Cell Viability Using A Fluorescent Redox Indicator Dye. Cell, 12(5).

Rix, U., & Superti-Furga, G. (2009). Target profiling of small molecules by chemical proteomics. Nature chemical biology, 5(9), 616-624.

Rodrigues, L., Ramos, J., Couto, I., Amaral, L., & Viveiros, M. (2011). Ethidium bromide transport across Mycobacterium smegmatis cell-wall: correlation with antibiotic resistance. BMC microbiology, 11(1), 35.

Russell, L. E., Yadav, J., Maldonato, B. J., Chien, H. C., Zou, L., Vergara, A. G., & Villavicencio, E. G. (2025). Transporter-mediated drug-drug interactions: regulatory guidelines, in vitro and in vivo methodologies and translation, special populations, and the blood-brain barrier. Drug Metabolism Reviews, 57(3), 244-271.

Sandoval-Motta, S., & Aldana, M. (2016). Adaptive resistance to antibiotics in bacteria: a systems biology perspective. Wiley Interdisciplinary Reviews: Systems Biology and Medicine, 8(3), 253-267.

Santos-Martins, D., Solis-Vasquez, L., Tillack, A. F., Sanner, M. F., Koch, A., & Forli, S. (2021). Accelerating AutoDock4 with GPUs and gradient-based local search. Journal of chemical theory and computation, 17(2), 1060-1073.

Savoia, D. (2012). Plant-derived antimicrobial compounds: alternatives to antibiotics. Future microbiology, 7(8), 979-990.

Scheffers, D. J., & Pinho, M. G. (2005). Bacterial cell wall synthesis: new insights from localization studies. Microbiology and molecular biology reviews, 69(4), 585-607.

Schmittgen, T. D., & Livak, K. J. (2008). Analyzing real-time PCR data by the comparative CT method. *Nature protocols*, *3*(6), 1101-1108.

Senadheera, D. B., Cordova, M., Ayala, E. A., Chavez de Paz, L. E., Singh, K., Downey, J. S., ... & Cvitkovitch, D. G. (2012). Regulation of bacteriocin production and cell death by the VicRK signaling system in Streptococcus mutans. Journal of bacteriology, 194(6), 1307-1316.

Senadheera, D., Krastel, K., Mair, R., Persadmehr, A., Abranches, J., Burne, R. A., & Cvitkovitch, D. G. (2009). Inactivation of VicK affects acid production and acid survival of Streptococcus mutans. Journal of bacteriology, 191(20), 6415-6424.

Seukep, A. J., Fokoua-Maxime, C. D., Mbuntcha, H. G., Chen, G., Assob, J. C. N., Tenniswood, M., ... & Ming-Quan, G. (2022). Bacterial drug efflux pump inhibitors from plants. In Antimicrobial Resistance: Underlying Mechanisms and Therapeutic Approaches (pp. 487-532). Singapore: Springer Nature Singapore.

Shankar, M., Mohapatra, S. S., Biswas, S., & Biswas, I. (2015). Gene regulation by the LiaSR two-component system in Streptococcus mutans. PLoS One, 10(5), e0128083.

Sharma, A., Biharee, A., Kumar, A., & Jaitak, V. (2020). Antimicrobial terpenoids as a potential substitute in overcoming antimicrobial resistance. Current Drug Targets, 21(14), 1476-1494.

Smith, E. G., & Spatafora, G. A. (2012). Gene regulation in S. mutans: complex control in a complex environment. Journal of dental research, 91(2), 133-141.

Soto, S. M. (2013). Role of efflux pumps in the antibiotic resistance of bacteria embedded in a biofilm. Virulence, 4(3), 223-229.

Sumrall, E. T., Keller, A. P., Shen, Y., & Loessner, M. J. (2020). Structure and function of Listeria teichoic acids and their implications. Molecular microbiology, 113(3), 627-637.

Tabana, Y., Babu, D., Fahlman, R., Siraki, A. G., & Barakat, K. (2023). Target identification of small molecules: an overview of the current applications in drug discovery. BMC biotechnology, 23(1), 44.

Tran, Q. T., Wong, W. F., & Chai, C. L. (2017). Labdane diterpenoids as potential anti-inflammatory agents. Pharmacological research, 124, 43-63.

Vázquez-Boland, J. A., Kuhn, M., Berche, P., Chakraborty, T., Domínguez-Bernal, G., Goebel, W., ... & Kreft, J. (2001). Listeria pathogenesis and molecular virulence determinants. Clinical microbiology reviews, 14(3), 584-640.

Webb, A. J., Homer, K. A., & Hosie, A. H. (2008). Two closely related ABC transporters in Streptococcus mutans are involved in disaccharide and/or oligosaccharide uptake. Journal of bacteriology, 190(1), 168-178.

Wright, G. D. (2007). The antibiotic resistome: the nexus of chemical and genetic diversity. Nature reviews microbiology, 5(3), 175-186.

Wright, G. D. (2007). The antibiotic resistome: the nexus of chemical and genetic diversity. Nature reviews microbiology, 5(3), 175-186.

Xavier, V., Spréa, R., Finimundy, T. C., Heleno, S. A., Amaral, J. S., Barros, L., & Ferreira, I. C. (2023). Terpenes. In Natural secondary metabolites: from nature, through science, to industry (pp. 107-156). Cham: Springer International Publishing.

Yonezawa, H., & Kuramitsu, H. K. (2005). Genetic analysis of a unique bacteriocin, Smb, produced by Streptococcus mutans GS5. Antimicrobial agents and chemotherapy, 49(2), 541-548.

Zarin, M. K. Z., Dehaen, W., Salehi, P., & Asl, A. A. B. (2023). Synthesis and modification of morphine and codeine, leading to diverse libraries with improved pain relief properties. *Pharmaceutics*, *15*(6), 1779.

Zhang, F., & Cheng, W. (2022). The mechanism of bacterial resistance and potential bacteriostatic strategies. Antibiotics, 11(9), 1215.

Zou, M., Zhou, H., Gu, L., Zhang, J., & Fang, L. (2024). Therapeutic target identification and drug discovery driven by chemical proteomics. Biology, 13(8), 555.

Publications:

1. **Nocera, R.,** Rosa, E., Parisi, V., Tuccinardi, T., Di Stefano, M., Donadio, G., Dal Piaz, F., De Tommasi, N. (2025). Disarming *Streptococcus mutans* in real time: live-cell DARTS uncovers ABC transporter targeting by manool. Submitted on *Communication Biology,* Status: under review
2. Vitiello, M., Vidotto, F., Camangi, F., Donadio, G., **Nocera, R.,** De Tommasi, N., Braca, A., De Leo, M. (2025). Antioxidant flavonol glycosides from the aerial parts of Atriplex halimus L. *Phytochemistry*, 114559.
3. Parisi, V., **Nocera, R.,** Rosa, E., Iobbi, V., Ebrahimi, S. N., Braca, A., De Tommasi, N., Donadio, G. Constituents from the Polar Extract of *Pisolithus arhizus* and Their Anti-inflammatory Activity. *Journal of Natural Products*, 87(3), 2024, 520-529.
4. Parisi, V., **Nocera, R.,** Franceschelli, S.; Tedesco, C.; De Riccardis, F.; Braca, A.; De Tommasi, N., Donadio, G., Cytotoxic triterpenoids from the ectomycorrhizal fungus *Pisolitus arhizus*. Phitochemistry 209 2023, 113635
5. **Nocera, R.,** Eletto, D.; Santoro, V.; Parisi, V.; Bellone, M.L.; Izzo, M.; Tosco, A.; Dal Piaz, F.; Donadio, G.; De Tommasi, N. Design of an Herbal Preparation Composed by a Combination of *Ruscus aculeatus* L. and *Vitis vinifera* L. Extracts, Magnolol and Diosmetin to Address Chronic Venous Diseases through an Anti-

Inflammatory Effect and AP-1 Modulation. *Plants*, 2023, 12, 1051

Attendance at congress/conferences/ schools:

- INTERNATIONAL CONGRESS ON NATURAL PRODUCTS RESEARCH, August-September, 31-1-2-3 th 2025, Naples, Italy.
- INTERNATIONAL CONGRESS ON NATURAL PRODUCTS RESEARCH, July, 13-14-15-16-17 th 2024, Krakow, Poland.
- Fitochimica e studio degli endemismi vegetali, February, 2024, Rome, Italy.
- "31st International Symposium on the Chemistry of Natural Products and the 11th International Congress on Biodiversity (IUPAC ISCNP31 & ICOB11), October, 15-16-17-18-19th 2023, Napoli, Italy.
- " METABOLOMICS IN NATURAL PRODUCT RESEARCH. From biomarker discovery to deep metabolome analysis and targeted isolation of bioactive compounds", Società Fitochimica Italiana, September 21-22-23rd 2023, Catania, Italy.
- "1° Congresso intersocietà sui prodotti vegetali per la salute: il ruolo delle piante medicinali nella medicina moderna. June 17-18-19th 2023, Padova, Italy